PHYSICAL REVIEW D **90,** 114001 (2014)

Variable-flavor-number scheme for final state jets in thrust

Piotr Pietrulewicz,[1] Simon Gritschacher,[2] Andre H. Hoang,[1,3] Ilaria Jemos,[1] and Vicent Mateu[1]
[1]*Fakultät für Physik, Universität Wien, Boltzmanngasse 5, 1090 Vienna, Austria*
[2]*Mathematical Institute, University of Oxford, Woodstock Road, Oxford OX2 6GG, United Kingdom*
[3]*Erwin Schrödinger International Institute for Mathematical Physics, University of Vienna, Boltzmanngasse 9, A-1090 Vienna, Austria*
(Received 25 June 2014; published 1 December 2014)

We present results for mass effects coming from secondary radiation of heavy quark pairs related to gluon splitting in the thrust distribution for e^+e^- collisions. The results are given in the dijet limit where the hard interaction scale and the scales related to collinear and soft radiation are widely separated. We account for the corresponding fixed-order corrections at $\mathcal{O}(\alpha_s^2)$ and the summation of all logarithmic terms related to the hard, collinear, and soft scales as well as the quark mass at N^{3}LL order. We also remove the $\mathcal{O}(\Lambda_{\rm QCD})$ renormalon in the partonic soft function, leading to an infrared evolution equation with a matching condition related to the massive quark threshold. The quark mass can be arbitrary, ranging from the infinitely heavy case, where decoupling takes place, down to the massless limit, where the results smoothly merge into the well-known predictions for massless quarks. Our results are formulated in the framework of factorization theorems for e^+e^- dijet production and provide universal threshold corrections for the renormalization group evolution of the hard current, the jet, and the soft functions at the scale where the massive quarks are integrated out. The results represent a first explicit realization of a variable-flavor-number scheme for final-state jets along the lines of the well-known flavor-number-dependent evolution of the strong coupling α_s and the parton distribution functions.

DOI: 10.1103/PhysRevD.90.114001 PACS numbers: 12.38.-t, 12.38.Bx, 13.66.Jn

I. INTRODUCTION

The systematic theoretical treatment of mass effects in collider observables represents an important area in collider phenomenology where substantial progress is required to take full advantage of present and upcoming data. This concerns in particular the mass of the top quark [1–3] affecting physics at the Large Hadron Collider (LHC) and at a potential future linear collider, but also the masses of lighter heavy quarks such as charm [4–6] and bottom quarks [7] relevant e.g., in deep-inelastic scattering and event shape analyses at LEP. In this context, examinations for the top quark may be also considered as study cases for the treatment of new massive colored particles that might be discovered in the near future. For inclusive cross sections at hadron colliders, a systematic approach to treat massive quarks from the large mass limit, where decoupling takes place, continuously down to the small-mass limit, where the description for massless quarks is approached, has been provided by Aivazis, Collins, Olness, and Tung [8,9]. Their work laid the basis of a variable-flavor-number scheme (VFNS) for inclusive processes in hadron collisions which, depending on the size of the quark mass in relation to the hard scattering and hadronization scales, allows us to factorize infrared-safe quark-mass-dependent hard coefficient corrections from flavor-number-dependent low-energy parton distribution functions. Since the concepts behind the work of Aivazis, Collins, Olness, and Tung are founded in the separation of close-to-mass-shell and off-shell modes, their approach is along the lines of effective field theory (EFT) methods such as Soft-Collinear Effective Theory (SCET) [10,11] and can be readily incorporated into it.

In this paper, we present results for a VFNS for final-state jets which are initiated by massless quarks and where massive quarks are produced through the radiation of gluons that split into a massive quark-antiquark pair; see Fig. 1. We call this type of heavy quark production mechanism *secondary* in contrast to the case where the massive quarks are produced directly in the hard current interaction, which we call *primary*. As for the VFNS scheme for inclusive processes in hadron collisions, the approach is valid from the large-mass limit, where the heavy quark decouples, continuously down to the small-mass limit, where the predictions approach the known results for massless quarks. As a concrete application used to discuss the results, we consider the secondary massive quark effects in the e^+e^- thrust distribution, where we define the thrust variable τ via

$$\tau = 1 - T = 1 - \frac{\sum_i |\vec{n}\cdot\vec{p}_i|}{\sum_j E_j} = 1 - \sum_i \frac{|\vec{n}\cdot\vec{p}_i|}{Q}. \quad (1)$$

Here $\vec{n}$ is the thrust axis, and the sum is performed over all final-state particles with momenta $\vec{p}_i$ and energies E_i.[1] In

[1]We define the thrust variable τ normalized with respect to the c.m. energy Q, which is the sum of all energies and also agrees with the variable 2-jettiness [12].

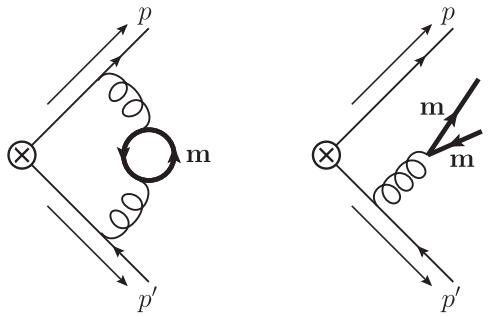

FIG. 1. Diagrams at $\mathcal{O}(\alpha_s^2)$ for virtual and real secondary radiation of massive quark pairs in primary massless quark production.

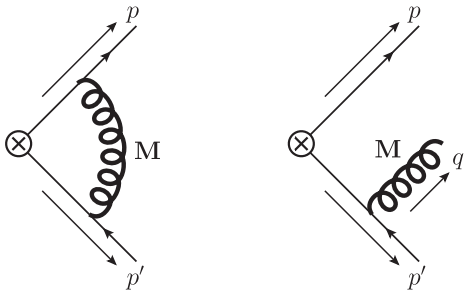

FIG. 2. Diagrams at $\mathcal{O}(\alpha_s)$ for virtual and real secondary radiation of gluons with mass M in primary massless quark production.

the dijet limit where τ is small, the final state is governed by two narrow back-to-back jets, and the scales of the hard interaction ($\sim Q$), of collinear radiation ($\sim Q\lambda$), and of soft radiation ($\sim Q\lambda^2$) are widely separated (with $\lambda \sim \max\{\tau^{1/2}, (\Lambda_{\rm QCD}/Q)^{1/2}\}$). In this context the dominant perturbative contributions in the thrust distribution for massless quarks are related to distributions in τ and can be factorized into a hard coefficient function, a universal jet function, and a soft function, all of which are defined in a gauge-invariant way. The latter has also a nonperturbative component which can be parametrized through a convolution with a soft model function that can be determined through fits to experimental data in a way free of $\mathcal{O}(\Lambda_{\rm QCD})$ renormalons [13]. The logarithmic terms within the dominant contributions can be summed using the anomalous dimensions of the hard coefficient and the jet and soft functions.

Accounting for quark masses in this context adds another nontrivial twist to the factorization setup, since quark masses represent additional scales that can in principle have any hierarchy with respect to the hard, collinear, and soft scales, which themselves depend on the value of τ.[2] The possible relations among these scales can therefore vary substantially even within a single thrust distribution for a fixed c.m. energy Q. Within the factorization formalism, the nonvanishing value of the quark mass can lead to a flavor-number-dependent renormalization group (RG) evolution, to threshold corrections in the evolution when crossing the quark mass scale and to additional mass-dependent fixed-order corrections in the hard coefficient and the jet and soft functions. The conceptual setup to define these quark-mass-dependent corrections is partially guided by identifying terms that are singular in the quark mass (in the small-mass limit). The framework of SCET—properly extended to account for massive quarks—provides a natural framework to carry out this task systematically.

The approach we propose is based on the seminal paper in Ref. [15], where it has been shown that the problem of secondary heavy quark production in the thrust distribution is closely related to the production of massive gauge bosons; see Fig. 2. The connection between these apparently different problems is related to the fact that the off-shell intermediate gluon that splits into the massive quark pair has an invariant mass that is bounded from below by twice the quark mass. So, concerning the setup of the field theoretic modes needed to construct effective field theories for the various possible scenarios (related to the possible hierarchies with respect to the hard, collinear, soft, and mass scales), both problems are quite similar, since each of the field theoretic formulations has to account for (collinear and/or soft) gluonic modes with a finite typical invariant mass. In Ref. [15] we have discussed in detail the field theoretic scenarios to treat all possible hierarchies involving the "gluon mass" and the hard, collinear, and soft scales, and we have provided the resulting form of the factorization theorems accounting for the required mass corrections, the changes of the RG evolution above and below the mass scale, and the associated threshold corrections at the mass scale ("mass mode method"). At this level, replacing the gluonic modes with massive quark modes at $\mathcal{O}(\alpha_s^2)$ can be computationally more challenging, but it does not lead to any additional conceptual complication. It was pointed out in Ref. [15] that for situations where the produced massive quark and antiquark enter a quantity coherently (i.e., only the sum of their momenta is relevant in the observable), one can obtain the corresponding $\mathcal{O}(\alpha_s^2)$ massive quark corrections from the $\mathcal{O}(\alpha_s)$ "massive gluon" result using a dispersion integration as illustrated in Fig. 3. It was in particular demonstrated in Ref. [15] that also the conceptual issues involving the so-called rapidity divergences, which are related to specific divergences of collinear and soft modes with the same typical invariant mass, and the soft-bin subtractions, which avoid double counting between collinear and soft mass modes, can be dealt with at the level of the massive gluon results. As was shown in Ref. [16], this computational trick can also be very useful for quantities where the quark and antiquark enter independently, as the dispersion integral might already give the bulk of the numerical effects.

The VFNS we propose in this paper is presented and discussed on the basis of the secondary massive quark

[2]Here we do not account for the effects of hadron masses (see Ref. [14]).

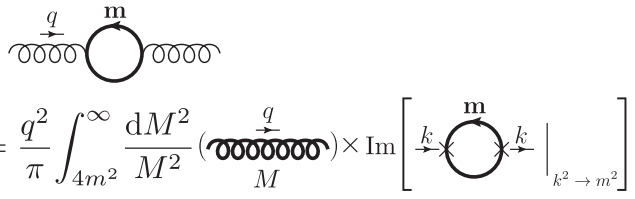

FIG. 3. Figure illustrating the dispersion method for the vacuum polarization correction to the gluon propagator in the subtracted version with $\Pi(q^2 = 0) = 0$ suitable for situations where the massive quark is not contributing to the renormalization group evolution. The explicit analytic form of the dispersion relations is discussed in Sec. IV A.

effects in the e^+e^- thrust distribution at N^{3}LL order in the conventional SCET counting.[3] Concerning a recent thrust distribution analysis based on the SCET factorization theorem for massless quarks [17], the dominant secondary massive quark effects come from bottom quarks and represent minor corrections, since that analysis was carried out with data where the bottom quark mass effects are small due to restrictions in the values of the c.m. energy Q and the fit range in τ.[4] In general, however, the effects from secondary massive quarks are sizeable for lower Q values or τ values in the peak and extreme dijet regions where the cross section depends strongly on the thrust value. Nevertheless, we consider the presentation of the VFNS given in this work primarily as a nontrivial showcase of the method which might serve as a guideline to apply the method to other problems involving final-state jets.

The content of this work is as follows: In Sec. II we review the notations and the massless thrust factorization theorem with an emphasis on the corrections related to the number of massless quarks n_f. In Sec. III we briefly summarize the four relevant field theory scenarios needed to describe the possible hierarchies of the quark mass with respect to the hard, jet, and soft scales. We describe the respective factorization theorems, which are analogous to the ones given in Ref. [15] for the case of the "massive gluon." We show explicitly the results of the $\mathcal{O}(\alpha_s^2 C_F T_F)$ massive quark corrections to the hard, jet, and soft functions including the results for the subtractions of $\mathcal{O}(\Lambda_{\mathrm{QCD}})$ renormalon contributions in the soft function using the gap scheme [13,18] and the threshold corrections that arise when the RG evolution of the hard current coefficient, the jet and soft functions, as well as the gap parameter, cross the massive quark pair flavor threshold. In Sec. IV we describe the computation of the $\mathcal{O}(\alpha_s^2 C_F T_F)$ massive quark corrections to the hard and jet functions, which were the remaining unknown ingredients in the factorization theorems at this order. In Sec. V we show that the massive threshold corrections are directly related to the matrix elements in the factorization theorems in different renormalization schemes. This will also illustrate that at the conceptual level, a separation into four different effective field theories is in principle not necessary, and that the factorization theorems merge continuously into each other. Furthermore, we explain in this section how the freedom to set up the RG evolution leads to consistency conditions among the various threshold corrections, underlining their universality. Finally, the results of this paper allow us to predict the singular $\mathcal{O}(\alpha_s^2 C_F T_F)$ fixed-order corrections arising from secondary massive quarks, which to our knowledge have not been given in an explicit form in the literature before. In Sec. VI we carry out a numerical analysis at N^{3}LL order for secondary massive bottom and top quarks at different c.m. energies. In particular, we investigate the size of the mass corrections compared to the massless limit, which turn out to be small in the tail region, but essential at the peak. Finally, Sec. VII contains our conclusions.

II. THE MASSLESS FACTORIZATION THEOREM FOR THRUST

In this section, we briefly review the known massless factorization theorem for the most singular contributions of the thrust distribution in the dijet limit, which are the dominant terms for small values of τ. The main purpose of this section is to set up the notations and to collect the perturbative results at $\mathcal{O}(\alpha_s^2 C_F T_F)$ for later comparison and reference concerning the massive quark contributions discussed in later sections. Due to consistency, the massive quark results must yield the massless expressions for vanishing quark mass. The factorization theorem for n_f massless quark flavors reads [19–21]

$$\begin{aligned}\frac{1}{\sigma_0}\frac{\mathrm{d}\sigma}{\mathrm{d}\tau} &= Q|C^{(n_f)}(Q,\mu_H)|^2|U_C^{(n_f)}(Q,\mu_H,\mu)|^2 \\ &\times \int \mathrm{d}s \int \mathrm{d}s' J^{(n_f)}(s',\mu_J) U_J^{(n_f)}(s-s',\mu,\mu_J) \\ &\times \int \mathrm{d}\ell\, S^{(n_f)}\left(Q\tau - \frac{s}{Q} - \ell, \mu_S\right) U_S^{(n_f)}(\ell,\mu,\mu_S),\end{aligned} \tag{2}$$

where σ_0 denotes the total partonic e^+e^- cross section at tree level, $C^{(n_f)}(Q,\mu)$ is the hard current matching condition, $J^{(n_f)}(s,\mu)$ the thrust jet function, and $S^{(n_f)}(\ell,\mu)$ the thrust soft function. The terms $U_C^{(n_f)}$, $U_J^{(n_f)}$, and $U_S^{(n_f)}$ are the RG evolution factors for the hard current matching, the jet, and the soft function, respectively. The superscript (n_f) indicates that the $\overline{\mathrm{MS}}$ scheme with n_f dynamic quark

[3] At N^{3}LL, one uses four-loop cusp and three-loop noncusp anomalous dimensions and two-loop matrix elements and matching conditions.

[4] In Ref. [17], some effects arising from the finite bottom mass related to primary production were accounted for, but none related to secondary bottom quark production.

flavors is used for all renormalized quantities, as is common when heavy quarks are not involved.

The functions $C^{(n_f)}$, $J^{(n_f)}$, and $S^{(n_f)}$ depend implicitly on n_f at $\mathcal{O}(\alpha_s)$ through the strong coupling constant. The explicit dependence on n_f starts at $\mathcal{O}(\alpha_s^2)$. The expansion of the hard current matching coefficient up to this order has the form

$$C^{(n_f)}(Q,\mu) = 1 + C^{(n_f,1)}(Q,\mu) + [C_{C_F}^{(n_f,2)}(Q,\mu) + C_{C_A}^{(n_f,2)}(Q,\mu) + C_{n_f}^{(n_f,2)}(Q,\mu)] + \mathcal{O}(\alpha_s^3), \tag{3}$$

where $C^{(n_f,1)}$, $C_{C_F}^{(n_f,2)}$, $C_{C_A}^{(n_f,2)}$, and $C_{n_f}^{(n_f,2)}$ denote the contributions at $\mathcal{O}(\alpha_s)$, $\mathcal{O}(\alpha_s^2 C_F^2)$, $\mathcal{O}(\alpha_s^2 C_F C_A)$, and $\mathcal{O}(\alpha_s^2 C_F T_F n_f)$, respectively. We use the analogous notation for $J^{(n_f)}$ and $S^{(n_f)}$, as well as for all other perturbative expressions throughout this work. The additional dependence on a finite quark mass will be indicated in the arguments.

The massless current matching coefficient $C^{(n_f)}(Q,\mu)$ is determined by matching SCET to QCD. The renormalized contribution at $\mathcal{O}(\alpha_s^2 C_F T_F)$ reads [22] [$\alpha_s^{(n_f)} \equiv \alpha_s^{(n_f)}(\mu)$]

$$C_{n_f}^{(n_f,2)}(Q,\mu) = \frac{(\alpha_s^{(n_f)})^2 C_F T_F n_f}{16\pi^2}\left\{-\frac{4}{9}L_{-Q}^3 + \frac{38}{9}L_{-Q}^2 - \left(\frac{418}{27}+\frac{4\pi^2}{9}\right)L_{-Q} + \frac{4085}{162}+\frac{23\pi^2}{27}+\frac{4}{9}\zeta_3\right\}, \tag{4}$$

where $L_{-Q} = \ln(-Q^2/\mu^2)$ (with $Q^2 \equiv Q^2 + i0$). The associated contributions to the current renormalization factor read

$$Z_{C,n_f}^{(n_f,2)}(Q,\mu) = \frac{(\alpha_s^{(n_f)})^2 C_F T_F n_f}{16\pi^2} \times \left\{-\frac{2}{\epsilon^3}+\frac{1}{\epsilon^2}\left[\frac{4}{3}L_{-Q}-\frac{8}{9}\right] + \frac{1}{\epsilon}\left[-\frac{20}{9}L_{-Q}+\frac{65}{27}+\frac{\pi^2}{3}\right]\right\}. \tag{5}$$

The jet function is given by a vacuum correlator of two jet fields in SCET and describes the collinear dynamics of the two back-to-back jets. The renormalized expression for $J^{(n_f)}(s,\mu)$ at $\mathcal{O}(\alpha_s^2 C_F T_F)$ reads [23]

$$\mu^2 J_{n_f}^{(n_f,2)}(s,\mu) = \frac{(\alpha_s^{(n_f)})^2 C_F T_F n_f}{16\pi^2} \times \left\{\left[-\frac{4057}{81}+\frac{136\pi^2}{27}+\frac{32}{9}\zeta_3\right]\delta(\bar{s}) + \left(\frac{988}{27}-\frac{16\pi^2}{9}\right)\left[\frac{\theta(\bar{s})}{\bar{s}}\right]_+ - \frac{232}{9}\left[\frac{\theta(\bar{s})\ln\bar{s}}{\bar{s}}\right]_+ + \frac{16}{3}\left[\frac{\theta(\bar{s})\ln^2\bar{s}}{\bar{s}}\right]_+\right\}, \tag{6}$$

with $\bar{s} \equiv s/\mu^2$. The corresponding contributions to the renormalization factor read

$$\mu^2 Z_{J,n_f}^{(n_f,2)}(s,\mu) = \frac{(\alpha_s^{(n_f)})^2 C_F T_F n_f}{16\pi^2} \times \left\{\left[\frac{8}{\epsilon^3}-\frac{4}{9\epsilon^2}-\frac{1}{\epsilon}\left(\frac{242}{27}+\frac{4\pi^2}{9}\right)\right]\delta(\bar{s}) - \left(\frac{16}{3\epsilon^2}-\frac{80}{9\epsilon}\right)\left[\frac{\theta(\bar{s})}{\bar{s}}\right]_+\right\}. \tag{7}$$

The thrust soft function $S^{(n_f)}(\ell,\mu)$ describes ultrasoft radiation between the two jets. It can be written as a convolution of the partonic soft function describing perturbative corrections at the soft scale and the nonperturbative hadronic soft function [13]. The renormalized expression for the partonic soft function at $\mathcal{O}(\alpha_s^2 C_F T_F)$ is [24,25]

$$\mu\hat{S}_{n_f}^{(n_f,2)}(\ell,\mu) = \frac{(\alpha_s^{(n_f)})^2 C_F T_F n_f}{16\pi^2} \times \left\{\left[\frac{80}{81}+\frac{74\pi^2}{27}-\frac{232}{9}\zeta_3\right]\delta(\bar{\ell}) + \left(-\frac{448}{27}+\frac{16\pi^2}{9}\right)\left[\frac{\theta(\bar{\ell})}{\bar{\ell}}\right]_+ + \frac{320}{9}\left[\frac{\theta(\bar{\ell})\ln\bar{\ell}}{\bar{\ell}}\right]_+ - \frac{64}{3}\left[\frac{\theta(\bar{\ell})\ln^2\bar{\ell}}{\bar{\ell}}\right]_+\right\}, \tag{8}$$

with $\bar{\ell} \equiv \ell/\mu$. The corresponding contributions to the renormalization factor read

$$\mu Z_{S,n_f}^{(n_f,2)}(\ell,\mu) = \frac{(\alpha_s^{(n_f)})^2 C_F T_F n_f}{16\pi^2} \times \left\{\left[-\frac{4}{\epsilon^3}+\frac{20}{9\epsilon^2}+\frac{1}{\epsilon}\left(\frac{112}{27}-\frac{2\pi^2}{9}\right)\right]\delta(\bar{\ell}) + \left(\frac{16}{3\epsilon^2}-\frac{80}{9\epsilon}\right)\left[\frac{\theta(\bar{\ell})}{\bar{\ell}}\right]_+\right\}. \tag{9}$$

The overlap between the partonic and the nonperturbative contributions in dimensional regularization leads to an

infrared sensitivity of the perturbative corrections implying factorially enhanced coefficients ("renormalon"). One can eliminate the renormalon problem for the leading $\mathcal{O}(\Lambda_{\rm QCD})$ power correction that arises in the operator production expansion (OPE) of the soft function for $\ell \gg \Lambda_{\rm QCD}$ by introducing a gap parameter $\Delta \sim \Lambda_{\rm QCD}$ in the hadronic soft model function related to a minimal hadronic energy deposit together with properly defined perturbative subtractions in the partonic soft function. This cancels the linear sensitivity to small momenta in the partonic soft function order by order in perturbation theory [13,18]. The complete function, including the renormalon subtractions, has the form

$$S^{(n_f)}(\ell,\mu) = \int \mathrm{d}\ell' \hat{S}^{(n_f)}(\ell-\ell'-2\delta^{(n_f)}(R,\mu),\mu) \times F(\ell'-2\bar{\Delta}^{(n_f)}(R,\mu)), \tag{10}$$

where $\delta^{(n_f)}(R,\mu)$ is the subtraction series, $\bar{\Delta}^{(n_f)}(R,\mu)$ is the gap parameter, which is free of the $\mathcal{O}(\Lambda_{\rm QCD})$ renormalon, and F is the soft model function. A convenient definition for $\delta^{(n_f)}(R,\mu)$ with consistent RG properties has been given in Ref. [18] and has the form

$$\delta^{(n_f)}(R,\mu) = \frac{R}{2} e^{\gamma_E} \frac{\mathrm{d}}{\mathrm{d}\ln(ix)} \ln \tilde{S}^{(n_f)}(x,\mu)|_{x=(iRe^{\gamma_E})^{-1}}, \tag{11}$$

where $\tilde{S}^{(n_f)}$ is the partonic soft function in configuration space, $\tilde{S}^{(n_f)}(x,\mu) = \int \mathrm{d}\ell \hat{S}^{(n_f)}(\ell,\mu) e^{-i\ell x}$. The $\mathcal{O}(\alpha_s^2 C_F T_F)$ correction reads

$$\delta_{n_f}^{(n_f,2)}(R,\mu) = \frac{(\alpha_s^{(n_f)})^2 C_F T_F n_f}{16\pi^2} R e^{\gamma_E} \times \left[\frac{8}{3}\ln^2\left(\frac{\mu^2}{R^2}\right) + \frac{80}{9}\ln\left(\frac{\mu^2}{R^2}\right) + \frac{224}{27} + \frac{8\pi^2}{9}\right]. \tag{12}$$

The renormalon-free gap parameter $\bar{\Delta}^{(n_f)}(R,\mu)$ is related to the ambiguous, but scale-independent "bare" gap parameter Δ by the relation[5]

$$\Delta = \bar{\Delta}^{(n_f)}(R,\mu) + \delta^{(n_f)}(R,\mu). \tag{13}$$

Thus, $\bar{\Delta}^{(n_f)}(R,\mu)$ is scale- and subtraction-scheme-dependent. The natural choice for the scale R of the renormalon-free gap parameter is $R \gtrsim \Lambda_{\rm QCD}$. On the other hand, the renormalon subtraction $\delta^{(n_f)}(R,\mu)$ should be evaluated for $\mu = \mu_S$, which is much larger than $\Lambda_{\rm QCD}$ in the tail region, in order to achieve a proper cancellation with the IR-sensitive terms in the soft function. This requires a resummation if the logarithm $\ln(\mu_S/\Lambda_{\rm QCD})$ is large, which can be performed by solving the evolution equations [13,18,26,27]

$$R\frac{\mathrm{d}}{\mathrm{d}R}\bar{\Delta}^{(n_f)}(R,R) = -R\frac{\mathrm{d}}{\mathrm{d}R}\delta^{(n_f)}(R,R) \equiv -R\gamma_R^{(n_f)}[\alpha_s^{(n_f)}(R)], \tag{14}$$

$$\mu\frac{\mathrm{d}}{\mathrm{d}\mu}\bar{\Delta}^{(n_f)}(R,\mu) \equiv -R\gamma_{\Delta,\mu}^{(n_f)} = 2Re^{\gamma_E}\Gamma_{\rm cusp}^{(n_f)}[\alpha_s^{(n_f)}(\mu)]. \tag{15}$$

Note that the R anomalous dimension $\gamma_R^{(n_f)}$, which is responsible for relating $\bar{\Delta}^{(n_f)}$ at different values of R to each other in a way free of the $\mathcal{O}(\Lambda_{\rm QCD})$ renormalon and free of large IR logarithms, happens to vanish at $\mathcal{O}(\alpha_s)$. Thus, the leading anomalous dimension at $\mathcal{O}(\alpha_s^2)$ depends both linearly and via the strong coupling constant on the number of active flavors n_f. The $\mathcal{O}(\alpha_s^2 C_F T_F)$ contribution reads

$$\gamma_{R,n_f}^{(n_f,2)} = \frac{(\alpha_s^{(n_f)})^2 C_F T_F n_f}{16\pi^2} e^{\gamma_E}\left(\frac{224}{27} + \frac{8\pi^2}{9}\right). \tag{16}$$

Note that the first moment of the soft model function $2\Omega_1$ also becomes a scheme- and scale-dependent quantity once we employ a renormalon-free gap scheme. The moment parameter $\Omega_1^{(n_f)}(R,\mu)$ is then related to the gap parameter $\bar{\Delta}^{(n_f)}(R,\mu)$ via

$$\Omega_1^{(n_f)}(R,\mu) \equiv \frac{1}{2}\int_0^\infty \mathrm{d}\ell\,\ell F(\ell - 2\bar{\Delta}^{(n_f)}(R,\mu)) = \bar{\Delta}^{(n_f)}(R,\mu) + \frac{1}{2}\int_0^\infty \mathrm{d}\ell\,\ell F(\ell). \tag{17}$$

Large logarithms between the characteristic scales of each sector, μ_H, μ_J, and μ_S, and the final, common renormalization scale of the factorization theorem μ are summed by the evolution factors $U_C^{(n_f)}$, $U_J^{(n_f)}$, and $U_S^{(n_f)}$. They satisfy the RG equations

$$\mu\frac{\mathrm{d}}{\mathrm{d}\mu}U_C^{(n_f)}(Q,\mu_H,\mu) = \gamma_C^{(n_f)}(Q,\mu)U_C^{(n_f)}(Q,\mu_H,\mu), \tag{18}$$

$$\mu\frac{\mathrm{d}}{\mathrm{d}\mu}U_J^{(n_f)}(s,\mu,\mu_J) = \int \mathrm{d}s'\gamma_J^{(n_f)}(s-s',\mu)U_J^{(n_f)}(s',\mu,\mu_J), \tag{19}$$

$$\mu\frac{\mathrm{d}}{\mathrm{d}\mu}U_S^{(n_f)}(\ell,\mu,\mu_S) = \int \mathrm{d}\ell'\gamma_S^{(n_f)}(\ell-\ell',\mu)U_S^{(n_f)}(\ell',\mu,\mu_S). \tag{20}$$

The evolution factors are already at leading logarithmic (LL) order, sensitive to the number of active flavors n_f due

[5]The "bare" gap parameter Δ is conceptually analogous to the heavy quark pole mass parameter, so all renormalon-free gap schemes can be related to each other unambiguously through their relation to the bare Δ. Frequently Δ is also called the "$\overline{\rm MS}$ gap parameter."

to the running of $\alpha_s^{(n_f)}$. Thus, modifying the number of active quark flavors in the evolution affects the thrust distribution already at LL through its dependence on α_s, which happens when a mass threshold is crossed. The explicit dependence of the anomalous dimensions on n_f starts at $\mathcal{O}(\alpha_s^2)$, and the corresponding $\mathcal{O}(\alpha_s^2 C_F T_F)$ terms read ($Q^2 \equiv Q^2 + i0$)

$$\gamma_{C,n_f}^{(n_f,2)}(Q,\mu) = \frac{(\alpha_s^{(n_f)})^2 C_F T_F n_f}{16\pi^2} \times \left[\Gamma_{n_f}^{(2)} \ln\left(-\frac{Q^2}{\mu^2}\right) + \frac{260}{27} + \frac{4\pi^2}{3}\right], \quad (21)$$

$$\mu^2 \gamma_{J,n_f}^{(n_f,2)}(s,\mu) = \frac{(\alpha_s^{(n_f)})^2 C_F T_F n_f}{16\pi^2} \left\{-4\Gamma_{n_f}^{(2)} \left[\frac{\theta(\bar{s})}{\bar{s}}\right]_+ - \left(\frac{968}{27} + \frac{16\pi^2}{9}\right)\delta(\bar{s})\right\}, \quad (22)$$

$$\mu \gamma_{S,n_f}^{(n_f,2)}(\ell,\mu) = \frac{(\alpha_s^{(n_f)})^2 C_F T_F n_f}{16\pi^2} \left\{4\Gamma_{n_f}^{(2)} \left[\frac{\theta(\bar{\ell})}{\bar{\ell}}\right]_+ + \left(\frac{448}{27} - \frac{8\pi^2}{9}\right)\delta(\bar{\ell})\right\}, \quad (23)$$

where $\Gamma_{n_f}^{(2)} = -80/9$ denotes the $\mathcal{O}(\alpha_s^2 C_F T_F n_f)$ coefficient of the cusp anomalous dimension $\Gamma_{\text{cusp}}^{(n_f)}$.

In Eq. (2), the choice of μ is arbitrary, and the dependence on μ cancels exactly, working to any given order in perturbation theory. In the following, we will present our results adopting the choice $\mu = \mu_S$, such that the evolution factor $U_S^{(1)}(\ell, \mu_S, \mu_S) = \delta(\ell)$ and can be dropped from Eq. (2). The fact that any other choice for μ can be implemented leads to a consistency relation between the renormalization group factors [21], which reads

$$Q|U_C^{(n_f)}(Q,\mu_0,\mu)|^2 U_J^{(n_f)}(Q\ell,\mu,\mu_0) = U_S^{(n_f)}(\ell,\mu_0,\mu). \quad (24)$$

It can also be written as a relation for the μ anomalous dimensions,

$$2\text{Re}[\gamma_C^{(n_f)}(Q,\mu)]\delta(\bar{\ell}) + Q\mu\gamma_J^{(n_f)}(Q\ell,\mu) = -\mu\gamma_S^{(n_f)}(\ell,\mu). \quad (25)$$

In the massive quark case, this consistency relation remains intact, since the UV divergences are mass independent. However, since the quark mass represents an additional relevant scale, the factorization theorem exhibits a richer structure due to the increased number of scales, and additional consistency relations emerge.

III. MASS MODE SETUP AND SUMMARY OF RESULTS

In this section, we briefly review the mass mode setup of Ref. [15], which is based on four different effective field theory scenarios associated with the hierarchies between the hard, jet, and soft scales and the quark mass. We also discuss the form of the resulting factorization theorems and present the final results for all mass-dependent perturbative corrections. The explicit calculations are described in detail in Sec. IV. An alternative conceptual (and likely more practical) view based only on a single effective theory below the hard scale, but with renormalization schemes for the different components of the factorization theorem that vary according to the relation between the hard, jet, and soft scales and the quark mass, is described in Sec. V.

For the discussion of the mass mode method we consider a generic setup with *one* massive quark flavor with mass m in addition to n_l massless flavors, and our notation is set up accordingly. It is convenient to define the ratio

$$\lambda_m = \frac{m}{Q}, \quad (26)$$

in addition to the regular power counting parameter $\lambda \sim \max\{\tau^{1/2}, (\Lambda_{\text{QCD}}/Q)^{1/2}\}$ that is already present in the purely massless setup. From the field theoretic point of view, we consider n-, $\bar{n}$-collinear, and soft mass modes. If kinematically allowed, these can have the momentum scaling and virtualities of their massless counterparts, but in addition one has to account for the fluctuations around their mass shell which have the scaling $p_n^\mu \sim Q(\lambda_m^2, 1, \lambda_m)$ and $p_{\bar{n}}^\mu \sim Q(1, \lambda_m^2, \lambda_m)$ for the n- and $\bar{n}$-collinear mass modes, respectively, and $p_s^\mu \sim Q(\lambda_m, \lambda_m, \lambda_m)$ for the soft mass modes. Since the typical invariant masses of the mass modes are bounded from below by $p_n^2 \sim p_{\bar{n}}^2 \sim p_s^2 \sim Q^2\lambda_m^2 \sim m^2$, dynamic real radiation effects can only occur if the typical collinear or soft scales are bigger than m^2. This means that depending on the relative sizes of λ_m and λ, collinear and soft mass mode fluctuations might not both contribute at the same time to the matrix elements, i.e., the jet and the soft functions, respectively. Since the hierarchy between the hard scale Q, the jet scale $Q\lambda$, and the soft scale $Q\lambda^2$ and their relation to the quark mass m can vary substantially, there are also different scenario-dependent threshold corrections when the RG evolution crosses the mass scale and the massive quark flavor is integrated out.[6]

Concerning Feynman rules, the collinear massive quark interactions are determined from a massive quark collinear

[6]Throughout this work, we adopt the convention that the effects of the massive quark flavor in the factorization theorems are integrated out globally at the scale $\mu_m \sim m$.

Lagrangian [28] which is a straightforward generalization of the massless collinear Lagrangian. In practice, since the collinear sector is essentially just a boosted version of usual QCD, the effects of the secondary massive quarks in the collinear sector can be calculated using regular QCD Feynman rules. We emphasize, however, that the consistency for calculations in the collinear sector with massive modes involves additional (nonvanishing) soft mass mode bin subtractions [29] in the collinear loop integrations to avoid double counting with the soft sector and to maintain collinear gauge invariance. As we have shown in Ref. [15], these soft mass mode bin subtractions are essential to obtain meaningful and gauge-invariant results. Concerning the interactions within the soft sector, the Feynman rules are anyway given by the usual QCD interactions and Feynman rules. This is sufficient for the treatment of the secondary soft massive quarks in this work.

Note that some of the notation, the formulation of the factorization theorems, and the organization of the RG evolution we use for the presentation of the results in this section are related to the choice that the final renormalization scale μ is set to be equal to the soft scale, $\mu = \mu_S$, such that the soft evolution factor $U_S(\ell, \mu_S, \mu_S) = \delta(\ell)$ and can be dropped. Thus, only the current and jet function RG evolution factors U_C and U_J, respectively, appear. The RG pattern of this "top-down" approach, together with a graphical display of how the collinear and soft massive modes give contributions, is illustrated in Fig. 4. Clearly, any other choice for μ is possible and can significantly affect the form as well as the interpretation of the various components of the factorization theorems in the different scenarios. Since the number of possibilities in connection with the different scenarios and the choices for μ in the factorization theorems proliferates strongly, we postpone a more general discussion to Sec. V, where we focus more on the RG properties of the hard coefficient and the jet and soft functions rather than on the full factorization theorem. This allows us to streamline the discussion significantly and to generalize our results to other processes.

A. Scenario I: $m > Q > Q\lambda > Q\lambda^2$

When the mass m is larger than the hard scale Q, the massive quark is not described in SCET but integrated out when SCET is matched to QCD. The factorization theorem is the one for n_l massless fermions in analogy to Eq. (2) up to the hard current matching coefficient, which acquires an additional contribution due to the heavy quark,

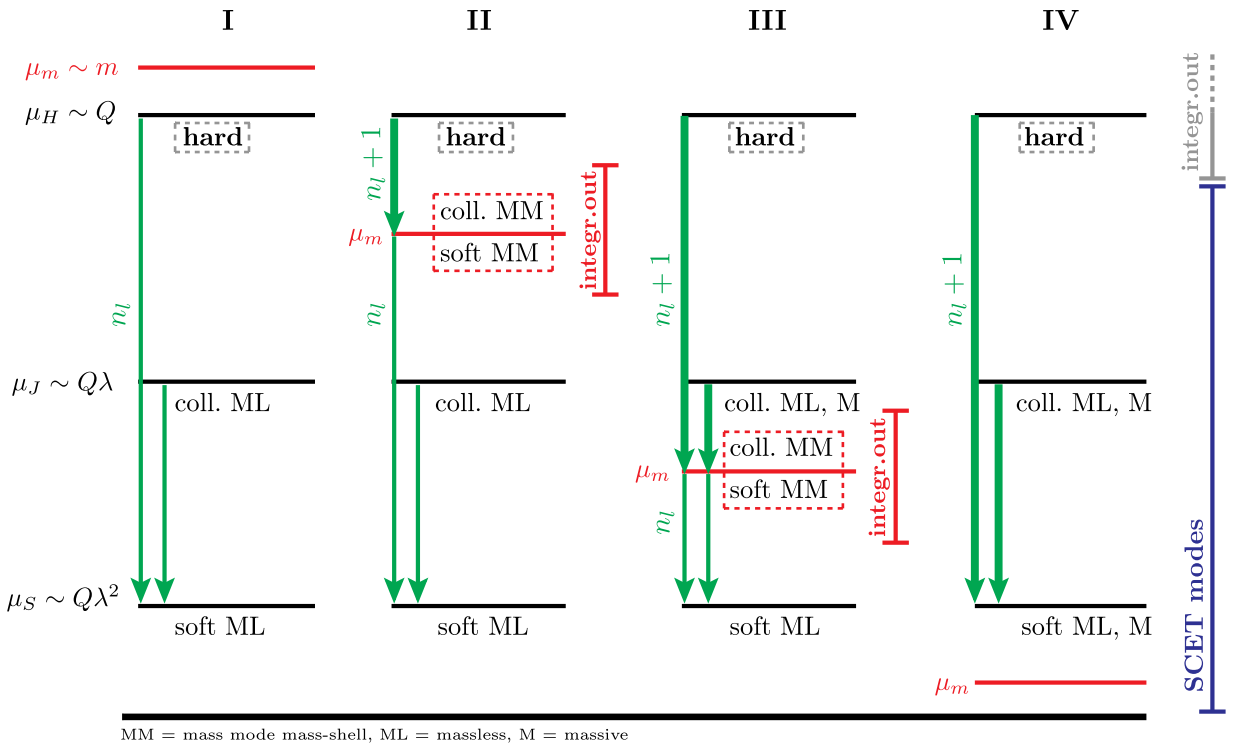

FIG. 4 (color online). The different scenarios depending on the hierarchy between the mass scale μ_m and the hard, jet, and ultrasoft scales. MM indicates mass shell scaling, and ML massless scaling. With M we denote modes that have a mass m but scale as their massless counterparts. The renormalization group evolution is also shown in the top-down evolution from the hard scale μ_H down to $\mu = \mu_S$. When the mass scale is crossed, the mass shell fluctuations are integrated out (dashed box). This leads to a matching condition and to a change in the evolution factor.

$$\frac{1}{\sigma_0}\frac{d\sigma}{d\tau} = Q|C^{(n_l)}(Q,m,\mu_H)|^2|U_C^{(n_l)}(Q,\mu_H,\mu_S)|^2 \times \int ds \int ds' J^{(n_l)}(s',\mu_J) U_J^{(n_l)}(s-s',\mu_S,\mu_J) \times S^{(n_l)}\left(Q\tau - \frac{s}{Q},\mu_S\right), \quad (27)$$

where

$$C^{(n_l)}(Q,m,\mu) = C^{(n_l)}(Q,\mu) + F_{\rm QCD}^{(n_l,2)}(Q,m). \quad (28)$$

The term $F_{\rm QCD}^{(n_l,2)}$ represents the massive quark bubble contribution to the QCD current form factor; see the diagram in Fig. 1(a). Scenario I is designed to show manifest decoupling in the infinite mass limit, i.e.,

$$C^{(n_l)}(Q,m\to\infty,\mu) \to C^{(n_l)}(Q,\mu). \quad (29)$$

This is achieved in $F_{\rm QCD}^{(n_l,2)}$ by two ingredients. First, the on-shell condition for the external quarks is related to a subtraction of the form factor at $Q^2=0$ concerning the virtual secondary massive quark effects. Second, the massive quark bubble contribution to the strong coupling constant is renormalized in the on-shell scheme rather than in $\overline{\rm MS}$.[7] So the massive quark is not an active dynamic flavor and does not contribute to the RG evolution of the strong coupling. One can derive the expression by first calculating the corresponding one-loop diagram with a massive gauge boson in Fig. 2(a) and then using the subtracted form of the dispersion relation according to Fig. 3. This yields[8] $[\alpha_s^{(n_l)} = \alpha_s^{(n_l)}(\mu)]$

$$F_{\rm QCD}^{(n_l,2)}(Q,m) \equiv F_{\rm QCD}^{(2,\rm OS)}(Q,m) = \frac{(\alpha_s^{(n_l)})^2 C_F T_F}{16\pi^2} f_{\rm QCD}^{(2)}(m/Q), \quad (30)$$

where the function $f_{\rm QCD}^{(2)}(x)$ is given by [30,31]

$$f_{\rm QCD}^{(2)}(x) = \left(\frac{46}{9}r^3 + \frac{10}{3}r\right)\left[{\rm Li}_2\left(\frac{r-1}{r+1}\right) - {\rm Li}_2\left(\frac{r+1}{r-1}\right)\right] + \left(-r^4+2r^2+\frac{5}{3}\right) \times \left[{\rm Li}_3\left(\frac{r-1}{r+1}\right) + {\rm Li}_3\left(\frac{r+1}{r-1}\right) - 2\zeta_3\right] + \left(\frac{110}{9}r^2 + \frac{200}{27}\right)\ln\left(\frac{1-r^2}{4}\right) + \frac{238}{9}r^2 + \frac{1213}{81}, \quad (31)$$

and we have defined

$$x^2 = \frac{m^2}{Q^2+i0}, \qquad r = \sqrt{1+4x^2}. \quad (32)$$

In the limit $m\to\infty$, the massive quark decouples indeed, i.e., $f_{\rm QCD}^{(2)}(x)\to 0$ for $x\to\infty$. For light fermions, i.e., $x\to 0$, we find

$$f_{\rm QCD}^{(2)}(x)|_{x\to 0} = \frac{4}{9}\ln^3(-x^2) + \frac{38}{9}\ln^2(-x^2) + \left(\frac{530}{27}+\frac{4\pi^2}{9}\right)\ln(-x^2) + \frac{3355}{81} + \frac{38\pi^2}{27} - \frac{16}{3}\zeta_3, \quad (33)$$

with subleading corrections going as $\mathcal{O}(x^2)$. Equation (33) does not bear any similarity to the massless result of Eq. (4) and further exhibits large unresummed mass logarithms. Thus, the QCD result of Eq. (30) is not suitable for taking the massless limit. This is because Eq. (30) still contains mass mode on-shell contributions which must be subtracted prior to taking the limit $m \ll Q$. This procedure is described in scenario II.

B. Scenario II: $Q > m > Q\lambda > Q\lambda^2$

The mass m is below the hard scale, but still above the jet and the soft scales. It is our aim (i) to resum the mass logarithms in Eq. (33) and (ii) to determine the hard current matching coefficient such that it contains no mass singularities and in particular approaches the massless limit for $m\to 0$. The collinear and soft mass modes are included into the SCET setup, so that they render the hard coefficient IR safe by subtracting the mass shell contributions in the matching procedure. They contribute as dynamic degrees of freedom to the RG evolution above m. In the RG evolution of the current from the hard to the jet scale, the mass shell fluctuations are finally integrated out at the scale m. The mass mode effects are purely virtual because the jet scale $Q\lambda$, the

[7]The massless quark bubble contributions are still renormalized in the $\overline{\rm MS}$ scheme as usual.

[8]Throughout the paper, we suppress the dependence on the renormalization scale μ in the arguments of terms which are just implicitly depending on the renormalization scale through α_s and the mass m.

typical invariant mass for real collinear particle radiation, is below m. Therefore, the jet and soft functions, as well as their RG evolution factors towards scales smaller than m, coincide with the ones for n_l massless quarks. The factorization theorem reads

$$\begin{aligned}\frac{1}{\sigma_0}\frac{\mathrm{d}\sigma}{\mathrm{d}\tau} &= Q|C^{(n_l+1)}(Q,m,\mu_H)|^2|U_C^{(n_l+1)}(Q,\mu_H,\mu_m)|^2 \\ &\times |\mathcal{M}_C(Q,m,\mu_m)|^2|U_C^{(n_l)}(Q,\mu_m,\mu_S)|^2 \\ &\times \int \mathrm{d}s \int \mathrm{d}s' J^{(n_l)}(s',\mu_J)U_J^{(n_l)}(s-s',\mu_S,\mu_J) \\ &\times S^{(n_l)}\left(Q\tau-\frac{s}{Q},\mu_S\right). \end{aligned} \tag{34}$$

Compared to $C^{(n_l)}(Q,m,\mu_H)$ in Eq. (28), the hard current coefficient $C^{(n_l+1)}(Q,m,\mu_H)$ acquires a subtractive contribution arising from the nonvanishing SCET diagrams involving virtual collinear and soft mass modes and contributions related to the use of the $\overline{\mathrm{MS}}$ renormalization prescription for the strong coupling rather than the OS one concerning the massive quark bubble. The latter correction means that the massive quark now contributes to the RG evolution, and that we employ $\alpha_s^{(n_l+1)}$. The result for $C^{(n_l+1)}(Q,m,\mu)$ reads

$$C^{(n_l+1)}(Q,m,\mu) = C^{(n_l+1)}(Q,\mu) + \delta F^{(n_l+1,2)}(Q,m). \tag{35}$$

The term $\delta F^{(n_l+1,2)}$ represents the corrections due to the nonvanishing mass of the heavy quark and can be written as $[\alpha_s^{(n_l+1)} = \alpha_s^{(n_l+1)}(\mu)]$

$$\begin{aligned}\delta F^{(n_l+1,2)}(Q,m) &= \frac{(\alpha_s^{(n_l+1)})^2 C_F T_F}{16\pi^2} \\ &\times [f_{\mathrm{QCD}}^{(2)}(m/Q) - f_{\mathrm{QCD}}^{(2)}(m/Q)|_{m\to 0}],\end{aligned} \tag{36}$$

which can be read off Eqs. (31) and (33). All calculational steps are explained in detail in Sec. IV B. One can check explicitly that all of the IR divergent mass shell contributions are removed and that the massless limit for Eq. (35) is recovered for $m \to 0$, i.e., $\delta F^{(n_l+1,2)}(Q,m) \xrightarrow{m\to 0} 0$. We note that in the results of the collinear, the soft, and the soft mass mode bin contributions, there are rapidity divergences that cancel in the sum of all terms. We stress, however, that for $\mu \sim Q$, no large (rapidity) logarithm remains in the hard current matching.

Note that the UV divergences of the bare SCET form factor are insensitive to the nonvanishing quark mass, such that we get in total the UV divergences from Eq. (5) for $n_f = n_l + 1$. This argument does not rely on a specific order in α_s, so the evolution factor $U_C^{(n_l+1)}$ obeys the RG equation

$$\mu\frac{\mathrm{d}}{\mathrm{d}\mu}U_C^{(n_l+1)}(Q,\mu_H,\mu) = \gamma_C^{(n_l+1)}(Q,\mu)U_C^{(n_l+1)}(Q,\mu_H,\mu) \tag{37}$$

to all orders in perturbative QCD for scales $\mu > \mu_m$.

At the scale μ_m, the mass shell fluctuations of the collinear and soft mass modes are integrated out. This leads to the current mass mode matching coefficient $\mathcal{M}_C(Q,m,\mu_m)$, which is the analogue of the well-known matching correction between the strong coupling schemes with n_l+1 and n_l running dynamic flavors $\alpha_s^{(n_l+1)}$ and $\alpha_s^{(n_l)}$, respectively. The result reads $[\alpha_s \ln(m^2/Q^2) \sim \mathcal{O}(1)]$

$$\begin{aligned}\mathcal{M}_C(Q,m,\mu_H,\mu_m) &= 1 + \left[\frac{(\alpha_s^{(n_l+1)})^2 C_F T_F}{(4\pi)^2}\ln\left(\frac{\mu_H^2}{\mu_m^2}\right)\left\{-\frac{4}{3}L_m^2 - \frac{40}{9}L_m - \frac{112}{27}\right\}\right]_{\mathcal{O}(\alpha_s)} \\ &+ \left[\frac{(\alpha_s^{(n_l+1)})^2 C_F T_F}{(4\pi)^2}\left\{\frac{4}{9}L_m^3 + \frac{38}{9}L_m^2 + \left(\frac{242}{27}+\frac{2\pi^2}{3}\right)L_m - \ln\left(-\frac{Q^2}{\mu_H^2}\right)\left\{\frac{4}{3}L_m^2 + \frac{40}{9}L_m + \frac{112}{27}\right\}\right.\right. \\ &\left.\left. + \frac{875}{54} + \frac{5\pi^2}{9} - \frac{52}{9}\zeta_3\right\} + \frac{(\alpha_s^{(n_l+1)})^3 C_F T_F}{(4\pi)^3}\ln\left(\frac{\mu_H^2}{\mu_m^2}\right)\left\{L_m^3\left[\frac{88}{27}C_A - \frac{64}{27}T_F - \frac{32}{27}T_F n_l\right]\right. \\ &+ L_m^2\left[\left(-\frac{92}{9}+\frac{8}{9}\pi^2\right)C_A + 12C_F - \frac{160}{27}T_F\right] + L_m\left[\left(-\frac{620}{81}+\frac{80\pi^2}{27}-\frac{112}{3}\zeta_3\right)C_A\right. \\ &\left.\left. + \left(-\frac{4}{3}+32\zeta_3\right)C_F - \frac{1088}{81}T_F n_l - \frac{992}{81}T_F\right] - \frac{\mathcal{M}_3^{C,+}}{C_F T_F}\right\} \\ &+ \left.\frac{(\alpha_s^{(n_l+1)})^4 C_F^2 T_F^2}{(4\pi)^4}\ln^2\left(\frac{\mu_H^2}{\mu_m^2}\right)\left\{\frac{8}{9}L_m^4 + \frac{160}{27}L_m^3 + \frac{416}{27}L_m^2 + \frac{4480}{243}L_m + \frac{6272}{729}\right\}\right]_{\mathcal{O}(\alpha_s^2)},\end{aligned} \tag{38}$$

where $Q^2 = Q^2 + i0$, $L_m \equiv \ln(m^2/\mu_m^2)$ and $\alpha_s^{(n_l+1)} = \alpha_s^{(n_l+1)}(\mu_m)$. The quark mass $m \equiv \bar{m}(\mu_m)$ is given in the $\overline{\text{MS}}$ scheme. We see that the result contains large logarithms $\ln(\mu_m^2/\mu_H^2)$, which are not summed by the RG μ evolution of the current. These logarithms are related to rapidity singularities that arise in the overlap region between the collinear and soft mass modes, all having invariant masses of order m^2. Analogous logarithmic terms were also found for the $\mathcal{O}(\alpha_s)$ massive gluon results discussed in Ref. [15]. There are several approaches to resum these rapidity logarithms [32–34], but the outcome is just a simple exponentiation which yields the term at $\mathcal{O}(\alpha_s^4 \ln^2(m^2/Q^2))$ in Eq. (38). We refer to Ref. [35] for a calculation of the anomalous dimension in rapidity space. We note that through the rapidity RG evolution, $\mathcal{M}_C$ depends at each order on two rapidity scales. For simplicity we correlate them with the two invariant mass scales μ_H and μ_m. We stress, however, that the dependence of $\mathcal{M}_C$ on the hard matching scale μ_H is actually spurious and cancels in an expansion at fixed order in α_s. The existence of the large logarithms has the important consequence that the $\mathcal{O}(\alpha_s^2 \ln(m^2/Q^2))$ corrections in Eq. (38) enter at the same order as the $\mathcal{O}(\alpha_s)$ fixed-order corrections based on the counting $\alpha_s \ln(m^2/Q^2) \sim \mathcal{O}(1)$, and thus contribute already at N^{2}LL order where one-loop fixed-order corrections to the hard coefficient and the jet and the soft function are accounted for. At N^{3}LL order, we therefore need the terms at $\mathcal{O}(\alpha_s^3 \ln(m^2/Q^2))$ and $\mathcal{O}(\alpha_s^4 \ln^2(m^2/Q^2))$.[9] We have indicated this counting by using the subscripts "$\mathcal{O}(\alpha_s)$" and "$\mathcal{O}(\alpha_s^2)$" in the result of Eq. (38). From the $\mathcal{O}(\alpha_s^3 \ln(m^2/Q^2))$ terms, the contributions explicitly depending on μ_m can be inferred using the μ_m independence of the factorization theorem and the explicit form of the current evolution factors $U_C^{(n_l+1)}$ and $U_C^{(n_l)}$. In Eq. (38), the full form of the $\mathcal{O}(\alpha_s^3 \ln(m^2/Q^2))$ term is displayed with the constant $\mathcal{M}_3^{C,+}$, which cannot be determined from RG arguments. This constant corresponds to a rapidity logarithm that is physically unrelated to logarithms of μ_m. Details of these computations can be found in Sec. V A.

C. Scenario III: $Q > Q\lambda > m > Q\lambda^2$

The mass is between the jet and the soft scales. The current evolution is the same as the one in scenario II, and the soft function still includes only the effects of the n_l massless quarks. Since the massless as well as the massive collinear modes both can now fluctuate in the collinear sector, the difference from scenario II concerns the jet function, where additional massive real and virtual contributions arise. The setup is constructed such that it (i) sums all mass logarithms that arise in the evolution of the jet function and (ii) ensures that the jet function approaches the known massless result for $n_l + 1$ flavors in the limit $m \to 0$. In analogy to the current, the RG evolution of the jet function is performed with $n_l + 1$ flavors above the mass threshold. Collinear mass shell fluctuations are integrated out at the mass scale, yielding a collinear mass mode matching coefficient $\mathcal{M}_J$, and the evolution continues with n_l light quarks down to the soft scale. Overall, the factorization theorem in this scenario has the form

$$\begin{aligned}\frac{1}{\sigma_0}\frac{\mathrm{d}\sigma}{\mathrm{d}\tau} &= Q|C^{(n_l+1)}(Q,m,\mu_H)|^2|U_C^{(n_l+1)}(Q,\mu_H,\mu_m)|^2 \\ &\quad\times|\mathcal{M}_C(Q,m,\mu_m)|^2|U_C^{(n_l)}(Q,\mu_m,\mu_S)|^2 \\ &\quad\times\int \mathrm{d}s\int \mathrm{d}s'\int \mathrm{d}s''\int \mathrm{d}s''' J^{(n_l+1)}(s''',m,\mu_J) \\ &\quad\times U_J^{(n_l+1)}(s''-s''',\mu_m,\mu_J)\mathcal{M}_J(s'-s'',m,\mu_m) \\ &\quad\times U_J^{(n_l)}(s-s',\mu_S,\mu_m)S^{(n_l)}\left(Q\tau-\frac{s}{Q},\mu_S\right), \end{aligned} \tag{39}$$

where the matching coefficients $C^{(n_l+1)}(Q,m,\mu_H)$ and $\mathcal{M}_C(Q,m,\mu_m)$ are the same as in scenario II; see Eqs. (35) and (38). The jet function $J^{(n_l+1)}(s,m,\mu)$ contains contributions related to virtual and real radiation of the massive secondary quarks and has the form

$$\begin{aligned}J^{(n_l+1)}(s,m,\mu) &= J^{(n_l+1)}(s,\mu) + \delta J_m^{\text{dist}}(s,m,\mu) \\ &\quad + \delta J_m^{\text{real}}(s,m),\end{aligned} \tag{40}$$

where the two latter terms represent corrections due to the quark mass. The computation is described in Sec. IV C. The expression for $\delta J_m^{\text{dist}}(s,m,\mu)$ contains only distributions and corresponds to collinear massive virtual corrections (including soft-bin subtractions), as well as terms related to the subtraction of the massless quark result contained in $J^{(n_l+1)}(s,\mu)$ [see Eq. (6)]. Its renormalized expression reads [$\bar{s} = s/\mu^2, \alpha_s^{(n_l+1)} = \alpha_s^{(n_l+1)}(\mu)$]

$$\begin{aligned}\mu^2\delta J_m^{\text{dist}}(s,m,\mu) &= \frac{(\alpha_s^{(n_l+1)})^2 C_F T_F}{16\pi^2}\Bigg\{\Bigg[\frac{16}{9}L_m^3+\frac{116}{9}L_m^2 \\ &\quad+\left(\frac{1436}{27}-\frac{16\pi^2}{9}\right)L_m+\frac{8650}{81}-\frac{116\pi^2}{27} \\ &\quad-\frac{64}{3}\zeta_3\Bigg]\delta(\bar{s})+\left(-\frac{16}{3}L_m^2-\frac{232}{9}L_m-\frac{1436}{27}\right. \\ &\quad\left.+\frac{16\pi^2}{9}\right)\left[\frac{\theta(\bar{s})}{\bar{s}}\right]_+ +\left(\frac{32}{3}L_m+\frac{232}{9}\right) \\ &\quad\times\left[\frac{\theta(\bar{s})\ln\bar{s}}{\bar{s}}\right]_+ -\frac{16}{3}\left[\frac{\theta(\bar{s})\ln^2\bar{s}}{\bar{s}}\right]_+\Bigg\}.\end{aligned} \tag{41}$$

[9] In the primed counting, one might still need to distinguish between terms enhanced by rapidity logarithms (and related to terms summed by the rapidity RGE) and the remaining terms in the series for the mass mode threshold factors.

The term $\delta J_m^{\rm real}(s,m)$ in Eq. (40) contributes only when the jet invariant mass is above the threshold $4m^2$ and thus corresponds to real production of the massive quarks. It is given by

$$\begin{aligned}\mu^2\delta J_m^{\rm real}(s,m) = {}& \frac{(\alpha_s^{(n_l+1)})^2 C_F T_F}{16\pi^2}\frac{1}{\bar{s}}\theta(s-4m^2)\\ &\times\left\{-\frac{64}{3}\mathrm{Li}_2\left(\frac{b-1}{b+1}\right)+\frac{32}{3}\ln\left(\frac{1-b^2}{4}\right)\right.\\ &\times\ln\left(\frac{1-b}{1+b}\right)-\frac{16}{3}\ln^2\left(\frac{1-b}{1+b}\right)\\ &+\left(b^4-2b^2+\frac{241}{9}\right)\ln\left(\frac{1-b}{1+b}\right)\\ &\left.-\frac{10}{27}b^3+\frac{482}{9}b-\frac{16\pi^2}{9}\right\},\end{aligned} \tag{42}$$

with

$$b=\sqrt{1-\frac{4m^2}{s}}. \tag{43}$$

Due to its physical character, it is UV finite and does not contain any explicit logarithmic μ dependence. Furthermore, $\delta J_m^{\rm real}$ and its first two derivatives in s vanish at the threshold, so that no discontinuity arises due to real radiation. Note that the range in τ where scenario III is employed may be chosen such that it fully includes the domain for collinear massive real radiation, namely $\tau \geq 4m^2/Q^2$, so that the threshold is properly accounted for through the analytic form of $\delta J_m^{\rm real}(s,m,\mu_m)$. For $m\to 0$, the jet function $J^{(n_l+1)}(s,m,\mu)$ yields correctly the fully massless jet function at $\mathcal{O}(\alpha_s^2)$, i.e.,

$$J^{(n_l+1)}(s,m,\mu)\xrightarrow{m\to 0}J^{(n_l+1)}(s,\mu). \tag{44}$$

We note that in the calculation of $\delta J_m^{\rm dist}$, rapidity divergences arise which cancel in the sum of the collinear diagrams and the corresponding soft-bin subtractions. We stress that for $\mu^2\sim s$, all associated logarithms cancel completely in the sum of $\delta J_m^{\rm real}$ and $\delta J_m^{\rm dist}$, so that no (large) rapidity logarithm remains in the jet function.

The UV divergences of the bare jet function $J_{\rm bare}^{(n_l+1)}(s,m,\mu)$ are mass independent and agree with the known massless ones for n_l+1 dynamic flavors. The $\mathcal{O}(\alpha_s^2 C_F T_F)$ contributions to the jet function counterterm are the ones from Eq. (7) for $n_f=n_l+1$. This statement holds to any order in α_s, so that the jet function evolution factor $U_J^{(n_l+1)}$ obeys

$$\begin{aligned}&\mu\frac{\mathrm{d}}{\mathrm{d}\mu}U_J^{(n_l+1)}(s,\mu,\mu_J)\\ &\quad=\int \mathrm{d}s'\gamma_J^{(n_l+1)}(s-s',\mu)U_J^{(n_l+1)}(s',\mu,\mu_J).\end{aligned} \tag{45}$$

At the scale μ_m, the mass shell fluctuations of the collinear mass modes are integrated out. These contributions are encoded in the jet mass mode matching coefficient $\mathcal{M}_J(s,m,\mu_m)$ and contain all virtual effects of the massive flavor such that for the scales $\mu<\mu_m$ massive collinear effects decouple. The result up to $\mathcal{O}(\alpha_s^2)$ reads

$$\begin{aligned}\mu_J^2\mathcal{M}_J^{(2)}(s,m,\mu_J,\mu_m) = {}& \delta(\tilde{s})+\left[\frac{(\alpha_s^{(n_l+1)})^2 C_F T_F}{(4\pi)^2}\delta(\tilde{s})\ln\left(\frac{\mu_J^2}{\mu_m^2}\right)\left(\frac{16}{3}L_m^2+\frac{160}{9}L_m+\frac{448}{27}\right)\right]_{\mathcal{O}(\alpha_s)}\\ &+\left[\frac{(\alpha_s^{(n_l+1)})^2 C_F T_F}{(4\pi)^2}\left\{\left[-\frac{16}{9}L_m^3-\frac{116}{9}L_m^2+\left(-\frac{932}{27}-\frac{8\pi^2}{9}\right)L_m-\frac{1531}{27}-\frac{20\pi^2}{27}+\frac{160}{9}\zeta_3\right]\delta(\tilde{s})\right.\right.\\ &\left.+\left[\frac{16}{3}L_m^2+\frac{160}{9}L_m+\frac{448}{27}\right]\left[\frac{\theta(\tilde{s})}{\tilde{s}}\right]_+\right\}+\frac{(\alpha_s^{(n_l+1)})^3 C_F T_F}{(4\pi)^3}\delta(\tilde{s})\\ &\times\ln\left(\frac{\mu_J^2}{\mu_m^2}\right)\left\{L_m^3\left[-\frac{352}{27}C_A+\frac{256}{27}T_F+\frac{128}{27}T_F n_l\right]+L_m^2\left[\left(\frac{368}{9}-\frac{32\pi^2}{9}\right)C_A-48C_F+\frac{640}{27}T_F\right]\right.\\ &\left.+L_m\left[\left(\frac{448}{3}\zeta_3+\frac{2480}{81}-\frac{320\pi^2}{27}\right)C_A+\left(\frac{16}{3}-128\zeta_3\right)C_F+\frac{4352}{81}T_F n_l+\frac{3968}{81}T_F\right]+\frac{\mathcal{M}_3^{J,+}}{C_F T_F}\right\}\\ &+\frac{(\alpha_s^{(n_l+1)})^4 C_F^2 T_F^2}{(4\pi)^4}\delta(\tilde{s})\ln^2\left(\frac{\mu_J^2}{\mu_m^2}\right)\left(\frac{128}{9}L_m^4+\frac{2560}{27}L_m^3+\frac{6656}{27}L_m^2+\frac{71680}{243}L_m+\frac{100352}{729}\right)\Bigg]_{\mathcal{O}(\alpha_s^2)},\end{aligned} \tag{46}$$

where $\tilde{s}\equiv s/\mu_J^2$, $L_m\equiv\ln(m^2/\mu_m^2)$, and $\alpha_s^{(n_l+1)}=\alpha_s^{(n_l+1)}(\mu_m)$. The quark mass $m=\bar{m}(\mu_m)$ is given in the $\overline{\rm MS}$ scheme. It is interesting to note that the result is a nontrivial distributive function of the jet invariant mass s and thus differs substantially from the local mass mode matching coefficient of the current [see Eq. (38)] or the strong coupling, which do not depend explicitly on any kinematic scale. As for the case of the current mass mode

matching coefficient, $\mathcal{M}_J$ contains large logarithms involving the ratio of the jet scale $s \sim \mu_J$ and the mass scale $m \sim \mu_m$, which are not summed by the RG μ evolution of the jet function. They are related to rapidity-type singularities that arise in the massive virtual corrections in the overlap region between the collinear mass mode contributions and their soft-bin subtractions. These logarithms exponentiate as in the case for the current mass mode matching coefficient. We note that, through the rapidity RG evolution, $\mathcal{M}_J$ depends at each order on two rapidity scales, which we correlate to the jet and the mass scales μ_J and μ_m, respectively. We stress, however, that the dependence of $\mathcal{M}_J$ on the jet scale μ_J cancels in a fixed-order expansion. Using the counting $\alpha_s \ln(m^2/s) \sim \mathcal{O}(1)$ concerning rapidity logarithms, the $\mathcal{O}(\alpha_s^2 \ln(m^2/s))$ corrections in Eq. (46) are counted as $\mathcal{O}(\alpha_s)$, while at $\mathcal{O}(\alpha_s^2)$ one has to include the terms of $\mathcal{O}(\alpha_s^4 \ln^2(m^2/s))$ and $\mathcal{O}(\alpha_s^3 \ln(m^2/s))$. From the latter terms, the contributions explicitly depending on μ_m can be inferred using the μ_m independence of the factorization theorem and the explicit form of the jet function evolution factors $U_J^{(n_l+1)}$ and $U_J^{(n_l)}$. In Eq. (46) we have displayed all terms that are counted as $\mathcal{O}(\alpha_s)$ and $\mathcal{O}(\alpha_s^2)$, as well as the constant $\mathcal{M}_3^{J,+}$, which is not constrained by RG arguments. The computations are described in detail in Sec. V B.

D. Scenario IV: $Q > Q\lambda > Q\lambda^2 > m$

The mass is below the ultrasoft scale. There is no separation between the collinear and soft mass modes and the corresponding collinear and soft massless modes, since the RG evolution following the top-down approach of Fig. 4 never crosses the massive quark threshold, and all evolution is carried out for $n_l + 1$ active dynamic flavors. So, compared to scenario III, there are no mass mode matching coefficients, and the soft function accounts for the secondary massive contributions. The factorization theorem reads

$$\frac{1}{\sigma_0}\frac{d\sigma}{d\tau} = Q|C^{(n_l+1)}(Q,m,\mu_H)|^2 |U_C^{(n_l+1)}(Q,\mu_H,\mu_S)|^2 \times \int ds \int ds' U_J^{(n_l+1)}(s-s',\mu_S,\mu_J) J^{(n_l+1)}(s',m,\mu_J) \times S^{(n_l+1)}\left(Q\tau - \frac{s}{Q}, m, \mu_S\right), \quad (47)$$

where the hard current matching coefficient $C^{(n_l+1)}(Q,m,\mu_H)$ is the same as in scenarios II and III, see Eq. (35), and the jet function $J^{(n_l+1)}(s,m,\mu_J)$ is the same as in scenario III, see Eq. (40). The soft function $S^{(n_l+1)}(\ell,m,\mu_S)$ contains virtual as well as real radiation contributions related to the massive quark. The partonic contribution can be written as

$$\hat{S}^{(n_l+1)}(\ell,m,\mu) = \hat{S}^{(n_l+1)}(\ell,\mu) + \delta S_m^{\rm dist}(\ell,m,\mu) + \delta S_m^{{\rm real},\theta}(\ell,m) + \delta S_m^{{\rm real},\Delta}(\ell,m), \quad (48)$$

where $\hat{S}^{(n_l+1)}(\ell,\mu)$ is the partonic soft function for n_l+1 massless quark flavors. The other terms represent the $\mathcal{O}(\alpha_s^2 C_F T_F)$ corrections due to the nonzero quark mass and were computed in Ref. [16]. For the convenience of the reader, we briefly review these results in the following.

The expression for $\delta S_m^{\rm dist}$ contains only distributions and corresponds to virtual massive quark radiation as well as to the terms related to the subtractions of the massless quark result [see Eq. (8)] to avoid double counting with the full massless result in the first term of Eq. (48). The renormalized expression reads [$\bar{\ell} = \ell/\mu$, $\alpha_s^{(n_l+1)} = \alpha_s^{(n_l+1)}(\mu)$]

$$\mu\delta S_m^{\rm dist}(\ell,m,\mu) = \frac{(\alpha_s^{(n_l+1)})^2 C_F T_F}{16\pi^2}\left\{\left[-\frac{8}{9}L_m^3 - \frac{40}{9}L_m^2 + \left(-\frac{448}{27}+\frac{8\pi^2}{9}\right)L_m - \frac{2048}{81} - \frac{64\pi^2}{27} + 32\zeta_3\right]\delta(\bar{\ell}) + \left(\frac{16}{3}L_m^2 + \frac{160}{9}L_m + \frac{896}{27} - \frac{16\pi^2}{9}\right)\left[\frac{\theta(\bar{\ell})}{\bar{\ell}}\right]_+ - \left(\frac{64}{3}L_m + \frac{320}{9}\right)\left[\frac{\theta(\bar{\ell})\ln\bar{\ell}}{\bar{\ell}}\right]_+ + \frac{64}{3}\left[\frac{\theta(\bar{\ell})\ln^2\bar{\ell}}{\bar{\ell}}\right]_+\right\}. \quad (49)$$

The term $\delta S_m^{{\rm real},\theta}$ describes real massive quark radiation for the prescription that the coherent sum of the massive quark and antiquark momentum (i.e., the virtual gluon momentum) enters the thrust definition.[10] It contains a threshold at $\ell = 2m$ and reads

$$\mu\delta S_m^{{\rm real},\theta}(\ell,m) = \frac{(\alpha_s^{(n_l+1)})^2 C_F T_F}{16\pi^2}\theta(\ell-2m)\frac{1}{\bar{\ell}}\left\{\frac{64}{3}{\rm Li}_2\left(\frac{w-1}{w+1}\right) - \frac{32}{3}\ln\left(\frac{1-w^2}{4}\right)\ln\left(\frac{1-w}{1+w}\right) + \frac{16}{3}\ln^2\left(\frac{1-w}{1+w}\right) - \frac{160}{9}\ln\left(\frac{1-w}{1+w}\right) + \frac{64}{27}w^3 - \frac{320}{9}w + \frac{16\pi^2}{9}\right\}, \quad (50)$$

[10]It was demonstrated in Ref. [16] that this prescription can be easily calculated analytically and agrees with the regular thrust prescription except when the quark and antiquark enter different hemispheres.

with

$$w = \sqrt{1 - \frac{4m^2}{\ell^2}}. \tag{51}$$

$\delta S_m^{\mathrm{real},\theta}$ and its first two derivatives in ℓ vanish at the threshold, so that no discontinuity arises due to real radiation. Since the momenta of the quark and antiquark enter the thrust prescription as different respective projections on one of the two light-cone axes, if they enter different hemispheres, $\delta S_m^{\mathrm{real},\theta}$ does not represent the complete real radiation contribution. For the part of the phase space where the massive quark and antiquark go into opposite hemispheres, one has to account for the additional, numerically small *hemisphere mismatch contribution* $\delta S_m^{\mathrm{real},\Delta}$ that has also been computed in Ref. [16]. This correction does not have a threshold and is nonvanishing for all positive thrust momenta ℓ. In the massless limit, $\delta S_m^{\mathrm{real},\Delta}$ approaches a δ distribution. In Ref. [16], a parametrization for $\delta S_m^{\mathrm{real},\Delta}$ was given that approximates this contribution up to better than 2% relative accuracy:

$$\delta S_m^{\mathrm{real},\Delta}(xm,m)|_{\mathrm{fit}} = \frac{(\alpha_s^{(n_l+1)})^2 C_F T_F}{16\pi^2} \frac{1}{m} \frac{x^5[a\ln^2(1+x^2) + b\ln(1+x^2) + c]}{dx^8 + ex^7 + fx^6 + gx^4 + hx^3 + jx^2 + 1}, \tag{52}$$

with $a = 8d$, $b = -80d$, $c = 8/15$, and $d = 6/(2400 + 360\pi + 73\pi^2)$ being fixed from imposing the correct asymptotic behavior for $m \gg \ell$ and $m \ll \ell$. The remaining five parameters were obtained using a fit with the constraint of satisfying the correct normalization corresponding to the massless analytic limit:

$$e = 0.0117, \qquad f = 0.100, \qquad g = -0.502,$$
$$h = 0.747, \qquad j = -0.180. \tag{53}$$

Note that both real radiation contributions are UV finite. For $m \to 0$, the soft function $\hat{S}^{(n_l+1)}(\ell, m, \mu)$ yields correctly the fully massless partonic soft function at $\mathcal{O}(\alpha_s^2)$, i.e.,

$$\hat{S}^{(n_l+1)}(\ell, m, \mu) \xrightarrow{m\to 0} \hat{S}^{(n_l+1)}(s, \mu). \tag{54}$$

We note that in the calculation of $\delta S_m^{\mathrm{dist}}$, rapidity divergences arise in the contributions coming from the different hemispheres which cancel in the sum of the terms. We stress, however, that for $\mu \sim \ell$, all associated logarithmic mass singularities cancel in the sum of $\delta S_m^{\mathrm{real},\theta}$ and $\delta S_m^{\mathrm{dist}}$, so that no (large) rapidity logarithm remains in the soft function.

The UV divergences of the bare soft function $\hat{S}_{\mathrm{bare}}^{(n_l+1)}(\ell, m, \mu)$ are mass independent and agree with the known massless ones for $n_l + 1$ dynamic flavors in Eq. (9) with the replacement $n_f = n_l + 1$. The evolution factor $U_S^{(n_l+1)}$ obeys

$$\mu \frac{\mathrm{d}}{\mathrm{d}\mu} U_S^{(n_l+1)}(\ell, \mu, \mu_S) = \int \mathrm{d}\ell' \gamma_S^{(n_l+1)}(\ell - \ell', \mu) U_S^{(n_l+1)}(\ell', \mu, \mu_S), \tag{55}$$

which holds to any order in the strong coupling.

E. Gap subtraction, evolution and matching

In scenarios I to III, the quark mass is above the soft scale, and therefore the massive quark does not affect the soft function. Thus, the gap subtraction agrees with the one from the factorization theorem for $n_f = n_l$ massless quarks as described in Sec. II. In scenario IV, for $m > \Lambda_{\mathrm{QCD}}$, the finite quark mass provides an infrared cutoff for the virtuality of the exchanged gluon in the partonic soft function such that the factorial growth of the coefficients related to the massive flavor at large orders in perturbation theory is suppressed and, in principle, a corresponding subtraction in the gap series $\delta(R, \mu)$ might be unnecessary. However, implementing the gap scheme along the lines of Eqs. (10) and (11) including the effects of the secondary massive quarks is useful in order to have a smooth interpolation of the gap scheme parameters to the massless quark limit. Since the resulting subtraction series $\delta^{(n_l+1)}(R, m, \mu)$ encodes infrared-sensitive perturbative contributions, it now becomes mass dependent. Thus, the complete soft function in scenario IV reads

$$S^{(n_l+1)}(\ell, m, \mu) = \int \mathrm{d}\ell' \hat{S}^{(n_l+1)}(\ell - \ell' - 2\delta^{(n_l+1)}(R, m, \mu), m, \mu) \times F(\ell' - 2\bar{\Delta}^{(n_l+1)}(R, m, \mu)). \tag{56}$$

The renormalon subtractions $\delta^{(n_l+1)}(R, m, \mu)$ can be written as

$$\delta^{(n_l+1)}(R, m, \mu) = \delta^{(n_l+1)}(R, \mu) + \delta_m(R, m), \tag{57}$$

where $\delta^{(n_l+1)}(R, \mu)$ is the series for $n_l + 1$ massless quark flavors and $\delta_m(R, m)$ represents the correction to the massless result due to the finite quark mass. In Ref. [16], the $\mathcal{O}(\alpha_s^2 C_F T_F)$ correction to $\delta_m(R, m)$ was calculated

according to Eq. (11), and the result can be parametrized by[11] $[\alpha_s^{(n_l+1)} = \alpha_s^{(n_l+1)}(\mu)]$

$$\delta_m(R, yR) = \frac{(\alpha_s^{(n_l+1)})^2 C_F T_F}{16\pi^2} R e^{\gamma_E} \tilde{g}(y), \tag{58}$$

$$\tilde{g}(y) = \tilde{h}(y) - \frac{\tilde{h}(y) + ay}{1 + by + cy^2} e^{-\alpha y^\beta}, \tag{59}$$

where

$$\alpha = 0.634, \qquad \beta = 1.035, \qquad a = 23.6,$$
$$b = -0.481, \qquad c = 1.19, \tag{60}$$

and

$$\tilde{h}(y) = -\frac{8}{3}\ln^2 y^2 - \frac{80}{9}\ln y^2 - \frac{448}{27} - \frac{8\pi^2}{9}. \tag{61}$$

The expression in Eq. (58) provides an approximation that is much better than 1% and that is constructed such that the massless limit in Eq. (57) is recovered for $m \to 0$, i.e., $\delta_m(R, m) \xrightarrow{m\to 0} 0$. Moreover, for $m/R \to \infty$, the parametrization yields the correct limit,

$$\delta_m(R, yR) \xrightarrow{y\to\infty} \frac{(\alpha_s^{(n_l+1)})^2 C_F T_F}{16\pi^2} R e^{\gamma_E} \tilde{h}(y). \tag{62}$$

The μ evolution of the gap parameter $\bar{\Delta}^{(n_l+1)}(R, m, \mu)$ is mass independent and thus the same as for the massless gap parameter as given in Eq. (15) with the replacement $n_f = n_l + 1$. With the quark-mass-dependent gap subtraction at $\mathcal{O}(\alpha_s^2 C_F T_F)$, however, the gap evolution in R becomes mass dependent, and one can determine the R-evolution equation directly from Eq. (57) using Eq. (14). The R anomalous dimension can then be written as $[\alpha_s^{(n_l+1)} = \alpha_s^{(n_l+1)}(R)]$

$$\gamma_R^{(n_l+1)}(m/R) = \gamma_R^{(n_l+1)} + \gamma_{R,m}(m/R), \tag{63}$$

$$\gamma_{R,m}(y) = \frac{(\alpha_s^{(n_l+1)})^2 C_F T_F}{16\pi^2} e^{\gamma_E} \left[1 - y\frac{\mathrm{d}}{\mathrm{d}y}\right] \tilde{g}(y), \tag{64}$$

where $\gamma_R^{(n_l+1)}$ denotes the R anomalous dimension with $n_l + 1$ massless quarks. Using the parametrization of Eq. (58), the result for the $\mathcal{O}(\alpha_s^2 C_F T_F)$ massive quark correction $\gamma_{R,m}(m/R)$ can be easily computed. It approximates the exact result within 2% (except for $m/R < 0.1$, where the correction is anyway tiny) and yields the correct massless limit in Eq. (63) for $m \to 0$, i.e., $\gamma_{R,m}(m/R) \xrightarrow{m\to 0} 0$. The explicit solution for the μ and R evolution for $\bar{\Delta}$ with massless quarks can be found in Eq. (41) of Ref. [17]. The quark mass just modifies the R-evolution terms of that solution. It affects the function $D^{(k)}(\alpha_s(R_1), \alpha_s(R_0))$, defined for massless quarks in Eq. (A31) of Ref. [17], where R_0 (R_1) is the initial (final) scale of the R evolution. Mass effects start contributing at N^{2}LL order and modify $D^{(2)}(\alpha_s(R_1), \alpha_s(R_0))$ in the following way:

$$\begin{aligned} D^{(2)}&(\alpha_s(R_1), \alpha_s(R_0), m) \\ &= D^{(2)}(\alpha_s(R_1), \alpha_s(R_0), m = 0) \\ &\quad + \frac{1}{4\beta_0^2}\int_{t_0}^{t_1} \mathrm{d}t e^{-t}(-t)^{-2-\frac{\beta_1}{2\beta_0^2}} \tilde{\gamma}_{R,m}\left(\frac{m e^{G(t)}}{\Lambda^{(2)}_{\mathrm{QCD}}}\right), \end{aligned} \tag{65}$$

with $t_i = -2\pi/(\alpha_s(R_i)\beta_0)$ and β_i being the coefficients of the perturbative expansion of the β function as defined in Eq. (109) and $\gamma_{R,m}(m/R) = \alpha_s^2/(16\pi^2)\tilde{\gamma}_{R,m}(m/R)$. Here the strong coupling α_s is understood to be in the $(n_\ell + 1)$-flavor scheme. The function $G(t)$ is given by

$$G(t) = t + \frac{\beta_1}{2\beta_0^2}\ln(-t) - \frac{\beta_1^2 - \beta_0\beta_2}{4\beta_0^4}\frac{1}{t}. \tag{66}$$

Eq. (65) can be obtained following the changes of variables as explained in Ref. [26]. A generalization to higher orders is straightforward.

To complete the discussion on the evolution of the gap parameter, we have to consider the matching relation between $\bar{\Delta}^{(n_l+1)}(R, m, \mu)$ for $R, \mu > \mu_m \sim m$, where the massive quark is an active dynamic flavor, and $\bar{\Delta}^{(n_l)}(R, \mu)$ for $R, \mu < \mu_m \sim m$, where the massive quark is integrated out. The matching relation is most easily derived using the fact that the "bare" gap parameter is scheme independent, very much like the massive quark pole mass. This gives the relation

$$\begin{aligned} \Delta &= \bar{\Delta}^{(n_l)}(R, \mu) + \delta^{(n_l)}(R, \mu) \\ &= \bar{\Delta}^{(n_l+1)}(R, m, \mu) + \delta^{(n_l+1)}(R, m, \mu), \end{aligned} \tag{67}$$

and we thus obtain $[L_m = \ln(m^2/\mu^2)]$

$$\begin{aligned} \bar{\Delta}^{(n_l)}(R, \mu) &= \bar{\Delta}^{(n_l+1)}(R, m, \mu) + \delta^{(n_l+1,2)}_{n_f=1}(R, \mu) \\ &\quad + \delta_m(R, m) - \frac{\alpha_s^{(n_l+1)} T_F}{3\pi} L_m \delta^{(n_l+1,1)}(R, \mu) \end{aligned} \tag{68}$$

with the one-loop gap subtraction

$$\delta^{(n_l+1,1)}(R, \mu) = \frac{\alpha_s^{(n_l+1)} C_F}{4\pi} R e^{\gamma_E} \left[-4\ln\left(\frac{\mu^2}{R^2}\right)\right]. \tag{69}$$

The latter term arises from the matching relation of the strong coupling between the n_l and $(n_l + 1)$ schemes. To

[11] This parametrization differs from the one given in Ref. [16]. It has better precision and interpolates the R anomalous dimension more smoothly for small values of m/R.

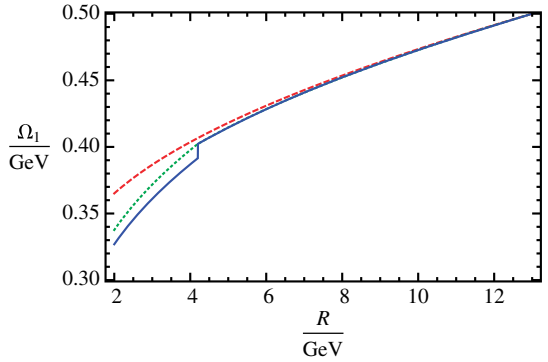

FIG. 5 (color online). R evolution of $\Omega_1(R,\mu=R)$ with a massive bottom quark at $\mathcal{O}(\alpha_s^3)$ as described in the text. The curves represent purely massless evolution (red, dashed), massive evolution including threshold matching at $\bar{m}_b(\bar{m}_b)$ (blue, solid), and massive evolution without threshold matching (green, dotted).

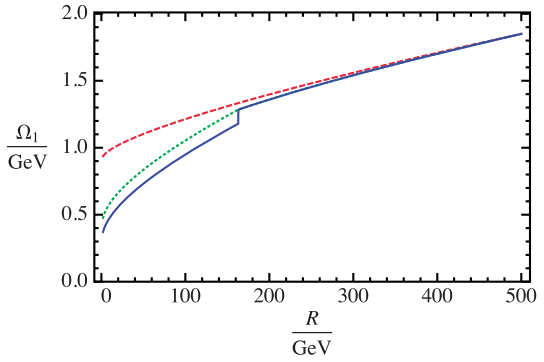

FIG. 6 (color online). R evolution of $\Omega_1(R,\mu=R)$ with a massive top quark at $\mathcal{O}(\alpha_s^3)$ as described in the text. The curves represent purely massless evolution (red, dashed), massive evolution including threshold matching at $\bar{m}_t(\bar{m}_t)$ (blue, solid), and massive evolution without threshold matching (green, dotted).

avoid large logarithms, the gap matching relation should be employed for $R\sim\mu\sim m$.

In Fig. 5 we show $\Omega_1(R,\mu=R)$ [see Eq. (17)] as a function of R in the range between 2 and 13 GeV using $\Omega_1^{(5)}(13\text{ GeV},13\text{ GeV})=0.5$ GeV and $\alpha_s^{(5)}(m_Z)=0.114$ as initial conditions. The choice of these initial conditions is motivated by recent fits for α_s and Ω_1 in Refs. [17,36], which involved only experimental data related to R-scale values above 10 GeV despite the fact that values for Ω_1 at $R=2$ GeV were quoted in the final result. The red, dashed curve shows the purely massless evolution using the R anomalous dimension at $\mathcal{O}(\alpha_s^3)$. The blue, solid curve shows the R dependence accounting for the finite bottom quark mass, taking $\bar{m}_b(\bar{m}_b)=4.2$ GeV as an input for the $\overline{\text{MS}}$ bottom quark mass and using the threshold matching relation of Eq. (68) at $R=\mu=\bar{m}_b(\bar{m}_b)$ when switching from the $n_f=5$ to the $n_f=4$ flavor scheme for the gap parameter. The difference between the blue and the red curve illustrates the impact of the finite bottom mass corrections on the R dependence. We see that the mass effects are relatively small for $R>\bar{m}_b(\bar{m}_b)$, which indicates that the mass corrections in the anomalous dimension in R represent only a minor effect. On the other hand, for $R<\bar{m}_b(\bar{m}_b)$, the bottom mass effects, which arise from the threshold matching corrections and from using the $n_f=4$ flavor anomalous dimension, are quite sizeable. This indicates that the latter two effects represent the most important effect due to the finite bottom mass. To visualize the impact of the bottom mass on the R evolution alone, we have also displayed the dependence on R when the threshold matching correction is ignored (green, dotted curve). Overall, we see that the impact due to the finite bottom quark mass is sizeable and non-negligible, particularly for scales below the bottom quark mass.

In Fig. 6 we display $\Omega_1(R,\mu=R)$ as a function of R in the range up to 500 GeV showing the same type of curves as in Fig. 5 in order to illustrate the impact of the finite top quark mass. All curves have the common input value $\Omega_1^{(6)}(500\text{ GeV},500\text{ GeV})=1.85$ GeV, using again $\alpha_s^{(5)}(m_Z)=0.114$, and the switch from the $n_f=6$ to the $n_f=5$ flavor scheme has been carried out exactly at the top quark mass $\bar{m}_t(\bar{m}_t)=163$ GeV. We can make observations that are very similar to the ones already discussed for the bottom quark threshold region. The difference is that the impact of the finite top quark mass effects are even more dramatic than for the bottom quark case, leading to a discrepancy of a factor of 2 between the appropriate mass dependence and the evolution for a massless top quark when Ω_1 is evolved down to the bottom quark scale. This is related to the fact that the threshold matching relation at $R\sim m_t$ involves the top quark mass [see Eq. (68)] and that the R evolution involves a linear dependence on R.

Note that the mass dependence of the R-evolution equations at $\mathcal{O}(\alpha_s^3)$ is currently unknown. We have therefore employed at $\mathcal{O}(\alpha_s^3)$ the known massless corrections with the appropriate number of flavors. As the $\mathcal{O}(\alpha_s^3)$ corrections amount to at most 25% of the $\mathcal{O}(\alpha_s^2)$ terms, and—as we have just shown above—the mass dependence in the R-evolution equation only represents a minor effect, this approach is certainly justified. We have checked that these $\mathcal{O}(\alpha_s^3)$ contributions in the R evolution lead to a total numerical impact in the bottom quark mass corrections for the thrust distribution that is less than half of the one generated by the variation of μ_m discussed in our numerical analysis of Sec. V. This indicates that the missing quark mass corrections at $\mathcal{O}(\alpha_s^3)$ might be safely ignored at this stage.

IV. COMPUTATIONS FOR THE HARD CURRENT COEFFICIENT AND JET FUNCTION

In this section, we give details on the calculations of the secondary massive quark corrections at $\mathcal{O}(\alpha_s^2 C_F T_F)$ to the hard current coefficient and the jet function, for masses below the hard and jet scales, respectively, i.e., for cases where

the massive quark represents an active dynamic flavor. The massive quark corrections to the partonic soft function for masses below the soft scale have been already computed in Ref. [16], and the corresponding results have been reviewed in Sec. III D. For all of these results the scheme with $n_l + 1$ running flavors is employed (also for the strong coupling) allowing us to recover the known results for massless quarks in the limit $m \to 0$. For the calculations, we use the dispersion relation method, which enables us to obtain the secondary massive quark corrections at $\mathcal{O}(\alpha_s^2 C_F T_F)$ from the d-dimensional results for a massive gauge boson at $\mathcal{O}(\alpha_s)$ via an integration over the imaginary part of the gluon vacuum polarization due to the massive quark-antiquark bubble [15]. The dispersion relation method facilitates in particular the treatment of the rapidity singularities and the soft-bin subtractions, since they can be dealt with completely at the level of the $\mathcal{O}(\alpha_s)$ diagrams with the massive gluon propagator. This allows us to separate these issues conveniently from the effects of the gluon splitting, which simplifies the calculations considerably.

A. Dispersion relations

We explain the dispersive method for a secondary massive quark-antiquark pair starting from the gluonic vacuum polarization $\Pi(m^2, p^2)$ due to a massive quark-antiquark bubble,

$$\Pi^{AB}_{\mu\nu}(m^2, p^2) = -i(p^2 g_{\mu\nu} - p_\mu p_\nu)\Pi(m^2, p^2)\delta^{AB} \equiv \int \mathrm{d}^4 x e^{ipx} \langle 0|T J^A_\mu(x) J^B_\nu(0)|0\rangle, \tag{70}$$

with the vector current $J^A_\mu(x) = i g_s \bar{q}(x) T^A \gamma_\mu q(x)$. The vacuum polarization function $\Pi(m^2, p^2)$ can be rewritten as a dispersion integral over its absorptive part. The unsubtracted (unrenormalized) dispersion integral reads

$$\Pi(m^2, p^2) = -\frac{1}{\pi}\int \mathrm{d}M^2 \frac{\mathrm{Im}[\Pi(m^2, M^2)]}{p^2 - M^2 + i\epsilon}, \tag{71}$$

and the subtracted (on-shell and finite) dispersion relation has the form

$$\Pi^{\mathrm{OS}}(m^2, p^2) = \Pi(m^2, p^2) - \Pi(m^2, 0) = -\frac{p^2}{\pi}\int \frac{\mathrm{d}M^2}{M^2} \frac{\mathrm{Im}[\Pi(m^2, M^2)]}{p^2 - M^2 + i\epsilon}. \tag{72}$$

The absorptive part in d dimensions reads

$$\mathrm{Im}[\Pi(m^2, p^2)] = \theta(p^2 - 4m^2) g^2 T_F \tilde{\mu}^{2\epsilon} (p^2)^{(d-4)/2} \times \frac{2^{3-2d}\pi^{(3-d)/2}}{\Gamma(\frac{d+1}{2})}\left(d - 2 + \frac{4m^2}{p^2}\right)\left(1 - \frac{4m^2}{p^2}\right)^{(d-3)/2}, \tag{73}$$

where $\tilde{\mu}^2 = \mu^2 e^{\gamma_E}/(4\pi)$. Equations (71) and (72) are valid for any d. The subtracted vacuum polarization function $\Pi^{\mathrm{OS}}(m^2, p^2)$ has the important feature that its insertion into the gluon line can be rewritten as a dispersion integration over a "massive gluon" propagator,

$$\frac{-ig^{\mu\rho}}{p^2 + i\epsilon}\Pi^{\mathrm{OS}}_{\rho\sigma}(m^2, p^2)\frac{-ig^{\sigma\nu}}{p^2 + i\epsilon} = \frac{1}{\pi}\int \frac{\mathrm{d}M^2}{M^2}\frac{-i(g^{\mu\nu} - \frac{p^\mu p^\nu}{p^2})}{p^2 - M^2 + i\epsilon}\mathrm{Im}[\Pi(m^2, M^2)], \tag{74}$$

where p^μ denotes the external gluon momentum, and we have dropped the overall color-conserving Kronecker δ^{AB}. Note that in Eq. (74) the propagator becomes transverse from the insertion of the vacuum polarization. In our calculations the contributions from the additional $p^\mu p^\nu$ term vanish due to gauge invariance and can be ignored. The insertion of the full unsubtracted vacuum polarization function $\Pi(m^2, p^2)$ can be recovered by subtracting a term with the massless gluon propagator times the zero-momentum vacuum polarization function,

$$\frac{-ig^{\mu\rho}}{p^2 + i\epsilon}\Pi_{\rho\sigma}(m^2, p^2)\frac{-ig^{\sigma\nu}}{p^2 + i\epsilon} = \frac{1}{\pi}\int \frac{\mathrm{d}M^2}{M^2}\frac{-i(g^{\mu\nu} - \frac{p^\mu p^\nu}{p^2})}{p^2 - M^2 + i\epsilon}\mathrm{Im}[\Pi(m^2, M^2)] - \frac{-i(g^{\mu\nu} - \frac{p^\mu p^\nu}{p^2})}{p^2 + i\epsilon}\Pi(m^2, 0). \tag{75}$$

Note that Eqs. (74) and (75) hold in any gauge employed on the lhs of the equalities. The zero-momentum vacuum polarization function at $\mathcal{O}(\alpha_s)$ in d dimensions reads

$$\Pi(m^2, 0) = \frac{\alpha_s T_F}{3\pi}\left(\frac{\mu^2 e^{\gamma_E}}{m^2}\right)^{2-\frac{d}{2}}\Gamma\left(2 - \frac{d}{2}\right). \tag{76}$$

Using the on-shell vacuum polarization insertion via Eq. (74) automatically implements the on-shell subtraction for the renormalization of the strong coupling with respect to the effects of the massive quark. So, using Eq. (72) implies that we employ the strong coupling in the n_l-flavor scheme, i.e., $\alpha_s^{(n_l)}$. The subtracted dispersion relation has the computational advantage that the integration over the virtual gluon mass is suppressed by an additional inverse power of M^2. This can make the dispersion integration UV finite and may allow us to carry out the integral directly in $d = 4$ dimensions. Using the full vacuum polarization insertion of Eq. (75) implies that the strong coupling is still unrenormalized with respect to the effects of the massive quark flavor.

The relations in Eqs. (74) and (75) show explicitly that we can obtain the result for the massive quark-antiquark pair from a dispersion integral over the corresponding result for a gluon with mass M. We note that the dispersion

relation method may not only be used to determine the effects of secondary virtual massive quarks, but also for real radiation corrections, as long as it is only the sum of the quark and antiquark momenta (i.e., the momentum of the gluon that splits into the massive quark pair) that enters the phase space constraint in the computation. Even if this is not the case, the dispersion integration may be useful to determine the dominant corrections or to deal with singular or divergent parts of the result; see e.g., Ref. [16] for such an application in the calculation of the $\mathcal{O}(\alpha_s^2 C_F T_F)$ massive quark contributions to the soft function.

B. Hard current matching coefficient for $m < Q$

Following Eq. (74), we can obtain the $\mathcal{O}(\alpha_s^2 C_F T_F)$ secondary massive quark form factor corrections relevant for the hard current matching calculation with the on-shell subtraction for the strong coupling by the relation

$$F^{(2,\mathrm{OS})}_{\mathrm{QCD(SCET)}}(Q,m,\mu) = \frac{1}{\pi}\int \frac{\mathrm{d}M^2}{M^2} F^{(1)}_{\mathrm{M,QCD(SCET)}}(Q,M,\mu) \times \mathrm{Im}[\Pi(m^2,M^2)], \tag{77}$$

where $F^{(1)}_{\mathrm{M,QCD}}$ ($F^{(1)}_{\mathrm{M,SCET}}$) denotes the one-loop massive gluon form factor in QCD (SCET). $F^{(2,\mathrm{OS})}_{\mathrm{QCD}}$ is both IR and UV finite, has been computed in Refs. [30,31], and is equivalent to $F^{(n_l,2)}_{\mathrm{QCD}}$ given in Eq. (30). The massive gluon form factor diagrams in SCET are displayed in Fig. 7, have been computed in Refs. [15,37], and read in d dimensions[12]

$$F^{(1)}_{\mathrm{M,SCET}}(Q,M,\mu) = \frac{\alpha_s C_F}{2\pi}\Gamma\left(2-\frac{d}{2}\right)\left(\frac{\mu^2 e^{\gamma_E}}{M^2}\right)^{2-\frac{d}{2}} \times \left[H_{\frac{d}{2}-1} - (-1)^{2-d/2}\Gamma\left(\frac{d}{2}\right)\Gamma\left(1-\frac{d}{2}\right) - \frac{4-6d+d^2}{d(d-2)} + \ln\left(\frac{M^2}{Q^2}\right)\right], \tag{78}$$

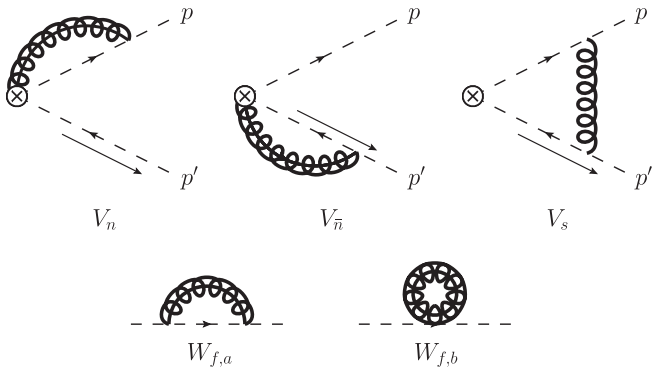

FIG. 7. Nonvanishing EFT diagrams for the computation of the hard matching coefficient; soft mass mode bin subtractions are implied for the collinear diagrams.

where H_n denotes the nth harmonic number. To avoid double counting and achieve gauge invariance, it is crucial to subtract the soft-bin contributions, which arise from the soft scaling regions of the collinear diagrams. The collinear diagrams V_n, $V_{\bar{n}}$, their soft-bin subtractions, and the soft diagram V_s in Fig. 7 are for themselves not fully regularized in dimensional regularization due to rapidity divergences. These cancel in the sum of all diagrams and leave behind the rapidity logarithm $\ln(M^2/Q^2)$. Due to the finite gluon mass, the soft-bin contributions are essential and nonvanishing for a general regularization of the rapidity singularities. Interestingly, this logarithm cancels in the difference of $F^{(1)}_{\mathrm{M,QCD}}$ and $F^{(1)}_{\mathrm{M,SCET}}$, so that there is no corresponding rapidity logarithm in the $\mathcal{O}(\alpha_s^2 C_F T_F)$ secondary massive quark corrections to the hard current matching coefficient at the scale $\mu_H \sim Q$. Thus, the rapidity singularities that arise in the SCET form factor computation do not leave any trace in the hard current matching coefficient.

Carrying out the convolution in Eq. (77) in $d = 4-2\epsilon$ dimensions and expanding in ϵ, we obtain [$x^2 \equiv m^2/(Q^2+i0)$, $L_{-Q} \equiv \ln[-(Q^2+i0)/\mu^2]$, $\alpha_s = \alpha_s^{(n_l)}(\mu)$]

$$\begin{aligned} F^{(2,\mathrm{OS})}_{\mathrm{SCET}}(Q,m,\mu) = {} & \frac{\alpha_s^2 C_F T_F}{(4\pi)^2}\left\{\frac{2}{\epsilon^3}+\frac{1}{\epsilon^2}\left[-\frac{8}{3}\ln(-x^2)-4L_{-Q}+\frac{8}{9}\right]+\frac{1}{\epsilon}\left[\frac{4}{3}\ln^2(-x^2)+\frac{16}{3}\ln(-x^2)L_{-Q}\right.\right. \\ & \left. +4L_{-Q}^2-4\ln(-x^2)-\frac{16}{9}L_{-Q}-\left(\frac{65}{27}+\frac{\pi^2}{9}\right)\right]-\frac{8}{3}L_{-Q}^3-\frac{16}{3}\ln(-x^2)L_{-Q}^2-\frac{8}{3}\ln^2(-x^2)L_{-Q}+\frac{56}{9}\ln^2(-x^2) \\ & \left. +8\ln(-x^2)L_{-Q}+\frac{16}{9}L_{-Q}^2+\left(\frac{242}{27}+\frac{4\pi^2}{9}\right)\ln(-x^2)+\left(\frac{130}{27}+\frac{2\pi^2}{9}\right)L_{-Q}+\frac{875}{54}+\frac{8\pi^2}{9}-\frac{20}{3}\zeta_3\right\}. \end{aligned} \tag{79}$$

Since $F^{(2,\mathrm{OS})}_{\mathrm{QCD}}$ and $F^{(2,\mathrm{OS})}_{\mathrm{SCET}}$ have been computed with the subtracted dispersion relation, they correspond to expressions in the n_l-flavor scheme for the strong coupling. To switch to the (n_l+1)-flavor scheme, one has to add the $\overline{\mathrm{MS}}$-subtracted vacuum polarization function at zero momentum times the corresponding one-loop form factor,

[12]Here we have corrected a typo in Eq. (71) of Ref. [15] concerning the factor $(-1)^{2-d/2}$ appearing in Eq. (78). For $d \to 4$, both expressions give the same terms up to terms of $\mathcal{O}(\epsilon)$.

$$F^{(2)}_{\mathrm{QCD(SCET)}}(Q,m,\mu,\Delta) = F^{(2,\mathrm{OS})}_{\mathrm{QCD(SCET)}}(Q,m,\mu) - \left(\Pi(m^2,0) - \frac{\alpha_s T_F}{3\pi}\frac{1}{\epsilon}\right) F^{(1)}_{\mathrm{QCD(SCET)}}(Q,\mu,\Delta), \quad (80)$$

where $F^{(1)}_{\mathrm{QCD}}$ ($F^{(1)}_{\mathrm{SCET}}$) is the massless gluon one-loop QCD (SCET) form factor calculated with an IR regulator Δ. To obtain the matching coefficient, we should in principle first renormalize both quantities and then calculate their difference where the dependence on Δ cancels. Since the QCD current is UV finite, it is convenient to revert this procedure, i.e., to first determine the difference of the unrenormalized quantities and renormalize the UV divergences in the SCET contribution at the very end. In this way the cancellation of the IR divergences can be made explicit from the beginning. The difference of the massless gluon one-loop QCD and SCET form factors has the form[13]

$$F^{(1)}_{\mathrm{QCD}}(Q,\mu) - F^{(1)}_{\mathrm{SCET}}(Q,\mu) = \frac{\alpha_s C_F}{4\pi}\left(-\frac{\mu^2 e^{\gamma_E}}{Q^2}\right)^{2-\frac{d}{2}} \times \frac{d^2-7d+16}{d-4}\,\frac{\Gamma(2-\frac{d}{2})\Gamma(\frac{d}{2}-1)^2}{\Gamma(d-2)}. \quad (81)$$

The additional term corresponding to the change from the n_l- to the (n_l+1)-flavor scheme thus reads

$$\begin{aligned}\delta F^{\mathrm{OS}\to\overline{\mathrm{MS}}}(Q,m,\mu) &= -\left(\Pi(m^2,0) - \frac{\alpha_s T_F}{3\pi}\frac{1}{\epsilon}\right)(F^{(1)}_{\mathrm{QCD}} - F^{(1)}_{\mathrm{SCET}}) \\ &= \frac{\alpha_s^2 C_F T_F}{(4\pi)^2}\left\{\frac{1}{\epsilon^2}\left[-\frac{8}{3}\ln(-x^2) - \frac{8}{3}L_{-Q}\right]\right. \\ &\quad + \frac{1}{\epsilon}\left[\frac{4}{3}\ln^2(-x^2) + \frac{16}{3}\ln(-x^2)L_{-Q} + 4L_{-Q}^2\right. \\ &\quad \left. - 4\ln(-x^2) - 4L_{-Q} + \frac{2\pi^2}{9}\right] - \frac{4}{9}\ln^3(-x^2) \\ &\quad - \frac{8}{3}\ln^2(-x^2)L_{-Q} - \frac{16}{3}\ln(-x^2)L_{-Q}^2 - \frac{28}{9}L_{-Q}^3 \\ &\quad + 2\ln^2(-x^2) + 8\ln(-x^2)L_{-Q} + 6L_{-Q}^2 \\ &\quad \left. - \frac{32}{3}\ln(-x^2) - \left(\frac{32}{3} + \frac{2\pi^2}{9}\right)L_{-Q} + \frac{\pi^2}{3} - \frac{8}{9}\zeta_3\right\}. \end{aligned} \quad (82)$$

Combining all contributions and including the $\overline{\mathrm{MS}}$ current counterterm contribution $Z^{(n_l+1,2)}_{C,n_f=1}$ given in Eq. (5), the result for the $\mathcal{O}(\alpha_s^2 C_F T_F)$ secondary massive quark contributions to the hard current coefficient in the (n_l+1)-flavor scheme reads [$\alpha_s = \alpha_s^{(n_l+1)}(\mu)$]

$$\delta C^{(n_l+1)}(Q,m,\mu) = F^{(2,\mathrm{OS})}_{\mathrm{QCD}}(Q,m) - F^{(2,\mathrm{OS})}_{\mathrm{SCET}}(Q,m,\mu) + \delta F^{\mathrm{OS}\to\overline{\mathrm{MS}}}(Q,m,\mu) - Z^{(n_l+1,2)}_{C,n_f=1}(Q,\mu). \quad (83)$$

Inserting Eqs. (5), (79), and (82) and subtracting from Eq. (83) the massless limit of Eq. (4) for one single flavor, we obtain the mass corrections to the form factor given in Eq. (35). We see from the result of Eq. (36) that the SCET matching procedure in the (n_l+1)-flavor scheme does in principle nothing other than exactly subtracting the asymptotic massless limit from the full QCD on-shell form factor correction.

C. Thrust jet function

The calculation of the $\mathcal{O}(\alpha_s^2 C_F T_F)$ secondary massive quark corrections to the jet function in the (n_l+1)-flavor scheme goes along the lines of the hard current coefficient. The $\mathcal{O}(\alpha_s)$ corrections to the jet function due to a massive gauge boson with QCD vector coupling have the form [15,37][14]

$$\delta J^{(1)}_M(s,M,\mu) = \delta J^{(1)}_{M,\mathrm{virt}}(s,M,\mu) + \delta J^{(1)}_{M,\mathrm{real}}(s,M). \quad (84)$$

The distributive part $\delta J^{(1)}_{M,\mathrm{virt}}$ corresponds to virtual radiation of the massive gauge boson, and the full expression in d dimensions reads

$$\mu^2\delta J^{(1)}_{M,\mathrm{virt}}(s,M,\mu) = \frac{2\alpha_s C_F}{\pi}\Gamma\left(2-\frac{d}{2}\right)\left(\frac{\mu^2 e^{\gamma_E}}{M^2}\right)^{2-\frac{d}{2}} \times \left\{\left[H_{\frac{d}{2}-1} - H_{1-\frac{d}{2}} + \ln\left(\frac{M^2}{\mu^2}\right) + \frac{2-d}{2d}\right]\delta(\bar{s}) - \left[\frac{\theta(\bar{s})}{\bar{s}}\right]_+\right\}. \quad (85)$$

The UV- and IR-finite real radiation contribution $\delta J^{(1)}_{M,\mathrm{real}}$ can for our purposes be evaluated for $d=4$, since it does not require any regularization for the convolution in the subtracted dispersion relation. It reads

$$\mu^2\delta J^{(1)}_{M,\mathrm{real}}(s,M) = \frac{\alpha_s C_F}{2\pi}\mu^2\theta(s-M^2) \times \left\{\frac{(M^2-s)(3s+M^2)}{s^3} + \frac{4}{s}\ln\left(\frac{s}{M^2}\right)\right\}. \quad (86)$$

[13]Using dimensional regularization for both UV and IR divergences, the SCET form factor for massless gluons vanishes identically.

[14]We consider directly the corrections to the total thrust jet function, which are exactly twice the contributions for the function of a single jet.

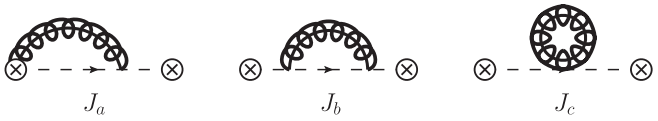

FIG. 8. Nonvanishing EFT diagrams for the computation of the jet function. The required soft mass mode bin subtractions are implicit. Concerning J_a, the right-symmetric diagram also has to be taken into account.

The calculation of $\delta J_M^{(1)}$ involves the collinear diagrams in Fig. 8, where the corresponding soft-bin subtractions are implied and contribute only to $\delta J_{M,\text{virt}}^{(1)}$. The soft-bin subtractions are crucial for gauge invariance as well as for a cancellation of all rapidity singularities [15]. As a remnant of this cancellation, we get a rapidity logarithm $\ln(M^2/\mu^2) \sim \ln(M^2/s)$ in $\delta J_{M,\text{virt}}^{(1)}$ in Eq. (85). For $M^2 \ll s$, a corresponding logarithm arises in the real radiation term $\delta J_{M,\text{real}}^{(1)}$ in Eq. (86) which cancels the rapidity logarithm from $\delta J_{M,\text{virt}}^{(1)}$. We emphasize, however, that in the calculation of $\delta J_{M,\text{real}}^{(1)}$, rapidity divergences do not arise anywhere. These properties are also inherited to the $\mathcal{O}(\alpha_s^2 C_F T_F)$ massive quark corrections discussed in the following.

The $\mathcal{O}(\alpha_s^2 C_F T_F)$ unrenormalized massive quark corrections to the jet function in the n_l-flavor scheme for α_s can be obtained with the subtracted dispersion relation

$$\begin{aligned}\delta J_m^{(2,\text{OS})}(s,m,\mu) &= \delta J_m^{(\text{OS,virt})}(s,m,\mu) + \delta J_m^{\text{real}}(s,m) \\ &= \frac{1}{\pi}\int \frac{\mathrm{d}M^2}{M^2}\,\delta J_M^{(1)}(s,M,\mu)\,\text{Im}[\Pi(m^2,M^2)].\end{aligned} \tag{87}$$

The convolution is performed separately for the d-dimensional virtual terms in Eq. (85) and the four-dimensional threshold term in Eq. (86), where for the latter no divergences arise in the M integration, and thus the $d=4$ version of the absorptive part of the vacuum polarization function in Eq. (73) can be used. This yields Eq. (42) for the real radiation term δJ_m^{real} and $[L_m = \ln(m^2/\mu^2), \alpha_s = \alpha_s^{(n_l)}(\mu)]$

$$\begin{aligned}&\mu^2 \delta J_m^{(\text{OS,virt})}(s,m,\mu) \\ &= \frac{\alpha_s^2 C_F T_F}{(4\pi)^2}\left\{\left[\frac{8}{\epsilon^3} + \frac{1}{\epsilon^2}\left(-\frac{32}{3}L_m - \frac{4}{9}\right)\right.\right. \\ &\quad + \frac{1}{\epsilon}\left(\frac{16}{3}L_m^2 - 8L_m - \frac{242}{27} + \frac{4\pi^2}{9}\right) \\ &\quad \left.+ \frac{152}{9}L_m^2 + \frac{932}{27}L_m + \frac{1531}{27} + \frac{38\pi^2}{27} - \frac{64}{3}\zeta_3\right]\delta(\bar{s}) \\ &\quad + \left[-\frac{16}{3\epsilon^2} + \frac{1}{\epsilon}\left(\frac{32}{3}L_m + \frac{80}{9}\right) - \frac{32}{3}L_m^2 - \frac{160}{9}L_m\right. \\ &\quad \left.\left. - \frac{448}{27} - \frac{8\pi^2}{9}\right]\left[\frac{\theta(\bar{s})}{\bar{s}}\right]_+\right\}.\end{aligned} \tag{88}$$

We switch to the (n_l+1)-flavor scheme for α_s by adding the $\overline{\text{MS}}$-renormalized $\Pi(0)$ times the (unrenormalized) massless one-loop contribution to the jet function which reads

$$J_{\text{bare}}^{(1)}(s,\mu) = \frac{\alpha_s C_F}{2\pi}\frac{1}{s}\left(\frac{\mu^2 e^{\gamma_E}}{s}\right)^{2-\frac{d}{2}}\frac{d+4}{d-4}\frac{\Gamma(\frac{d}{2})}{\Gamma(d-2)}. \tag{89}$$

Thus, the corresponding contribution needed to change from the n_l- to the (n_l+1)-flavor scheme reads

$$\begin{aligned}&\delta J_m^{\text{OS}\to\overline{\text{MS}}}(s,m,\mu) \\ &= -\left(\Pi(m^2,0) - \frac{\alpha_s T_F}{3\pi}\frac{1}{\epsilon}\right)J_{\text{bare}}^{(1)}(s,\mu) \\ &= \frac{\alpha_s^2 C_F T_F}{(4\pi)^2}\left\{\left[\frac{32}{3\epsilon^2}L_m + \frac{1}{\epsilon}\left(-\frac{16}{3}L_m^2 + 8L_m - \frac{8\pi^2}{9}\right)\right.\right. \\ &\quad + \frac{16}{9}L_m^3 - 4L_m^2 + \left(\frac{56}{3} - \frac{16\pi^2}{9}\right)L_m - \frac{2\pi^2}{3} + \frac{32}{9}\zeta_3\Big]\delta(\bar{s}) \\ &\quad + \left[-\frac{32}{3\epsilon}L_m + \frac{16}{3}L_m^2 - 8L_m + \frac{8\pi^2}{9}\right]\left[\frac{\theta(\bar{s})}{\bar{s}}\right]_+ \\ &\quad \left.+ \frac{32}{3}L_m\left[\frac{\theta(\bar{s})\log(\bar{s})}{\bar{s}}\right]_+\right\}.\end{aligned} \tag{90}$$

Combining all contributions and renormalizing the result with the jet counterterm contribution $Z_{J,n_f=1}^{(n_l+1,2)}$ in Eq. (7) finally gives

$$\begin{aligned}\delta J_m^{\text{virt}}(s,m,\mu) &= \delta J_m^{(\text{OS,virt})}(s,m,\mu) + \delta J_m^{\text{OS}\to\overline{\text{MS}}}(s,m,\mu) \\ &\quad - Z_{J,n_f=1}^{(n_l+1,2)}(s,\mu).\end{aligned} \tag{91}$$

Inserting Eqs. (7), (88), (90) and subtracting from Eq. (91) the massless limit of Eq. (6) for one single flavor, we obtain the virtual massive quark corrections to the jet function given in Eq. (41).

V. RENORMALIZATION CONDITIONS, THRESHOLD CORRECTIONS AND CONSISTENCY RELATIONS

In this section, we discuss the RG properties of the individual ingredients of the factorization theorem, namely the hard current coefficient, the jet function, and the soft function, rather than the factorization theorem as a whole. Since the hard coefficient and the jet and soft functions are gauge-invariant quantities, they can also be renormalized independently. This fact can be used to determine the threshold correction factors $\mathcal{M}_C$ for the hard coefficient [see Eq. (38)] and $\mathcal{M}_J$ for the jet function [see Eq. (46)], as well as the threshold correction factor $\mathcal{M}_S$ for the soft function [see Eq. (144)]. The latter becomes relevant if one sets the final renormalization scale μ above the soft scale

and the RG evolution of the soft function crosses the massive quark threshold. Instead of using different effective theories that follow the strict guideline of having the massive quark modes either as fluctuating fields contributing to the RG evolution in the same way as the massless quarks or excluded completely (i.e., integrated out), we use only a single theory which contains the massive quark modes but employs different renormalization conditions for the quantum corrections that arise from the massive quark modes. These renormalization conditions are either the $\overline{\text{MS}}$ prescription or an on-shell (or low-energy momentum subtraction) prescription. The former leads to the usual $\overline{\text{MS}}$ feature that massless quarks and the massive flavor all contribute to the RG evolution in the same way, so one uses the (n_l+1) running flavor scheme. The latter also subtracts finite and scale-dependent contributions such that the massive flavor does not lead to any contribution in the RG evolution, so there are only n_l running flavors. This concerns the strong coupling α_s (see Sec. IV A), as well as the hard coefficient and the jet and soft functions.

Obviously, the $\overline{\text{MS}}$ prescription is suitable to cover the situation where the quark mass becomes small (where "suitable" means that no large mass logarithms arise in the massless limit) and, as already demonstrated in Sec. IV, leads to results which give the known results for massless quarks in the limit $m \to 0$. The on-shell prescription is suitable to cover the decoupling limit, such that the effects of the massive quark vanish in the infinite-mass limit. The decoupling condition renders the finite subtraction unique for all calculations within SCET. This method of using different renormalization conditions for the RG evolution schemes with (n_l+1) and n_l running flavors also has the advantage that the kinematic thresholds of the jet and soft functions due to the quark mass are fully contained in them regardless of which type of renormalization scheme is used. This is unlike the case of using the effective theory method, where the massive quark is completely excluded from the n_l-flavor theory, and one is forced to take care of the fact that the real radiation thresholds are always located in the (n_l+1)-flavor theory.

The differences of the renormalized quantities with respect to both of these renormalization prescriptions constitute threshold matching conditions that uniquely define the mass mode matching threshold correction factors $\mathcal{M}_C$, $\mathcal{M}_J$, and $\mathcal{M}_S$. Since the hard current coefficient, the jet, and the soft functions are independent and in principle not tied to the particular factorization theorem for thrust, the important outcome is that the threshold correction factors can be determined from these quantities and do not rely on a separate perturbative calculation of the thrust distribution in full QCD. From the form of the factorization theorem for thrust we can therefore *predict* the singular $\mathcal{O}(\alpha_s^2 C_F T_F)$ massive quark corrections to the thrust distribution in full fixed-order QCD. To our knowledge they have not been calculated in an explicit form before in the literature.

The fact that the hard coefficients, the jet and soft functions, and the massive quark threshold corrections factors that appear in the factorization theorems in the four scenarios (in schemes with either n_l or n_l+1 running flavors) are conceptually connected through different choices of renormalization schemes and not related in any way to expansions in either small or large quantities makes it evident that the predictions of the different factorization theorems at their respective borders of validity have an overlap region and are continuous.[15]

We believe that it is worth discussing this issue briefly in the following. In Sec. III, we have discussed four scenarios one needs to distinguish for treating the possible hierarchies between the quark mass m on the one side and the hard scale Q, the jet scale $\sim Q\lambda$, and the soft scale $Q\lambda^2$ on the other. Concerning the power counting, we may assume the canonical strong hierarchy between these scales (such as $Q \gg m \gg Q\lambda \gg Q\lambda^2$) when discussing the effective theory setup, the RG evolution, the results for hard current coefficient, jet, and soft functions, and the mass mode threshold corrections that result when the massive modes are integrated out. However, since the components of the factorization theorems are related simply by different choices of renormalization conditions, each factorization theorem also applies in cases where hierarchies involving the mass are only marginal or nonexistent (such as $Q \gg m \gtrsim Q\lambda \gg Q\lambda^2$ or $Q \gtrsim m \gg Q\lambda \gg Q\lambda^2$). In these cases, the RG evolution between close-by scales is equivalent to a perturbative treatment, so that the factors of concern might be simply expanded out. Since this might be as well applied to the two neighboring scenarios within some range, we have continuity between the two descriptions, and the transition point where one switches between them can be picked freely within this range. This feature is very similar to (but distinguished from) the property that the scale μ_m where the quark mass m is integrated out can be picked freely within some range in a practical application. The freedom in these choices causes changes in the numerical predictions due to the truncation of the perturbative expansion and might contribute to estimating the remaining perturbative uncertainty.

The fact of having four different scales relevant for setting up the RG evolution (μ_H, μ_J, μ_S, and μ_m) leads to another interesting feature related to the proliferation of possibilities to pick the final renormalization scale $\mu = \mu_{\text{final}}$ to which the hard current coefficient, the jet function, and the soft function are being evolved in the different factorization theorems. See Fig. 9 for an illustration of three equivalent choices for scenario III, where we display the situations in which μ_{final} lies (a) between the mass and soft scales, (b) between the jet and mass scales, and (c) between the hard and jet scales. The different possibilities and their

[15]We mean continuity up to higher-order perturbative corrections which are not enhanced by large logarithms.

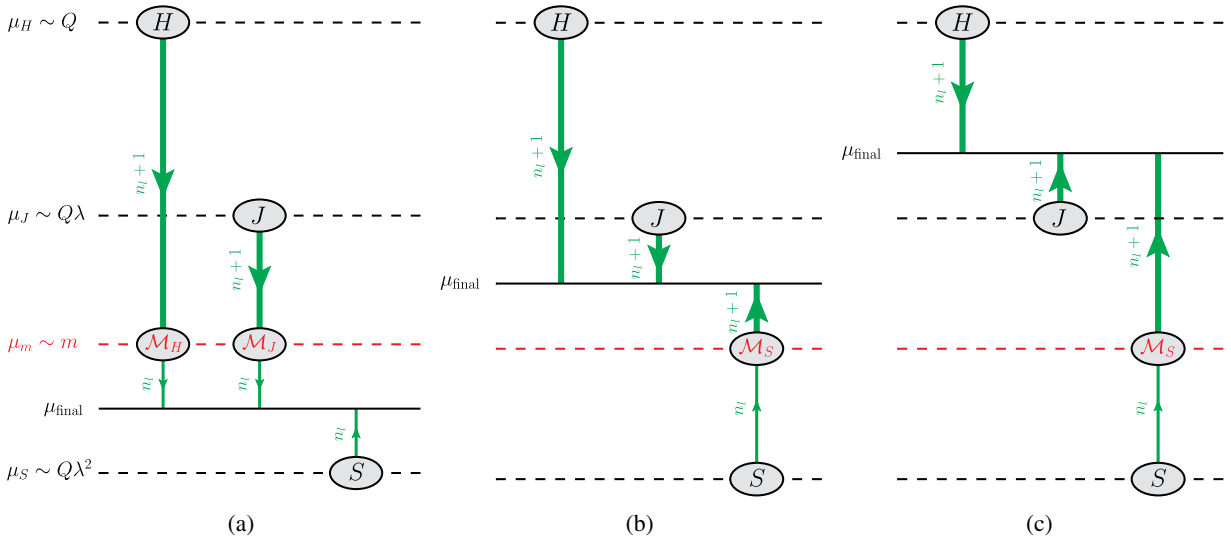

FIG. 9 (color online). Illustration of the different RG setups for scenario III ($\mu_J > \mu_m > \mu_S$) leading to the consistency relations mentioned in the text. Shown are the cases where the final renormalization scale $\mu_{\rm final}$ satisfies (a) $\mu_m > \mu_{\rm final} > \mu_S$, (b) $\mu_J > \mu_{\rm final} > \mu_m$, and (c) $\mu_H > \mu_{\rm final} > \mu_J$.

equivalence concerning predictions point to one of the deeper conceptual properties of factorization theorems. On the one hand, they imply the well-known consistency conditions between the RG evolution factors $U_C^{(n_f)}$, $U_J^{(n_f)}$, and $U_S^{(n_f)}$ for $n_f = n_l$ and $n_f = n_l + 1$, see Eq. (24). However, in the context of the RG evolution crossing a massive quark threshold, they also imply a consistency relation between the mass mode threshold matching correction factors $\mathcal{M}_C$, $\mathcal{M}_J$, and $\mathcal{M}_S$. This can be used to gain interesting general insights into properties of mass singularities, and at the practical level, may be used as a nontrivial tool for consistency checks.

Apart from providing consistency checks of theoretical calculations, these relations also have computational power, as they can be used to calculate properties of gauge-invariant and independent field theoretic objects once it has become clear that they represent building blocks of a factorization theorem. In the case of thrust, these building blocks are the hard (vector or axial) current coefficient, the jet function, and the soft function. Hereby, one of the most interesting aspects is that the various building blocks can appear in different factorization theorems, and one may gain insights into the mass singularities of apparently unrelated quantities.

In the following Secs. V A–V C, we discuss the evolution and the mass mode threshold corrections for the hard current coefficient, the jet function, and the soft function using the renormalization method described above. The calculations are fast and concise and are based on the $\mathcal{O}(\alpha_s^2 C_F T_F)$ massive quark results given in Sec. IV. Using RG-invariance with respect to the scale where one switches between n_l- and (n_l+1)-flavor schemes, we also examine terms of $\mathcal{O}(\alpha_s^3)$ and $\mathcal{O}(\alpha_s^4)$ which are enhanced by rapidity logarithms and may be counted as $\mathcal{O}(\alpha_s^2)$ in the logarithmic counting $\alpha_s \ln \sim \mathcal{O}(1)$. In Sec. V D we discuss the consistency conditions among the mass mode matching corrections $\mathcal{M}_C$, $\mathcal{M}_J$, and $\mathcal{M}_S$, and we also show that they are also relevant for the perturbative equivalence of the factorization theorems of neighboring scenarios in their overlap region. In Sec. V E, we present the explicit result for the singular $\mathcal{O}(\alpha_s^2 C_F T_F)$ massive quark correction of the thrust distribution in full QCD in the fixed-order expansion.

A. Current mass mode matching coefficient

The mass mode threshold factor $\mathcal{M}_C(Q, m, \mu_m)$ arises when the RG evolution of the hard current coefficient crosses the massive quark threshold. In the following we describe how it is related to the renormalization conditions for the hard current. The bare and the renormalized current coefficients $C^{(0)}(Q, m, \mu)$ and $C^{(n_f)}(Q, m, \mu)$ are related to each other via

$$C^{(0)}(Q, m, \mu) = Z_C^{(n_f)}(Q, m, \mu) C^{(n_f)}(Q, m, \mu), \qquad (92)$$

where $Z_C^{(n_f)}(Q, m, \mu)$ is the renormalization factor in a n_f-flavor scheme. In the following, we will omit all $\mathcal{O}(\alpha_s^2 C_F^2)$ and $\mathcal{O}(\alpha_s^2 C_F C_A)$ terms, as they are irrelevant for our considerations. For scales $\mu > m$ we use the (n_l+1)-flavor scheme, so we employ the $\overline{\rm MS}$ subtractions for the UV divergent contributions to the strong coupling and the current. The counterterm is mass independent and reads with the notation of Sec. II

$$Z_C^{(n_l+1)}(Q,\mu) = 1 + Z_C^{(n_l+1,1)}(Q,\mu) + Z_{C,n_l+1}^{(n_l+1,2)}(Q,\mu). \qquad (93)$$

The $\mathcal{O}(\alpha_s^2 C_F T_F)$ contribution $Z_{C,n_l+1}^{(n_l+1,2)}(Q,\mu)$ is given in Eq. (5) with $n_f = n_l + 1$, whereas the $\mathcal{O}(\alpha_s)$ term reads $[L_{-Q} = \ln(-(Q^2 + i0)/\mu^2)]$

$$Z_C^{(n_l+1,1)}(Q,\mu) = \frac{\alpha_s^{(n_l+1)}(\mu) C_F}{4\pi}\left(-\frac{2}{\epsilon^2} - \frac{3}{\epsilon} + \frac{2}{\epsilon} L_{-Q}\right). \quad (94)$$

Note that the contribution from the massive quark agrees with the one related to a massless flavor. The renormalized current coefficient reads

$$C^{(n_l+1)}(Q,m,\mu) = 1 + C^{(n_l+1,1)}(Q,\mu) + C_{n_l+1}^{(n_l+1,2)}(Q,\mu) + \delta F^{(n_l+1,2)}(Q,m), \quad (95)$$

which is the one for the case $m < Q$ (scenarios II, III, and IV) given in Eq. (35). The massless result at $\mathcal{O}(\alpha_s)$ reads

$$C^{(n_l+1,1)}(Q,\mu) = \frac{\alpha_s^{(n_l+1)}(\mu) C_F}{4\pi}\left(-L_{-Q}^2 + 3L_{-Q} - 8 + \frac{\pi^2}{6}\right). \quad (96)$$

In the n_l-flavor scheme, we intend to implement the renormalization condition that the massive quark corrections vanish for $Q \sim \mu \ll m$. Following the computation described in Sec. IV B, we now do *not* include the scheme change contribution $\delta F^{\mathrm{OS}\to\overline{\mathrm{MS}}}$, which implies that we use $\alpha_s^{(n_l)}$, i.e., the n_l-flavor scheme for the strong coupling. The resulting expressions for the counterterm and the renormalized current coefficient read

$$Z_C^{(n_l)}(Q,\mu) = 1 + Z_C^{(n_l,1)}(Q,\mu) + Z_{C,n_l}^{(n_l,2)}(Q,\mu) + Z_{\mathrm{C,OS}}^{(n_l,2)}(Q,m,\mu) \quad (97)$$

and

$$C^{(n_l)}(Q,m,\mu) = 1 + C^{(n_l,1)}(Q,\mu) + C_{n_l}^{(n_l,2)}(Q,\mu) + F_{\mathrm{QCD}}^{(2,\mathrm{OS})}(Q,m) - F_{\mathrm{SCET}}^{(2,\mathrm{OS})}(Q,m,\mu) - Z_{\mathrm{C,OS}}^{(n_l,2)}(Q,m,\mu), \quad (98)$$

where the one-loop terms $Z_C^{(n_l,1)}(Q,\mu)$ and $C^{(n_l,1)}(Q,\mu)$ are analogous to Eq. (94) and (96), respectively. The two-loop massless contributions $Z_{C,n_l}^{(n_l,2)}(Q,\mu)$, $C_{n_l}^{(n_l,2)}(Q,\mu)$ are given in Eqs. (5) and (4) with $n_f = n_l$, and the two-loop massive quark contributions $F_{\mathrm{QCD}}^{(2,\mathrm{OS})}(Q,m)$ and $F_{\mathrm{SCET}}^{(2,\mathrm{OS})}(Q,m,\mu)$ are given in Eqs. (30) and (79), respectively, with the corresponding counterterm contribution denoted by $Z_{\mathrm{C,OS}}^{(n_l,2)}(Q,m,\mu)$. The condition of decoupling requires that the massive quark contributions in Eq. (98) vanish for $m \to \infty$, so we obtain

$$Z_{\mathrm{C,OS}}^{(n_l,2)}(Q,m,\mu) = -F_{\mathrm{SCET}}^{(2,\mathrm{OS})}(Q,m,\mu). \quad (99)$$

Note that the QCD term $F_{\mathrm{QCD}}^{(2,\mathrm{OS})}(Q,m)$ automatically decouples for $m \gg Q$, so that it does not lead to any contributions in the counterterm. The renormalized current coefficient in this scheme is thus identical to the result for $\mu_m > \mu_H$ given in Eq. (28), where the effective theory scenario I was discussed.

It is now straightforward to determine the matching relation between the renormalized hard current coefficients in the two schemes at the scale μ_m. The matching accounts for the difference between the two schemes; thus, it is obtained by the relation

$$\mathcal{M}_C(Q,m,\mu_m) = \frac{C^{(n_l)}(Q,m,\mu_m)}{C^{(n_l+1)}(Q,m,\mu_m)} = \frac{Z_C^{(n_l+1)}(Q,\mu_m)}{Z_C^{(n_l)}(Q,m,\mu_m)}. \quad (100)$$

Since the difference in the factorization theorems for scenarios I and II in Eqs. (27) and (34) concerns just the current matching conditions and evolution, Eq. (100) makes evident that the condition for the current mass mode matching coefficient automatically implements a continuous transition between these two scenarios at $m \sim \mu_m \sim \mu_H \sim Q$. Comparing the factorization theorems of scenarios I and II in this region, we see that the same mass-shell contributions are just swapped between the Wilson coefficient and the mass mode matching coefficient.

Since the expressions in Eq. (100) are written in different schemes for α_s, one has to relate them by the decoupling relation for α_s[16] $[L_m = \ln(m^2/\mu_m^2)]$

$$\alpha_s^{(n_l)}(\mu_m) = \alpha_s^{(n_l+1)}(\mu_m) \times \left[1 + \frac{\alpha_s^{(n_l+1)}(\mu_m) T_F}{3\pi} L_m + \mathcal{O}(\alpha_s^2)\right]. \quad (101)$$

Using the structure of the Wilson coefficients in Eqs. (28) and (35), we obtain at $\mathcal{O}(\alpha_s^2)$ in the fixed-order counting

$$\mathcal{M}_C(Q,m,\mu_m) = 1 + F_{\mathrm{QCD}}^{(n_l,2)}(Q,m) - C_{n_f=1}^{(n_l+1,2)}(Q,\mu_m) - \delta F^{(n_l+1,2)}(Q,m,\mu_m) + \frac{\alpha_s^{(n_l+1)}(\mu_m) T_F}{3\pi} \times L_m C^{(n_l+1,1)}(Q,\mu_m) + \mathcal{O}(\alpha_s^3). \quad (102)$$

[16]Using the ratio of the counterterms instead of the ratio of the renormalized matching coefficients in Eq. (100), we need in Eq. (101) terms up to $\mathcal{O}(\epsilon^2)$. These can be easily determined from the result for $\Pi(m^2, 0)$ in Eq. (76) in d dimensions. Otherwise, the calculation is straightforward and completely equivalent to the one based on the renormalized expressions.

Inserting all explicit expressions gives at $\mathcal{O}(\alpha_s^2)$ in the fixed-order counting ($Q^2 = Q^2 + i0$),

$$\mathcal{M}_C^{(2)}(Q,m,\mu_m) = \frac{\alpha_s^2 C_F T_F}{16\pi^2}\left\{\left[\frac{4}{3}L_m^2 + \frac{40}{9}L_m + \frac{112}{27}\right]\ln\left(-\frac{m^2}{Q^2}\right) - \frac{8}{9}L_m^3 - \frac{2}{9}L_m^2 + \left(\frac{130}{27} + \frac{2\pi^2}{3}\right)L_m + \frac{875}{54} + \frac{5\pi^2}{9} - \frac{52}{9}\zeta_3\right\}. \quad (103)$$

Since there are no $\mathcal{O}(\alpha_s)$ one-loop corrections, the schemes of α_s and the mass appearing in Eq. (103) do not need to be specified at this point. In Eq. (103), we see explicitly the large rapidity logarithm $\ln(-m^2/Q^2)$, which enforces the counting $\alpha_s \ln(m^2/Q^2) \sim 1$. One can set up a RG evolution in rapidity space as described in Refs. [33,34] to resum the associated higher-order logarithms, which we postpone to a later publication [35].[17] For our purposes, the outcome—namely that this logarithm exponentiates—is sufficient. This allows us to determine the term of $\mathcal{O}(\alpha_s^4 \ln^2(m^2/Q^2)) \sim \mathcal{O}(\alpha_s^2)$.

For a complete analysis at N^{3}LL, we would also need the term at $\mathcal{O}(\alpha_s^3 \ln(m^2/Q^2)) \sim \mathcal{O}(\alpha_s^2)$. We can determine its μ_m-dependent contribution from the identity

$$\mathcal{M}_C(Q,m,\mu_m) = U_C^{(n_l+1)}(Q,\mu_m,m)\mathcal{M}_C(Q,m,m) \times U_C^{(n_l)}(Q,m,\mu_m), \quad (104)$$

or equivalently,

$$\mu\frac{\mathrm{d}}{\mathrm{d}\mu}\mathcal{M}_C(Q,m,\mu) = (\gamma_C^{(n_l)}(Q,\mu) - \gamma_C^{(n_l+1)}(Q,\mu))\mathcal{M}_C(Q,m,\mu). \quad (105)$$

Expanding consistently in α_s gives the perturbative result for the μ_m-dependent terms. Including the relevant term at $\mathcal{O}(\alpha_s^3 \ln(m^2/Q^2))$ in the exponent the structure of the mass mode matching coefficient reads [$\alpha_s^{(n_l+1)} = \alpha_s^{(n_l+1)}(\mu_m)$, $m = \bar{m}(\mu_m) = \bar{m}^{(n_l+1)}(\mu_m)$]

$$\begin{aligned}\mathcal{M}_C(Q,m,\mu_m) = {}& \left\{1 + \frac{(\alpha_s^{(n_l+1)})^2}{(4\pi)^2}\left[\frac{1}{12}L_m^3\Gamma_0^C\Delta\beta_0 + \frac{1}{4}L_m^2(\Delta\Gamma_1^C + \gamma_0^C\Delta\beta_0) + \frac{1}{2}L_m(\Delta\gamma_1^C + 2\mathcal{M}_2^{C,+}) + \mathcal{M}_2^C\right]\right\} \\ & \times \exp\left\{\frac{(\alpha_s^{(n_l+1)})^2}{(4\pi)^2}L_{-Q}\left[-\frac{1}{4}L_m^2\Gamma_0^C\Delta\beta_0 - \frac{1}{2}L_m\Delta\Gamma_1^C - \mathcal{M}_2^{C,+}\right] + \frac{(\alpha_s^{(n_l+1)})^3}{(4\pi)^3}L_{-Q}\left[\frac{1}{6}L_m^3\Gamma_0^C(\beta_0+\Delta\beta_0)\Delta\beta_0\right. \\ & + \frac{1}{4}L_m^2(-\Gamma_0^C\Delta\beta_1 - 2\Gamma_1^C\Delta\beta_0 + 2(\beta_0+\Delta\beta_0)\Delta\Gamma_1^C + 4\Delta\beta_0\Gamma_0^C\gamma_0^m) + \frac{1}{2}L_m(-\Delta\Gamma_2^C + 4\beta_0\mathcal{M}_2^{C,+} + c_{\mathrm{dec}}\Gamma_0^C \\ & \left.+ 2\Delta\Gamma_1^C\gamma_0^m) - \mathcal{M}_3^{C,+}\right]\Big\}. \end{aligned} \quad (106)$$

Here $\Delta\eta \equiv \eta^{(n_l+1)} - \eta^{(n_l)}$ is the difference between an evolution constant η in the (n_l+1)- and n_l-schemes. The terms Γ_i^C, γ_i^C, γ_i^m, and β_i denote the coefficients of the cusp and noncusp current anomalous dimensions, the mass anomalous dimension, and the beta function with n_l+1 light quarks, respectively:

$$\frac{\mu}{C}\frac{\mathrm{d}C}{\mathrm{d}\mu} = \sum_{i\geq 0}\left(\frac{\alpha_s^{(n_l+1)}}{4\pi}\right)^{i+1}[-\Gamma_i^C L_{-Q} + \gamma_i^C], \quad (107)$$

$$\frac{\mu}{\bar{m}}\frac{\mathrm{d}\bar{m}}{\mathrm{d}\mu} = -2\sum_{i\geq 0}\left(\frac{\alpha_s^{(n_l+1)}}{4\pi}\right)^{i+1}\gamma_i^m, \quad (108)$$

$$\frac{\mu}{\alpha_s}\frac{\mathrm{d}\alpha_s}{\mathrm{d}\mu} = -2\sum_{i\geq 0}\left(\frac{\alpha_s^{(n_l+1)}}{4\pi}\right)^{i+1}\beta_i. \quad (109)$$

In this notation, we have e.g., for the one-loop terms $\Gamma_0^C = -4C_F$, $\gamma_0^C = -6C_F$, $\gamma_0^m = 3C_F$, and $\beta_0 = \frac{11}{3}C_A - \frac{4}{3}T_F(n_l+1)$ with $\Delta\beta_0 = -\frac{4}{3}T_F$. The terms $\mathcal{M}_i^{C,+}$ ($\mathcal{M}_i^C$) indicate the renormalization-scale-independent constants, which multiply (do not multiply) the rapidity logarithm $\ln(-m^2/Q^2)$ in the matching coefficient $\mathcal{M}_C(Q,m,m)$, and c_{dec} is the coefficient of the two-loop correction in the decoupling relation between the strong couplings in the n_l- and (n_l+1)-flavor schemes at the scale of the mass that is being employed, i.e.,

[17] The result will then depend on two rapidity scales which should be varied independently of the invariant mass scales. This dependence can be easily restored in the result of Eq. (106) by replacements of the scales in the exponentiated logarithm L_{-Q}. The analogous statement holds also for the jet and soft mass mode matching coefficients in Eqs. (124) and (142).

$$\alpha_s^{(n_l)}(m) = \alpha_s^{(n_l+1)}(m)\left[1 + \left(\frac{\alpha_s^{(n_l+1)}(m)}{4\pi}\right)^2 c_{\rm dec}\right]. \quad (110)$$

For the $\overline{\rm MS}$ mass $m = \bar{m}(\mu_m)$, we have $c_{\rm dec} = 22/9$. The inclusion of the μ_m-dependent terms at $\mathcal{O}(\alpha_s^3 \ln(m^2/Q^2))$ can play an important role for obtaining the correct remaining μ_m dependence in numerical predictions at N^{3}LL order. Inserting the values for all of the constants and expanding Eq. (106) using the logarithmic counting $\alpha_s \ln(m^2/Q^2) \sim 1$ gives our final result in Eq. (38).

B. Jet mass mode matching coefficient

The mass mode threshold factor $\mathcal{M}_J(s, m, \mu_m)$ arises when the RG evolution of the jet function crosses the massive quark threshold. The derivation goes along the lines of the current mass mode threshold factor, and we will again omit all $\mathcal{O}(\alpha_s^2 C_F^2)$ and $\mathcal{O}(\alpha_s^2 C_F C_A)$ terms. The bare and the renormalized jet functions $J^{(0)}(s, m, \mu)$ and $J^{(n_f)}(s, m, \mu)$ are related to each other via

$$J^{(0)}(s,m,\mu) = \int {\rm d}s' Z_J^{(n_f)}(s-s',m,\mu) J^{(n_f)}(s',m,\mu), \quad (111)$$

where $Z_J^{(n_f)}(s, m, \mu)$ is the counterterm in a n_f-flavor scheme. For scales $\mu > m$, we use the $(n_l + 1)$-flavor scheme, so we employ the $\overline{\rm MS}$ subtractions for the UV divergent contributions to the strong coupling and the jet function. The counterterm is mass independent and reads with the notation of Sec. II

$$Z_J^{(n_l+1)}(s,\mu) = \delta(s) + Z_J^{(n_l+1,1)}(s,\mu) + Z_{J,n_l+1}^{(n_l+1,2)}(s,\mu). \quad (112)$$

The $\mathcal{O}(\alpha_s^2 C_F T_F)$ contribution $Z_{J,n_l+1}^{(n_l+1,2)}(s,\mu)$ is given in Eq. (7) with $n_f = n_l + 1$, whereas the $\mathcal{O}(\alpha_s)$ term reads ($\bar{s} = s/\mu^2$)

$$\mu^2 Z_J^{(n_l+1,1)}(s,\mu) = \frac{\alpha_s^{(n_l+1)}(\mu) C_F}{4\pi}\left\{\left(\frac{8}{\epsilon^2} + \frac{6}{\epsilon}\right)\delta(\bar{s}) - \frac{8}{\epsilon}\left[\frac{\theta(\bar{s})}{\bar{s}}\right]_+\right\}. \quad (113)$$

The renormalized jet function reads

$$J^{(n_l+1)}(s,m,\mu) = \delta(s) + J^{(n_l+1,1)}(s,\mu) + J^{(n_l+1,2)}(s,\mu) + \delta J_m^{\rm dist}(s,m,\mu) + \delta J_m^{\rm real}(s,m), \quad (114)$$

which is the one for the case $m^2 < s \sim \mu_J$ (scenarios III and IV) given in Eq. (40). The massless result at $\mathcal{O}(\alpha_s)$ reads

$$\mu^2 J^{(n_l+1,1)}(s,\mu) = \frac{\alpha_s^{(n_l+1)}(\mu) C_F}{4\pi}\left\{(14 - 2\pi^2)\delta(\bar{s}) - 6\left[\frac{\theta(\bar{s})}{\bar{s}}\right]_+ + 8\left[\frac{\theta(\bar{s})\ln\bar{s}}{\bar{s}}\right]_+\right\}. \quad (115)$$

In the n_l-flavor scheme, we intend to implement the renormalization condition that the massive quark corrections vanish for $s \sim \mu^2 \ll m^2$. Following the computation described in Sec. IV C, we now do *not* include the scheme change contribution $\delta J_m^{\rm OS\to\overline{MS}}$, which implies that we use $\alpha_s^{(n_l)}$. The resulting expressions for the counterterm and the renormalized jet function read

$$Z_J^{(n_l)}(s,m,\mu) = \delta(s) + Z_J^{(n_l,1)}(s,\mu) + Z_{J,n_l+1}^{(n_l+1,2)}(s,\mu) + Z_J^{(2,{\rm OS})}(s,m,\mu) \quad (116)$$

and

$$J^{(n_l)}(s,m,\mu) = \delta(s) + J^{(n_l,1)}(s,\mu) + J^{(n_l,2)}(s,\mu) + \delta J_m^{({\rm OS,virt})}(s,m,\mu) + \delta J_m^{\rm real}(s,m) - Z_J^{(2,{\rm OS})}(s,m,\mu), \quad (117)$$

where the one-loop terms $Z_J^{(n_l,1)}(s,\mu)$ and $J^{(n_l,1)}(s,\mu)$ are analogous to Eqs. (113) and (115), respectively. The two-loop massless contributions $Z_{J,n_l}^{(n_l,2)}(s,\mu)$ and $J_{n_l}^{(n_l,2)}(s,\mu)$ are given in Eqs. (7) and (6) with $n_f = n_l$, and the two-loop massive quark contributions $\delta J_m^{({\rm OS,virt})}(s,m,\mu)$ and $\delta J_m^{\rm real}(s,m)$ are given in Eqs. (88) and (42), respectively, with the corresponding counterterm contribution denoted by $Z_J^{(2,{\rm OS})}(s,m,\mu)$. The condition of decoupling requires that the rhs of Eq. (117) vanishes for $m \to \infty$, and we obtain

$$Z_J^{(2,{\rm OS})}(s,m,\mu) = \delta J_m^{({\rm OS,virt})}(s,m,\mu). \quad (118)$$

Note that the real radiation term $\delta J_m^{\rm real}(s,m)$ automatically decouples for $4m^2 > s$, so that it does not lead to any contributions in the counterterm. The renormalized jet function in this scheme is the one to be used for $m^2 \gtrsim s$ (in scenarios I and II). We note that $\delta J_m^{\rm real}(s,m)$ is part of the result and can contribute when kinematically allowed.

The matching procedure is accounting for the difference between the two schemes, thus the mass mode matching coefficient is obtained by the relation

$$\mathcal{M}_J(s,m,\mu_m) = \int {\rm d}s' J^{(n_l)}(s-s',m,\mu_m)(J^{(n_l+1)}(s',m,\mu_m))^{-1} = \int {\rm d}s' Z_J^{(n_l+1)}(s-s',\mu_m)(Z_J^{(n_l)}(s',m,\mu_m))^{-1}. \quad (119)$$

Since the difference in the factorization theorems for the scenarios II and III in Eqs. (34) and (39) concerns just the jet function and its evolution, Eq. (119) shows that the matching condition for the jet function automatically implements a continuous transition between these two scenarios at $m^2 \sim \mu_m^2 \sim \mu_J^2 \sim s$, since the real radiation term $\delta J_m^{\text{real}}(s,m)$ is fully included in both scenarios.

Relating the schemes of α_s via Eq. (101), we obtain at $\mathcal{O}(\alpha_s^2)$ in fixed-order counting $\left[\alpha_s^{(n_l+1)} = \alpha_s^{(n_l+1)}(\mu_m)\right]$

$$\mathcal{M}_J(s,m,\mu_m) = \delta(s) + \frac{\alpha_s^{(n_l+1)} T_F}{3\pi} L_m J^{(n_l+1,1)}(s,\mu_m) - J^{(n_l+1,2)}_{n_f=1}(s,\mu_m) - \delta J_m^{\text{dist}}(s,m,\mu_m) + \mathcal{O}(\alpha_s^3). \tag{120}$$

Note that, using the renormalized jet functions for the matching calculation, the real radiation terms cancel in Eq. (119) and do not contribute to the threshold correction factor. Inserting all explicit expressions gives at $\mathcal{O}(\alpha_s^2)$ in the fixed-order counting ($\bar{s} = s/\mu_m^2$),

$$\begin{aligned}\mu_m^2 \mathcal{M}_J^{(2)}(s,m,\mu_m) &= \frac{\alpha_s^2 C_F T_F}{16\pi^2}\left\{\left[-\frac{16}{9}L_m^3 - \frac{116}{9}L_m^2 - \left(\frac{932}{27} + \frac{8\pi^2}{9}\right)L_m - \frac{1531}{27} - \frac{20\pi^2}{27} + \frac{160}{9}\zeta_3\right]\delta(\bar{s}) \right.\\ &\left. + \left(\frac{16}{3}L_m^2 + \frac{160}{9}L_m + \frac{448}{27}\right)\left[\frac{\theta(\bar{s})}{\bar{s}}\right]_+\right\}. \end{aligned} \tag{121}$$

Since there are no $\mathcal{O}(\alpha_s)$ one-loop corrections, the schemes of α_s and the mass appearing in Eq. (121) do not need to be specified at this point. Equation (121) contains a large logarithm $\ln(m^2/s)$, which can be better seen by using the invariant mass variable $\tilde{s} = s/\mu_J^2 \sim \mathcal{O}(1)$ rather than $\bar{s} = s/\mu_m^2$. As for the current mass mode matching coefficient, this is a rapidity logarithm which enforces the counting $\alpha_s \ln(m^2/s) \sim \mathcal{O}(1)$. The logarithm is known to exponentiate, which allows us to determine the terms of $\mathcal{O}(\alpha_s^4 \ln^2(m^2/s)) \sim \mathcal{O}(\alpha_s^2)$. For a complete analysis at N^{3}LL, we also need the term at $\mathcal{O}(\alpha_s^3 \ln(m^2/s)) \sim \mathcal{O}(\alpha_s^2)$. We can determine its μ_m-dependent contribution from the identity

$$\mathcal{M}_J(s,m,\mu_m) = \int \mathrm{d}s' \int \mathrm{d}s'' U_J^{(n_l+1)}(s-s',m,\mu_m) \times \mathcal{M}_J(s'-s'',m,m) U_J^{(n_l)}(s'',\mu_m,m), \tag{122}$$

or equivalently, from

$$\mu \frac{\mathrm{d}}{\mathrm{d}\mu}\mathcal{M}_J(s,m,\mu) = \int \mathrm{d}s' \mathcal{M}_J(s',m,\mu) \times (\gamma_J^{(n_l)}(s-s',\mu) - \gamma_J^{(n_l+1)}(s-s',\mu)). \tag{123}$$

Expanding consistently in α_s gives the perturbative result for the μ_m-dependent terms. Including the relevant term at $\mathcal{O}(\alpha_s^3 \ln(s/m^2))$ in the exponent, the structure of the mass mode matching coefficient reads [$\alpha_s^{(n_l+1)} = \alpha_s^{(n_l+1)}(\mu_m)$, $m = \bar{m}(\mu_m)$, $\tilde{s} = s/\mu_J^2$]

$$\begin{aligned}\mu_J^2 \mathcal{M}_J(s,m,\mu_m,\mu_J) &= \left\{\delta(\tilde{s}) + \frac{(\alpha_s^{(n_l+1)})^2}{(4\pi)^2}\delta(\tilde{s})\left[\frac{1}{12}L_m^3\Gamma_0^J\Delta\beta_0 + \frac{1}{4}L_m^2(\Delta\Gamma_1^J + \gamma_0^J\Delta\beta_0) + \frac{1}{2}L_m(\Delta\gamma_1^J - 2\mathcal{M}_2^{J,+}) + \mathcal{M}_2^J\right]\right.\\ &\left. + \frac{(\alpha_s^{(n_l+1)})^2}{(4\pi)^2}\left[-\frac{1}{4}L_m^2\Gamma_0^J\Delta\beta_0 - \frac{1}{2}L_m\Delta\Gamma_1^J + \mathcal{M}_2^{J,+}\right]\left[\frac{\theta(\tilde{s})}{\tilde{s}}\right]_+\right\}\\ &\times \exp\left\{\frac{(\alpha_s^{(n_l+1)})^2}{(4\pi)^2}\ln\left(\frac{\mu_J^2}{\mu_m^2}\right)\left[-\frac{1}{4}L_m^2\Gamma_0^J\Delta\beta_0 - \frac{1}{2}L_m\Delta\Gamma_1^J + \mathcal{M}_2^{J,+}\right] + \frac{(\alpha_s^{(n_l+1)})^3}{(4\pi)^3}\ln\left(\frac{\mu_J^2}{\mu_m^2}\right)\right.\\ &\times \left[\frac{1}{6}L_m^3\Gamma_0^J(\beta_0+\Delta\beta_0)\Delta\beta_0 + \frac{1}{4}L_m^2(-\Gamma_0^J\Delta\beta_1 - 2\Gamma_1^J\Delta\beta_0 + 2(\beta_0+\Delta\beta_0)\Delta\Gamma_1^J + 4\Delta\beta_0\Gamma_0^J\gamma_0^m)\right.\\ &\left.\left. + \frac{1}{2}L_m(-\Delta\Gamma_2^J - 4\beta_0\mathcal{M}_2^{J,+} + c_{\text{dec}}\Gamma_0^J + 2\Delta\Gamma_1^J\gamma_0^m) + \mathcal{M}_3^{J,+}\right]\right\}. \end{aligned} \tag{124}$$

Here $\Delta\eta \equiv \eta^{(n_l+1)} - \eta^{(n_l)}$ is the difference between an evolution constant η in the (n_l+1) and n_l schemes. The terms Γ_i^J and γ_i^J denote the coefficients of the cusp and noncusp jet function anomalous dimensions with n_l+1 flavors defined by

$$\mu\frac{\mathrm{d}}{\mathrm{d}\mu}J(s) = \sum_{i\geq 0}\left(\frac{\alpha_s^{(n_l+1)}}{4\pi}\right)^{i+1}\int \mathrm{d}s'\left[-\frac{\Gamma_i^J}{\mu^2}\left[\frac{\mu^2\theta(s-s')}{s-s'}\right]_+ + \gamma_i^J\delta(s-s')\right]J(s'), \tag{125}$$

i.e., with the one-loop terms $\Gamma_0^J = 16C_F$ and $\gamma_0^J = 12C_F$. The terms γ_i^m and β_i denote the mass anomalous dimension and the beta function, respectively, as defined in Eqs. (108) and (109). Note that we have defined $J(s,\mu)$ as the thrust jet function, so the terms in the anomalous dimension on the rhs of Eq. (125) are twice the ones known for the jet function of a single jet. The terms $\mathcal{M}_i^{J,+}$ and $\mathcal{M}_i^J$ indicate the μ_m-independent coefficients of the plus-distribution $1/m^2[m^2\theta(s)/s]_+$ and the delta distribution $\delta(s)$ in the matching coefficient $\mathcal{M}_J(s,m,m)$ (i.e., for $\mu_m = m$), respectively, and $c_{\rm dec}$ is the mass-scheme-dependent two-loop decoupling constant for α_s, see Eq. (110). Inserting the values for all of the constants and expanding Eq. (124) using the logarithmic counting $\alpha_s \ln(m^2/s) \sim \mathcal{O}(1)$ gives our final result in Eq. (46).

C. Soft mass mode matching

The mass mode threshold factor $\mathcal{M}_S(\ell, m, \mu_m)$ arises when the RG evolution of the soft function crosses the massive quark threshold. This does not happen in the RG setup we discussed in Sec. III, since there the final renormalization scale has always been set to the soft scale. However, if we choose a different final renormalization scale, e.g., the jet scale μ_J, we can get a factorization theorem depending on $\mathcal{M}_S(\ell, m, \mu_m)$. This happens e.g., in scenario III ($\mu_J > \mu_m > \mu_S$):

$$\begin{aligned}\frac{1}{\sigma_0}\frac{\mathrm{d}\sigma}{\mathrm{d}\tau} &= Q|C^{(n_l+1)}(Q,m,\mu_H)|^2|U_C^{(n_l+1)}(Q,\mu_H,\mu_J)|^2 \\ &\quad\times \int \mathrm{d}s \int \mathrm{d}\ell \int \mathrm{d}\ell' \int \mathrm{d}\ell'' J^{(n_l+1)}(s,m,\mu_J) \\ &\quad\times U_S^{(n_l+1)}\left(\ell - \frac{s}{Q},\mu_J,\mu_m\right)\mathcal{M}_S(\ell'-\ell,m,\mu_m) \\ &\quad\times U_S^{(n_l)}(\ell''-\ell',\mu_m,\mu_S)S^{(n_l)}(Q\tau-\ell'',\mu_S). \end{aligned} \tag{126}$$

The derivation of $\mathcal{M}_S(\ell, m, \mu_m)$ proceeds along the lines of the current and jet mass mode threshold factor, and we will again omit all terms at $\mathcal{O}(\alpha_s^2 C_F^2)$ and $\mathcal{O}(\alpha_s^2 C_F C_A)$. The bare and the renormalized soft functions $S^{(0)}(\ell, m, \mu)$ and $S^{(n_f)}(\ell, m, \mu)$ are related to each other via

$$S^{(0)}(\ell,m,\mu) = \int \mathrm{d}\ell' Z_S^{(n_f)}(\ell-\ell',m,\mu)S^{(n_f)}(\ell',m,\mu), \tag{127}$$

where $Z_S^{(n_f)}(\ell, m, \mu)$ is the counterterm in a n_f-flavor scheme. For scales $\mu > m$ we use the (n_l+1)-flavor scheme, so we employ the $\overline{\rm MS}$ subtractions for the UV divergent contributions to the strong coupling and the soft function. The counterterm is mass independent and reads with the notation of Sec. II

$$Z_S^{(n_l+1)}(\ell,\mu) = \delta(\ell) + Z_S^{(n_l+1,1)}(\ell,\mu) + Z_{S,n_l+1}^{(n_l+1,2)}(\ell,\mu). \tag{128}$$

The $\mathcal{O}(\alpha_s^2 C_F T_F)$ contribution $Z_{S,n_l+1}^{(n_l+1,2)}(\ell,\mu)$ is given in Eq. (9) with $n_f = n_l + 1$, whereas the $\mathcal{O}(\alpha_s)$ term reads ($\bar\ell = \ell/\mu$)

$$\mu Z_S^{(n_l+1,1)}(\ell,\mu) = \frac{\alpha_s^{(n_l+1)}(\mu)C_F}{4\pi}\left\{-\frac{4}{\epsilon^2}\delta(\bar\ell) + \frac{8}{\epsilon}\left[\frac{\theta(\bar\ell)}{\bar\ell}\right]_+\right\}. \tag{129}$$

The renormalized soft function reads

$$\begin{aligned}\hat S^{(n_l+1)}(\ell,m,\mu) &= \delta(\ell) + \hat S^{(n_l+1,1)}(\ell,\mu) + \hat S^{(n_l+1,2)}(\ell,\mu) \\ &\quad + \delta S_m^{\rm dist}(\ell,m,\mu) + \delta S_m^{{\rm real},\theta}(\ell,m) \\ &\quad + \delta S_m^{{\rm real},\Delta}(\ell,m) \end{aligned} \tag{130}$$

and is the one for the case $m < \ell \sim \mu_S$ (scenario IV) given in Eq. (48). The massless result at $\mathcal{O}(\alpha_s)$ reads

$$\mu\hat S^{(n_l+1,1)}(\ell,\mu) = \frac{\alpha_s^{(n_l+1)}(\mu)C_F}{4\pi}\left\{\frac{\pi^2}{3}\delta(\bar\ell) - 16\left[\frac{\theta(\bar\ell)\ln\bar\ell}{\bar\ell}\right]_+\right\}. \tag{131}$$

In the n_l-flavor scheme, we intend to implement the renormalization condition that the massive quark corrections vanish for $\ell \sim \mu \ll m$. Analogously to the computation of the hard current coefficient and the jet function, we now do *not* include a corresponding scheme change contribution $\delta S_m^{\rm OS\to\overline{MS}}$ [see Eq. (14) in Ref. [16] for the explicit expression], which implies that we use $\alpha_s^{(n_l)}$. The resulting expressions for the counterterm and the renormalized soft function read

$$\begin{aligned} Z_S^{(n_l)}(\ell,m,\mu) &= \delta(\ell) + Z_S^{(n_l,1)}(\ell,\mu) + Z_{S,n_l}^{(n_l,2)}(\ell,\mu) \\ &\quad + Z_S^{(2,{\rm OS})}(\ell,m,\mu) \end{aligned} \tag{132}$$

and

$$\begin{aligned}\hat S^{(n_l)}(\ell,m,\mu) &= \delta(\ell) + \hat S^{(n_l,1)}(\ell,\mu) + \hat S^{(n_l,2)}(\ell,\mu) \\ &\quad + \delta S_m^{({\rm OS,virt})}(\ell,m,\mu) + \delta S_m^{{\rm real},\theta}(\ell,m) \\ &\quad + \delta S_m^{{\rm real},\Delta}(\ell,m) - Z_S^{(2,{\rm OS})}(\ell,m,\mu), \end{aligned} \tag{133}$$

where the one-loop terms $Z_S^{(n_l,1)}(\ell,\mu)$ and $\hat S^{(n_l,1)}(\ell,\mu)$ are analogous to Eqs. (129) and (131), respectively. The two-loop massless contributions $Z_{S,n_l}^{(n_l,2)}(\ell,\mu)$, $\hat S_{n_l}^{(n_l,2)}(\ell,\mu)$ are given in Eqs. (9) and (8) with $n_f = n_l$, and the two-loop massive quark contributions $\delta S_m^{{\rm real},\theta}(\ell,m)$, $\delta S_m^{{\rm real},\Delta}(\ell,m)$ and $\delta S_m^{({\rm OS,virt})}(\ell,m,\mu)$ are given in Eqs. (50) and (52), and by [16]

$$\mu\delta S_m^{(\mathrm{OS,virt})}(\ell,m,\mu)=\frac{\alpha_s^2 C_F T_F}{16\pi^2}\Bigg\{\delta(\bar{\ell})\Bigg[-\frac{4}{\epsilon^3}+\frac{1}{\epsilon^2}\left(\frac{16}{3}L_m+\frac{20}{9}\right)+\frac{1}{\epsilon}\left(-\frac{8}{3}L_m^2+\frac{112}{27}-\frac{2\pi^2}{3}\right)-\frac{40}{9}L_m^2+\left(-\frac{448}{27}+\frac{8\pi^2}{9}\right)L_m-\frac{656}{27}+\frac{10\pi^2}{27}+8\zeta_3\Bigg]+\left[\frac{16}{3\epsilon^2}+\frac{1}{\epsilon}\left(-\frac{32}{3}L_m-\frac{80}{9}\right)+\frac{32}{3}L_m^2+\frac{160}{9}L_m+\frac{448}{27}+\frac{8\pi^2}{9}\right]\left[\frac{\theta(\ell)}{\ell}\right]_+\Bigg\},\tag{134}$$

respectively. The corresponding counterterm contribution is denoted by $Z_S^{(2,\mathrm{OS})}(\ell,m,\mu)$. The condition of decoupling requires that the rhs of Eq. (133) vanishes for $m\to\infty$, and we obtain

$$Z_S^{(2,\mathrm{OS})}(\ell,m,\mu)=\delta S_m^{(\mathrm{OS,virt})}(\ell,m,\mu).\tag{135}$$

Note that the real radiation term $\delta S_m^{\mathrm{real},\theta}(\ell,m)$ automatically decouples for $2m>\ell$ and $\delta S_m^{\mathrm{real},\Delta}(s,m)$ vanishes for $m/\ell\to\infty$, so that these terms do not lead to any contributions in the counterterm. The renormalized soft function in this scheme is thus the one to be used for $m\gtrsim\ell$ (in scenarios I, II, and III). We note that the real radiation terms $\delta S_m^{\mathrm{real},\theta}(\ell,m)$ and $\delta S_m^{\mathrm{real},\Delta}(\ell,m)$ are part of the renormalized soft function in both schemes and contribute when kinematically allowed.

The matching procedure has to take care of the difference between the two schemes; thus the mass mode matching coefficient at the mass scale is obtained by the relation

$$\begin{aligned}\mathcal{M}_S(\ell,m,\mu_m)&=\int \mathrm{d}\ell'\,\hat{S}^{(n_l+1)}(\ell-\ell',m,\mu_m)(\hat{S}^{(n_l)}(\ell',m,\mu_m))^{-1}\\&=\int \mathrm{d}\ell' Z_S^{(n_l)}(\ell-\ell',m,\mu_m)(Z_S^{(n_l+1)}(\ell',\mu_m))^{-1}.\end{aligned}\tag{136}$$

In the RG setup, where the final renormalization scale is the jet scale μ_J, the difference in the factorization theorems for scenario III, given in Eq. (126), and for scenario IV, given by

$$\begin{aligned}\frac{1}{\sigma_0}\frac{\mathrm{d}\sigma}{\mathrm{d}\tau}&=Q|C^{(n_l+1)}(Q,m,\mu_H)|^2|U_C^{(n_l+1)}(Q,\mu_H,\mu_J)|^2\\&\times\int \mathrm{d}s\int \mathrm{d}\ell J^{(n_l+1)}(s,m,\mu_J)U_S^{(n_l+1)}\Big(\ell-\frac{s}{Q},\mu_J,\mu_S\Big)\\&\times S^{(n_l+1)}(Q\tau-\ell,m,\mu_S),\end{aligned}\tag{137}$$

concerns just the soft function and its evolution. Thus, Eq. (136) shows that the condition for the soft function automatically implements a continuous transition between these two scenarios in the region $m\sim\mu_m\sim\mu_S\sim\ell$, when the real radiation terms $\delta S_m^{\mathrm{real},\theta}(\ell,m)$ and $\delta S_m^{\mathrm{real},\Delta}(\ell,m)$ are included in both scenarios. From the viewpoint of the factorization theorems in the top-down evolution to the soft scale given in Eqs. (39) and (47), respectively, the continuity seems less obvious. However, since the final renormalization scale is unphysical, these two RG setups are related to each other via consistency relations, which we discuss in Sec. V D.

Relating the schemes of α_s via Eq. (101), we obtain at $\mathcal{O}(\alpha_s^2)$ in the fixed-order counting

$$\begin{aligned}\mathcal{M}_S(\ell,m,\mu_m)=\delta(\ell)&-\frac{\alpha_s^{(n_l+1)}T_F}{3\pi}L_m\hat{S}^{(n_l+1,1)}(\ell,\mu_m)\\&+\hat{S}^{(n_l+1,2)}_{n_f=1}(\ell,\mu_m)+\delta S_m^{\mathrm{dist}}(\ell,m,\mu_m)+\mathcal{O}(\alpha_s^3).\end{aligned}\tag{138}$$

Note that the real radiation terms cancel in the ratio in Eq. (136) and do not contribute to the threshold correction factor. Inserting all explicit expressions, this gives at $\mathcal{O}(\alpha_s^2)$ in the fixed-order counting ($\bar{\ell}=\ell/\mu_m$)

$$\begin{aligned}\mu_m\mathcal{M}_S^{(2)}(\ell,m,\mu_m)&=\frac{\alpha_s^2 C_F T_F}{16\pi^2}\Bigg\{\Bigg[-\frac{8}{9}L_m^3-\frac{40}{9}L_m^2+\left(-\frac{448}{27}+\frac{4\pi^2}{9}\right)L_m-\frac{656}{27}+\frac{10\pi^2}{27}+\frac{56}{9}\zeta_3\Bigg]\delta(\bar{\ell})\\&+\left[\frac{16}{3}L_m^2+\frac{160}{9}L_m+\frac{448}{27}\right]\left[\frac{\theta(\bar{\ell})}{\bar{\ell}}\right]_+\Bigg\}.\end{aligned}\tag{139}$$

Since there are no $\mathcal{O}(\alpha_s)$ corrections, the schemes of α_s and the mass appearing in Eq. (139) do not need to be specified at this point. Equation (139) contains a large logarithm, which can be better seen using the rescaled soft energy variable $\tilde{\ell}=\ell/\mu_S\sim\mathcal{O}(1)$ rather than $\bar{\ell}=\ell/\mu_m$. As for the current mass mode matching coefficient, this is a rapidity logarithm which enforces the counting $\alpha_s\ln(m/\ell)\sim\mathcal{O}(1)$. This logarithm is known to exponentiate, which allows us to determine the terms of $\mathcal{O}(\alpha_s^4\ln^2(m/\ell))\sim\mathcal{O}(\alpha_s^2)$. For a complete analysis at N^{3}LL, we also need the term at $\mathcal{O}(\alpha_s^3\ln(m/\ell))\sim\mathcal{O}(\alpha_s^2)$. We can determine its μ_m-dependent contribution from the identity

$$\mathcal{M}_S(\ell,m,\mu_m)=\int \mathrm{d}\ell' \int \mathrm{d}\ell'' U_S^{(n_l)}(\ell-\ell',m,\mu_m)\mathcal{M}_S(\ell'-\ell'',m,m)U_S^{(n_l+1)}(\ell'',\mu_m,m), \tag{140}$$

or equivalently, from

$$\mu\frac{\mathrm{d}}{\mathrm{d}\mu}\mathcal{M}_S(\ell,m,\mu)=\int \mathrm{d}\ell' \mathcal{M}_S(\ell',m,\mu)(\gamma_S^{(n_l+1)}(\ell-\ell',\mu)-\gamma_S^{(n_l)}(\ell-\ell',\mu)). \tag{141}$$

Expanding consistently in α_s gives the perturbative result for the μ_m-dependent terms. Including the relevant term at $\mathcal{O}(\alpha_s^3\ln(s/m^2))$ in the exponent, the structure of the mass mode matching coefficient reads [$\alpha_s^{(n_l+1)}=\alpha_s^{(n_l+1)}(\mu_m)$, $m=\bar{m}(\mu_m),\tilde{\ell}=\ell/\mu_S$]

$$\begin{aligned}
\mu_S\mathcal{M}_S(\ell,m,\mu_m,\mu_S)=&\left\{\delta(\tilde{\ell})+\frac{(\alpha_s^{(n_l+1)})^2}{(4\pi)^2}\delta(\tilde{\ell})\left[-\frac{1}{12}L_m^3\Gamma_0^S\Delta\beta_0-\frac{1}{4}L_m^2(\Delta\Gamma_1^S+\gamma_0^S\Delta\beta_0)\right.\right.\\
&\left.-\frac{1}{2}L_m(\Delta\gamma_1^S+\mathcal{M}_2^{S,+})+\mathcal{M}_2^S\right]+\frac{(\alpha_s^{(n_l+1)})^2}{(4\pi)^2}\left[\frac{\theta(\tilde{\ell})}{\tilde{\ell}}\right]_+\left[\frac{1}{2}L_m^2\Gamma_0^S\Delta\beta_0+L_m\Delta\Gamma_1^S+\mathcal{M}_2^{S,+}\right]\Bigg\}\\
&\times\exp\left\{\frac{(\alpha_s^{(n_l+1)})^2}{(4\pi)^2}\ln\left(\frac{\mu_S^2}{\mu_m^2}\right)\left[\frac{1}{4}L_m^2\Gamma_0^S\Delta\beta_0+\frac{1}{2}L_m\Delta\Gamma_1^S+\frac{1}{2}\mathcal{M}_2^{S,+}\right]+\frac{(\alpha_s^{(n_l+1)})^3}{(4\pi)^3}\ln\left(\frac{\mu_S^2}{\mu_m^2}\right)\right.\\
&\times\left[-\frac{1}{6}L_m^3\Gamma_0^S(\beta_0+\Delta\beta_0)\Delta\beta_0+\frac{1}{4}L_m^2(\Gamma_0^S\Delta\beta_1+2\Gamma_1^S\Delta\beta_0-2(\beta_0+\Delta\beta_0)\Delta\Gamma_1^S-4\Delta\beta_0\Gamma_0^S\gamma_0^m)\right.\\
&\left.\left.+\frac{1}{2}L_m(\Delta\Gamma_2^S-2\beta_0\mathcal{M}_2^{S,+}-c_{\mathrm{dec}}\Gamma_0^S-2\Delta\Gamma_1^S\gamma_0^m)+\frac{1}{2}\mathcal{M}_3^{S,+}\right]\right\},
\end{aligned} \tag{142}$$

Here $\Delta\eta\equiv\eta^{(n_l+1)}-\eta^{(n_l)}$ is the difference between an evolution constant η in the (n_l+1) and n_l schemes. The terms Γ_i^S and γ_i^S denote the coefficients of the cusp and noncusp soft function anomalous dimensions with n_l+1 flavors given by

$$\mu\frac{\mathrm{d}}{\mathrm{d}\mu}S(\ell)=\sum_{i\geq 0}\left(\frac{\alpha_s^{(n_l+1)}}{4\pi}\right)^{i+1}\int \mathrm{d}\ell'\left[-\frac{2\Gamma_i^S}{\mu}\left[\frac{\mu\theta(\ell-\ell')}{\ell-\ell'}\right]_+ +\gamma_i^S\delta(\ell-\ell')\right]S(\ell'), \tag{143}$$

i.e., with the one-loop terms $\Gamma_0^S=-8C_F$ and $\gamma_0^S=0$. The terms γ_i^m and β_i denote the mass anomalous dimension and the beta function, respectively, as defined in Eqs. (108) and (109). The terms $\mathcal{M}_i^{S,+}$ and $\mathcal{M}_i^S$ indicate the μ_m-independent coefficients of the plus-distribution $1/m[m\theta(\ell)/\ell]_+$ and delta distribution $\delta(\ell)$ in the matching coefficient $\mathcal{M}_S(\ell,m,m)$ (i.e., for $\mu_m=m$), respectively, and c_{dec} is the mass-scheme-dependent two-loop decoupling constant for α_s, see Eq. (110). Inserting the values for all of the constants and expanding Eq. (142) using the logarithmic counting $\alpha_s\ln(m^2/\ell^2)\sim\mathcal{O}(1)$ gives our final result,

$$\begin{aligned}
\mu_S\mathcal{M}_S^{(2)}(\ell,m,\mu_S,\mu_m)=&\,\delta(\tilde{\ell})+\left[\frac{(\alpha_s^{(n_l+1)})^2C_FT_F}{(4\pi)^2}\delta(\tilde{\ell})\ln\left(\frac{\mu_S^2}{\mu_m^2}\right)\left\{\frac{8}{3}L_m^2+\frac{80}{9}L_m+\frac{224}{27}\right\}\right]_{\mathcal{O}(\alpha_s)}\\
&+\left[\frac{(\alpha_s^{(n_l+1)})^2C_FT_F}{(4\pi)^2}\left\{\delta(\tilde{\ell})\left[-\frac{8}{9}L_m^3-\frac{40}{9}L_m^2+\left(-\frac{448}{27}+\frac{4\pi^2}{9}\right)L_m-\frac{656}{27}+\frac{10\pi^2}{27}+\frac{56}{9}\zeta_3\right]\right.\right.\\
&\left.+\left[\frac{16}{3}L_m^2+\frac{160}{9}L_m+\frac{448}{27}\right]\left[\frac{\theta(\tilde{\ell})}{\tilde{\ell}}\right]_+\right\}+\frac{(\alpha_s^{(n_l+1)})^3C_FT_F}{(4\pi)^3}\delta(\tilde{s})\ln\left(\frac{\mu_S^2}{\mu_m^2}\right)\\
&\times\left\{L_m^3\left[-\frac{176}{27}C_A+\frac{128}{27}T_F+\frac{64}{27}T_Fn_l\right]+L_m^2\left[\left(\frac{184}{9}-\frac{16}{9}\pi^2\right)C_A-24C_F+\frac{320}{27}T_F\right]\right.\\
&+L_m\left[\left(\frac{1240}{81}-\frac{160\pi^2}{27}+\frac{224}{3}\zeta_3\right)C_A+\left(\frac{8}{3}-64\zeta_3\right)C_F+\frac{2176}{81}T_Fn_l+\frac{1984}{81}T_F\right]+\left.\frac{\mathcal{M}_3^{S,+}}{2C_FT_F}\right\}\\
&+\left.\frac{(\alpha_s^{(n_l+1)})^4C_F^2T_F^2}{(4\pi)^4}\delta(\tilde{s})\ln^2\left(\frac{\mu_S^2}{\mu_m^2}\right)\left\{\frac{32}{9}L_m^4+\frac{640}{27}L_m^3+\frac{1664}{27}L_m^2+\frac{17920}{243}L_m+\frac{25088}{729}\right\}\right]_{\mathcal{O}(\alpha_s^2)}.
\end{aligned} \tag{144}$$

D. Consistency relations

As already discussed in the introduction of Sec. V, the mass mode threshold factors $\mathcal{M}_C$ for the hard current mass mode matching, $\mathcal{M}_J$ for the jet mass mode matching, and $\mathcal{M}_S$ for the soft mass mode matching are related by consistency of RG running in analogy to the well-known relation between the evolution factors and anomalous dimensions shown in Eqs. (24) and (25), respectively. This consistency relation can be easily read off Eqs. (39) and (126), which show the factorization theorems for $Q > Q\lambda > m > Q\lambda^2$ (scenario III) with the final renormalization scale μ set equal to the soft and the jet scale, respectively. It reads

$$\mathcal{M}_S(\ell, m, \mu_S, \mu) = Q|\mathcal{M}_C(Q, m, \mu_H, \mu)|^2 \times \mathcal{M}_J(Q\ell, m, \mu_J, \mu). \tag{145}$$

The relation implies in particular that the rapidity logarithms (and singularities) that arise in the hard, collinear, and soft sectors are intrinsically related to each other. Relation (145) holds identically at each finite order for $\mu_J = \sqrt{\mu_S \mu_H}$ using the counting explained in Eqs. (106), (124), and (142). For $\mu_J \sim \sqrt{\mu_S \mu_H}$, the relation holds up to terms at higher order. The consistency condition further implies that the currently unknown constants $\mathcal{M}_3^{J,+}$, $\mathcal{M}_3^{S,+}$, and $\mathcal{M}_3^{C,+}$, which are enhanced by a rapidity logarithm but not constrained by the μ anomalous dimension are related by

$$\mathcal{M}_3^{J,+} = \mathcal{M}_3^{S,+} = 4\mathcal{M}_3^{C,+}. \tag{146}$$

Using the structure of the matching coefficients given in Eqs. (102), (120), and (138), the consistency relation at $\mathcal{O}(\alpha_s^2)$ in the fixed-order expansion has the explicit form

$$\begin{aligned} &2\,\mathrm{Re}[F_{\mathrm{QCD}}^{(n_l,2)}(Q,m) - C_{n_f=1}^{(n_l+1,2)}(Q,\mu) - \delta F^{(n_l+1,2)}(Q,m,\mu)]\delta(\tau) \\ &- Q^2[J_{n_f=1}^{(n_l+1,2)}(Q^2\tau,\mu) + \delta J_m^{\mathrm{dist}}(Q^2\tau,m,\mu)] - Q[\hat{S}_{n_f=1}^{(n_l+1,2)}(Q\tau,\mu) + \delta S_m^{\mathrm{dist}}(Q\tau,m,\mu)] \\ &+ \frac{\alpha_s T_F}{3\pi} L_m\{2\mathrm{Re}[C^{(n_l+1,1)}(Q,\mu)]\delta(\tau) + Q^2 J^{(n_l+1,1)}(Q^2\tau,\mu) + Q\hat{S}^{(n_l+1,1)}(Q\tau,\mu)\} = 0. \end{aligned} \tag{147}$$

Here $C_{n_f=1}^{(n_l+1,2)}(Q,\mu)$, $J_{n_f=1}^{(n_l+1,2)}(s,\mu)$, and $\hat{S}_{n_f=1}^{(n_l+1,2)}(\ell,\mu)$ are the $\mathcal{O}(\alpha_s^2 C_F T_F)$ massless contributions to the hard current coefficient, jet, and soft functions for one single flavor corresponding to the expressions in Eqs. (4), (6), and (8), respectively. The corrections due to the quark mass given by $F_{\mathrm{QCD}}^{(n_l,2)}(Q,m)$, $\delta F^{(n_l+1,2)}(Q,m,\mu)$, $\delta J_m^{\mathrm{dist}}(s,m,\mu)$, and $\delta S_m^{\mathrm{dist}}(\ell,m,\mu)$ can be found in Eqs. (30), (36), (41), and (49). These do not involve terms related to real radiation of heavy quarks and yield together with the massless terms the virtual quark contributions to the SCET current, the jet function and the soft function (in the $\overline{\mathrm{MS}}$ scheme). Finally, also the one-loop terms $C^{(n_l+1,1)}(Q,\mu)$, $J^{(n_l+1,1)}(s,\mu)$, and $\hat{S}^{(n_l+1,1)}(\ell,\mu)$ given in Eqs. (96), (115), and (131) appear due to the virtual heavy quark contributions to the strong coupling encoded in the decoupling relation of α_s between the n_l- and (n_l+1)-flavor schemes. Equation (147) relates the virtual quark contributions to the hard current coefficient, the jet function, the soft function, and α_s to one another and is a consequence of the consistency of the mass mode setup. Moreover, Eq. (147) is also the analytic relation behind the fact that the transition between the factorization theorems in Eqs. (39) and (47) for scenarios III and IV, respectively, is continuous.[18]

We emphasize again that the form of the threshold factors and the validity of the consistency relation in Eq. (145) are not restricted to thrust, but arise in analogous form for other observables, which exhibit factorization theorems with a similar structure, i.e., involving a hard current coefficient, a jet function, and a soft function as building blocks.

E. Fixed-order QCD result

The factorization theorems discussed in the previous sections each contain all information about the singular $\mathcal{O}(\alpha_s^2 C_F T_F)$ secondary massive quark corrections to the thrust distribution in the fixed-order expansion in full QCD. As these fixed-order corrections have not been made available in literature in an explicit form, we give them in the following. Besides the virtual contributions, the singular fixed-order corrections consist of the singular collinear and soft real radiation contributions which arise for $\tau \sim m^2/Q^2 \ll 1$ and $\tau \sim m/Q \ll 1$, respectively, in the dijet regime.[19] Setting $\mu = \mu_H = \mu_J = \mu_S$, using the n_l-flavor scheme for α_s and ignoring the gap subtraction, we obtain

[18] Note that the gap parameter in the soft model function and the renormalon subtractions to the partonic soft function also change. However, they compensate each other for $\mu_m \sim \mu_S$ due to the matching relation in Eq. (68).

[19] Note that at the corresponding thresholds $\tau = 4m^2/Q^2$ and $\tau = 2m/Q$, respectively, in the fixed-order expansion, the nonsingular contributions can be numerically larger than the singular terms $\delta J_m^{\mathrm{real}}$ and $\delta S_m^{\mathrm{real},\theta}$, since the latter vanish at the respective thresholds. This feature was already discussed in Ref. [15] for the case of massive gauge bosons at one loop.

$$\left.\frac{1}{\sigma_0}\frac{\mathrm{d}\sigma}{\mathrm{d}\tau}\right|_{\mathcal{O}(\alpha_s^2 C_F T_F)} = 2\mathrm{Re}[F_{\mathrm{QCD}}^{(n_l,2)}(Q,m)]\delta(\tau) + Q^2\delta J_m^{\mathrm{real}}(Q^2\tau,m) + Q\delta S_m^{\mathrm{real},\theta}(Q\tau,m) + Q\delta S_m^{\mathrm{real},\Delta}(Q\tau,m), \tag{148}$$

where $F_{\mathrm{QCD}}^{(n_l,2)}(Q,m)$, $\delta J_m^{\mathrm{real}}(s,m)$, $\delta S_m^{\mathrm{real},\theta}(\ell,m)$, and $\delta S_m^{\mathrm{real},\Delta}(\ell,m)$ have been given in Eqs. (30), (42), (50), and (52), respectively. Writing out Eq. (148) explicitly for the convenience of the reader, we get

$$\begin{aligned}
\left.\frac{1}{\sigma_0}\frac{\mathrm{d}\sigma}{\mathrm{d}\tau}\right|_{\mathcal{O}(\alpha_s^2 C_F T_F)} &= \left(\frac{\alpha_s^{(n_l)}(\mu)}{4\pi}\right)^2 C_F T_F \times \Bigg\{\delta(\tau)\Bigg[\left(-r^4+2r^2+\frac{5}{3}\right)\left(4\mathrm{Li}_3\left(\frac{r-1}{r+1}\right)+\frac{1}{3}\ln^3\left(\frac{r-1}{r+1}\right)-\frac{2\pi^2}{3}\ln\left(\frac{r-1}{r+1}\right)-4\zeta_3\right) \\
&\quad + \left(\frac{46}{9}r^3+\frac{10}{3}r\right)\left(4\mathrm{Li}_2\left(\frac{r-1}{r+1}\right)+\ln^2\left(\frac{r-1}{r+1}\right)-\frac{2\pi^2}{3}\right)+\left(\frac{220}{9}+\frac{400}{27}r^2\right)\ln\left(\frac{1-r^2}{4}\right)+\frac{476}{9}r^2+\frac{2426}{81}\Bigg] \\
&\quad + \frac{1}{\tau}\theta\left(\tau-\frac{4m^2}{Q^2}\right)\Bigg[-\frac{64}{3}\mathrm{Li}_2\left(\frac{b-1}{b+1}\right)+\frac{32}{3}\ln\left(\frac{1-b^2}{4}\right)\ln\left(\frac{1-b}{1+b}\right)-\frac{16}{3}\ln^2\left(\frac{1-b}{1+b}\right) \\
&\quad + \left(b^4-2b^2+\frac{241}{9}\right)\ln\left(\frac{1-b}{1+b}\right)-\frac{10}{27}b^3+\frac{482}{9}b-\frac{16\pi^2}{9}\Bigg] \\
&\quad + \frac{1}{\tau}\theta\left(\tau-\frac{2m}{Q}\right)\Bigg[\frac{64}{3}\mathrm{Li}_2\left(\frac{w-1}{w+1}\right)-\frac{32}{3}\ln\left(\frac{1-w^2}{4}\right)\ln\left(\frac{1-w}{1+w}\right)+\frac{16}{3}\ln^2\left(\frac{1-w}{1+w}\right)-\frac{160}{9}\ln\left(\frac{1-w}{1+w}\right) \\
&\quad + \frac{64}{27}w^3-\frac{320}{9}w+\frac{16\pi^2}{9}\Bigg]\Bigg\} + Q\delta S_m^{\mathrm{real},\Delta}(Q\tau,m),
\end{aligned} \tag{149}$$

with

$$r \equiv \sqrt{1+\frac{4m^2}{Q^2}}, \qquad b \equiv \sqrt{1-\frac{4m^2}{Q^2\tau}}, \qquad w \equiv \sqrt{1-\frac{4m^2}{Q^2\tau^2}}. \tag{150}$$

An important difference in the SCET setup to this fixed-order QCD expansion is that in the factorization theorems, the various components are calculated in different flavor number schemes to allow for the summation of logarithms involving ratios of the scales Q, $Q\lambda$, $Q\lambda^2$, and m. A maybe even more notable difference is that the consistent and IR-safe definitions of the jet and the soft functions entail that virtual corrections have nonvanishing support for finite values of τ, so that they do not only arise in coefficients of $\delta(\tau)$, but also in coefficients involving plus-distributions $(\ln^n\tau/\tau)_+$. In contrast, the fixed-order expansion contains only real radiation corrections for finite values of τ and virtual corrections proportional to $\delta(\tau)$, each of which is individually IR regular for $m \to 0$. The rearrangement of virtual and mass-singular corrections, which is intrinsically connected to the consistency relation of Eqs. (145) and (147), is the basis of rendering the hard coefficient and the jet and the soft functions in the factorization theorems infrared safe in the limit $m \to 0$. This may provide a guideline to understanding the factorization from the point of view of the fixed-order expansion.

VI. NUMERICAL ANALYSIS

In the following, we investigate the numerical effects of secondary bottom and top quarks in the thrust distribution related to the mass-dependent factorization theorems we have described and presented in the previous sections. The emphasis is on a comparison to the predictions where the mass of the secondary quark is neglected. In Ref. [15], a similar examination was carried out which, however, did not account for nonperturbative effects (described by the soft model function F), for the renormalon subtractions and the associated gap formalism.[20] We note that our analysis does not include the nonsingular contributions, which might be sizeable in the tail and the far-tail region, so some of the conclusions concerning the tail region, e.g., concerning the scale variations, are preliminary, and final conclusions are postponed to a complete phenomenological analysis which also includes the effects of primary massive quark production.

The results in our analysis are calculated at N^{3}LL order in the usual SCET counting, so we use the beta function and the cusp anomalous dimension up to four loops and the noncusp anomalous dimensions including R evolution up

[20]The soft model function and the gap subtraction lead to significant changes in the thrust distribution and affect the secondary quark mass effects as well as the contributions from the massless quarks. Our partonic results are in complete agreement with the results shown in Ref. [15].

to three loops.[21] The perturbative corrections to the matrix elements and matching conditions are included up to $\mathcal{O}(\alpha_s^2)$ and expanded out within the factorized expressions to avoid higher-order cross terms. There are many ingredients concerning the RG evolution and matrix elements involving massless quarks which we have not discussed in detail in this paper, but which are used in our analysis. For these contributions, we employed the results given in Ref. [17] with top-down evolution. We have further checked that the massless limit of the factorization theorem for scenario IV agrees with the N^{3}LL thrust distribution given in Ref. [17] for massless quarks up to implementation-dependent higher-order corrections.

For the renormalization scales of the individual structures and the renormalon subtraction scale we use the τ-dependent profile functions for the hard, jet, soft, and R scale given in Ref. [17], which contain an appropriate generic scaling and smoothly interpolate between peak, tail, and far-tail regimes. Adding an additional profile for the τ-independent mass mode matching scale, the profile functions have the form

$$\mu_H = e_H Q, \tag{151}$$

$$\mu_S(\tau) = \begin{cases} \mu_0 + \frac{b}{2t_1}\tau^2, & 0 \le \tau \le t_1, \\ b\tau + d, & t_1 \le \tau \le t_2, \\ \mu_H - \frac{b}{1-2t_2}(\frac{1}{2}-\tau)^2 & t_2 \le \tau \le \frac{1}{2}, \end{cases} \tag{152}$$

$$\mu_J(\tau) = \left(1 + e_J\left(\frac{1}{2}-\tau\right)^2\right)\sqrt{\mu_H \mu_S(\tau)}, \tag{153}$$

$$R(\tau) = \begin{cases} R_0 + \mu_1\tau + \mu_2\tau^2 & 0 \le \tau \le t_1 \\ \mu_S(\tau), & t_1 \le \tau \le \frac{1}{2}, \end{cases} \tag{154}$$

$$\mu_m = e_m m_b. \tag{155}$$

As default values we use

$$e_H = e_m = 1, \quad e_J = 0, \quad \mu_0 = 2\text{ GeV}, \quad R_0 = 0.85\mu_0,$$
$$t_2 = 0.25, \quad n_1 \equiv \frac{Q t_1}{1\text{ GeV}} = \begin{cases} 5, & Q \ge \frac{5\text{ GeV}}{t_2}, \\ \frac{Q t_2}{1\text{ GeV}}, & Q \le \frac{5\text{ GeV}}{t_2}, \end{cases} \tag{156}$$

and b, d, μ_1, and μ_2 are fixed by demanding smoothness of the profiles as in Ref. [17]. Compared to Ref. [17], we have modified the default value of the parameter n_1 for the case $Q \le 5\text{ GeV}/t_2$ such that one always has $t_1 \le t_2$, and the profiles can remain smooth for small values of Q.

We perform the convolution with the soft model function directly in momentum space, since the mass-dependent corrections to the jet and the soft functions cannot be easily treated in Fourier space. This requires a thorough treatment of fractional plus-distributions of the form $[\ln^n(x)/x^{1+\omega}]_+$, where ω can be larger than 0. For convenience, the corresponding rules are given in the Appendix. As a model function we use

$$F(\ell) = \frac{128\ell^3}{3\lambda^4} e^{-4\ell/\lambda}, \tag{157}$$

which is properly normalized to unity. The parameter λ is a measure for the width of the function and therefore contributes as in Eq. (17) together with the gap parameter to the first nonperturbative moment, $\Omega_1 = \bar{\Delta} + \lambda/2$. As a default we use the following parameters:

$$\Omega_1^{(5)}(13\text{ GeV}, 13\text{ GeV}) = 0.5\text{ GeV}, \quad \lambda = 0.65\text{ GeV},$$
$$\alpha_s^{(5)}(m_Z) = 0.114, \quad \bar{m}_b(\bar{m}_b) = 4.2\text{ GeV},$$
$$\bar{m}_t(\bar{m}_t) = 163\text{ GeV}. \tag{158}$$

We have checked that the basic characteristics of the results for the mass effects are rather weakly depending on these parameters within their known accuracy and on details of the shape of the soft model function, so our observations represent generic properties of the mass effects from secondary massive quarks.

An important aspect of the practical implementation of the VFNS concerns the prescription of how the predictions within the various scenarios discussed in the previous sections are patched together to obtain the complete spectrum of the thrust distribution. As described in Sec. III, one switches between neighboring scenarios when the mass scale is close to one of the kinematic scales related to the hard coefficient and the jet and the soft functions. It is therefore natural to tie the prescription for the transition to the τ-dependent profile functions for μ_m, μ_H, μ_J, and μ_S. In Figs. 10 and 11 the default profile functions (including the subtraction scale R) are shown for $Q = 14$ GeV with $\mu_m = \bar{m}_b(\bar{m}_b)$ and $Q = 500$ GeV with $\mu_m = \bar{m}_t(\bar{m}_t)$, respectively. The prescription we adopt is that the transition concerning the scenarios II, III, and IV is carried out when μ_m is equal to μ_J or μ_S, respectively. For each choice of the profile functions and the mass mode matching scale this leads to a unique value of τ for the transition. The resulting τ regions for the scenarios II, III, and IV are indicated in Figs. 10 and 11 by the black dotted vertical lines. We note that the general freedom to choose the transition value for τ in some range causes variations in the predictions that are related to higher-order corrections in the same way as changes of the renormalization and matching scales μ_m, μ_H,

[21] For Γ_3^{cusp}, we use the Padé approximation of Ref. [17]. The remaining missing ingredients for a complete N^{3}LL analysis are logarithmic enhanced coefficients $\mathcal{M}_3^{C,+}$ and $\mathcal{M}_3^{J,+}$ in the mass mode threshold factors at $\mathcal{O}(\alpha_s^3)$ (which we set to zero) and the massive R-anomalous dimension at $\mathcal{O}(\alpha_s^3)$ (for which we use the massless approximation; see discussion in Sec. III E).

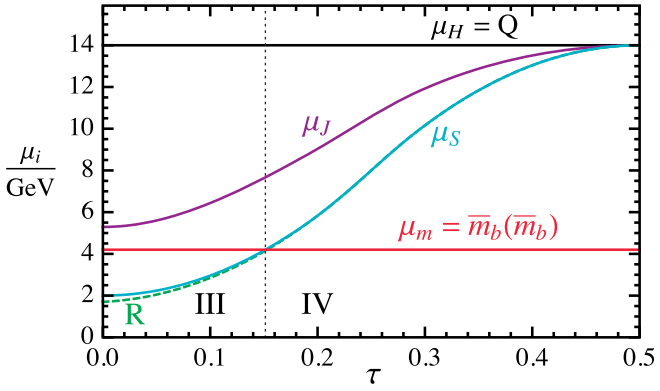

FIG. 10 (color online). Default profiles for $Q = 14$ GeV. The transition value for τ between the scenarios III and IV is indicated by the dotted line.

μ_J, and μ_S in their respective ranges. Our prescription ties the choices made for their profile functions to the range in τ of the scenarios.

The practical implementation of the factorization theorems from the different scenarios at N^{3}LL involves a treatment of perturbative terms at higher orders that arise from cross terms of the perturbative series for the hard, jet, and soft functions and the mass mode threshold factors. As mentioned above, we use the common approach to expand out the perturbative terms in the matrix elements and matching factors to $\mathcal{O}(\alpha_s^2)$, but to keep the RG evolution factors multiplying all expanded terms to the highest order. This approach has been proven advantageous to avoid spurious higher-order corrections in the fixed-order expansion and to obtain reliable information on the remaining renormalization scale dependence at the corresponding order. This approach is also crucial to achieving a good numerical agreement of the factorization theorems in overlap regions where two different scenarios can be employed. In the same spirit, to avoid gaps at the transition points between neighboring scenarios related to spurious higher-order terms and to obtain a continuous distribution,

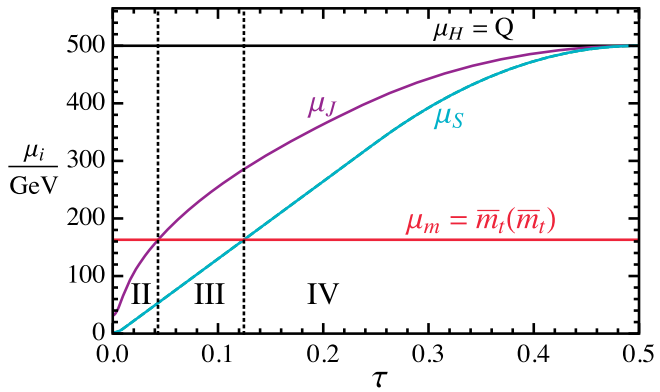

FIG. 11 (color online). Default profiles for $Q = 500$ GeV. The transition values for τ between the scenarios II and III and between the scenarios III and IV are indicated by dotted lines.

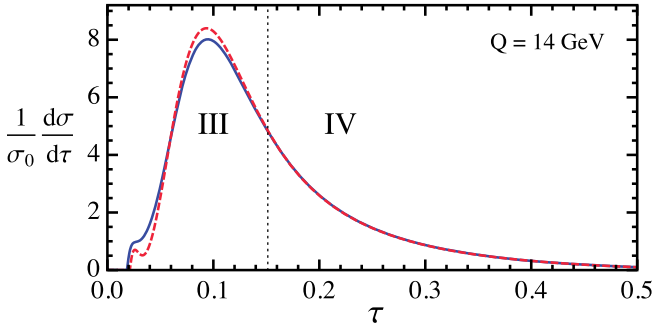

FIG. 12 (color online). The thrust distribution at $Q = 14$ GeV including secondary massive bottom effects (blue, solid) compared to keeping the bottom quark massless (red, dashed).

we also adopt the approach to expand in the series (at the scale μ_m) for the decoupling relations of the strong coupling and the gap parameter $\bar{\Delta}$ up to $\mathcal{O}(\alpha_s^2)$, see Eqs. (101) and (68).

In Fig. 12, the thrust distribution (for primary production of the four light quark flavors and secondary production of the light flavors and the bottom quark) normalized to the Born cross section σ_0 is shown for $Q = 14$ GeV at N^{3}LL order, based on the factorization theorems for secondary massive bottom quarks with $\mu_m = \bar{m}_b(\bar{m}_b)$ (blue, solid line) and in the massless approximation (red, dashed line). We see that the finite bottom mass effects are significant at and below the peak, but small in the tail region. Overall, the secondary quark mass effects lead to a significant decrease in the peak cross section. Interestingly, at the peak the deviations are only weakly depending on the value of Q. This is illustrated in Fig. 13, where we display for $Q = 14$ GeV (blue, solid curve), $Q = 35$ GeV (red, dashed curve), and $Q = m_Z$ (green, dotted curve) the relative change due to the finite mass of the secondary massive bottom quarks $\Delta\sigma(m_b)$, with

$$\Delta\sigma(m) \equiv \frac{\frac{d\sigma}{d\tau}(m) - \frac{d\sigma}{d\tau}(m=0)}{\frac{d\sigma}{d\tau}(m=0)}. \tag{159}$$

Here $\frac{d\sigma}{d\tau}(m)$ is the complete thrust distribution at N^{3}LL for primary massless quarks and for secondary quark production which includes the proper number of light

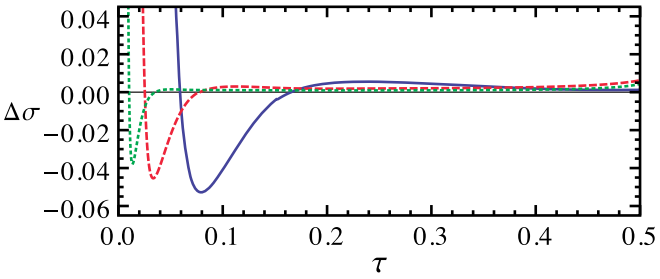

FIG. 13 (color online). Relative secondary massive bottom effects for $Q = 14$ GeV (blue, solid), $Q = 35$ GeV (red, dashed) and $Q = m_Z$ (green, dotted).

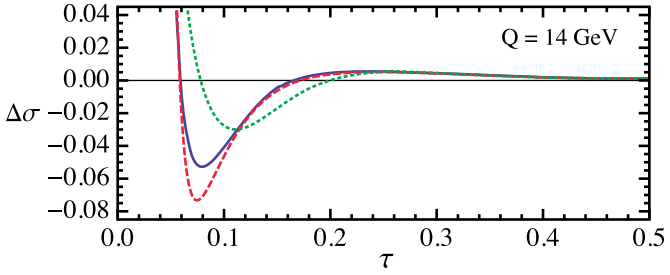

FIG. 14 (color online). Dependence of $\Delta\sigma$ on the mass mode matching scale μ_m for secondary bottom quarks for $Q = 14$ GeV: $\mu_m = m_b$ (blue, solid), $\mu_m = m_b/2$ (red, dashed), $\mu_m = 2m_b$ (green, dotted).

quarks and an additional flavor with mass m. We see that in the peak region $\Delta\sigma$ is up to $\sim -5\%$ and depends only weakly on the Q value. In the tail region, the mass effects from secondary bottom quarks amount to relative corrections below 1% for $Q = 14$ GeV, and they quickly decrease for larger values of Q.

It is also important to discuss the scale variations of the mass correction $\Delta\sigma$. In Fig. 14, the impact of the variations of μ_m is illustrated for the bottom quark case for $Q = 14$ GeV. The curves are for μ_m equal to the $\overline{\text{MS}}$ bottom mass and for variations by factors of 2 and 0.5. The μ_m dependence is quite small in the tail and far-tail regions. In the peak region, on the other hand, the variation of $\Delta\sigma$ increases to 4% and grows even further below the peak, where $\Delta\sigma$ changes sign. This behavior is generic for the bottom quark case and very similar for other values of Q. This behavior might appear formidable for $\Delta\sigma$, but it should be judged taking into account that in the peak region the dependence on μ_m is related to missing higher-order corrections of the complete thrust distribution and not only to $\Delta\sigma$. In other words, the finite mass of the secondary heavy quark leads to a modification of the peak behavior which represents a property of the complete thrust distribution and not just of $\Delta\sigma$ itself. The result shows that variations of μ_m need to be accounted for when estimating perturbative uncertainties in the peak region.

In this context it is also important to examine the variation of $\Delta\sigma$ due to changes of the profile functions for μ_H, μ_J, and μ_S, as well as for R. In Fig. 15, $\Delta\sigma$ is shown for the bottom quark case at $Q = 14$ GeV for variations of the parameters e_H, e_J, μ_0, n_1, and t_2, see Eqs. (151)–(154), which parametrize changes of the profile functions. The ranges of variation are described in the figure caption and are identical to the ones used for the thrust analysis of Ref. [17] (except for n_1, which requires a lower range for low Q values). These variations induce visible changes in $\Delta\sigma$, but they are in general much smaller than the dependence on μ_m discussed just above. This outcome is again generic for other values of Q and also for the top quark case and shows that independent variations of the profile functions *and* of μ_m are essential for a thorough assessment of the scale variations of the complete thrust distribution.

We complete our analysis by showing in Fig. 16 the thrust distribution for primary light quark production at $Q = 500$ GeV with $n_l = 5$ massless flavors and a secondary massive top quark (blue, solid line). The figure also shows the prediction for the case where the secondary top quark is treated as massless (red, dashed line). For all parameters the default values mentioned above are used. It is visible that the finite top quark mass causes, besides a reduction of the distribution at the peak, as we have observed in the bottom quark case, also a shift of the peak to lower τ values. This effect is related to the top quark mass effects in the R-scale dependence of the gap

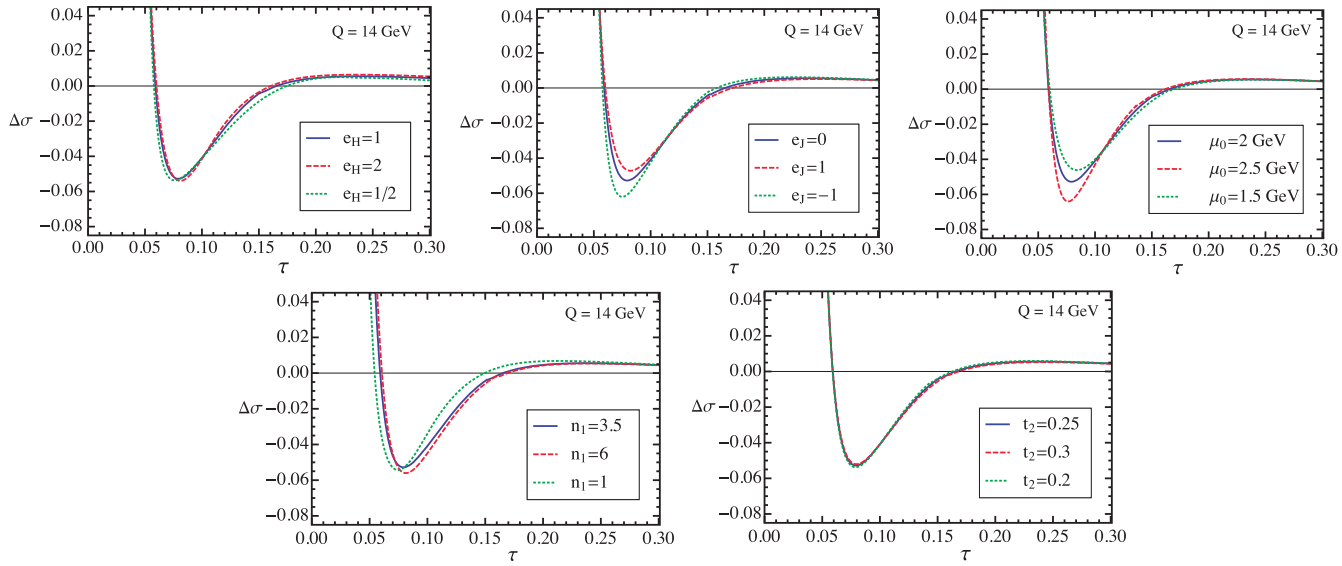

FIG. 15 (color online). Relative secondary bottom mass effects for $Q = 14$ GeV under variation of the profile parameters for the hard, jet, and soft scales.

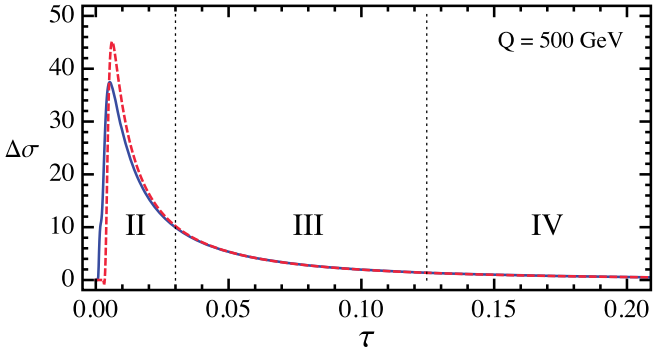

FIG. 16 (color online). The thrust distribution at $Q = 500$ GeV including secondary massive top effects (blue, solid) compared to keeping the top quark massless (red, dashed).

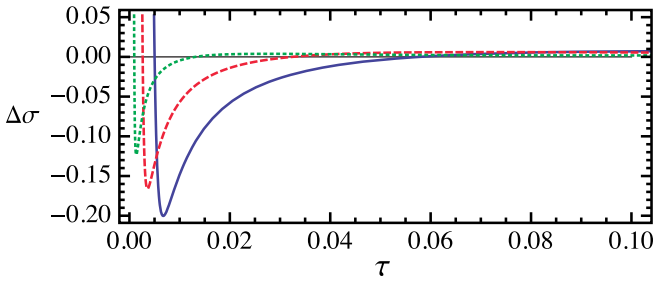

FIG. 17 (color online). Relative secondary massive top effects for $Q = 500$ GeV (blue, solid), $Q = 1000$ GeV (red, dashed), and $Q = 3000$ GeV (green, dotted).

parameter, which is significantly modified below the massive threshold as described in Sec. III E. In Fig. 17, $\Delta\sigma$ is shown for the top quark case for $Q = 500$ GeV (blue, solid line), $Q = 1000$ GeV (red, dashed line), and $Q = 3000$ GeV (green, dotted line). We find again sizable mass effects at and below the peak of the distribution. In the tail region, on the other hand, the top mass effects are relatively small. At the peak the mass effects amount to 10%–20% and remain significant even for large values of Q. In contrast to the bottom quark case, the size of the top mass effects is larger than the variations due to changes of the mass mode matching scale μ_m which amount to 1 to 2% in the total cross section. We note that in the top quark case and for these c.m. energies the decoupling limit, i.e., the thrust distribution with just five massless flavors and a decoupled top quark, is at the peak much closer to the VFNS prediction than the massless top approximation (shown in the red dashed curve). This is because in the peak region, the top mass is significantly larger than the jet and the soft scales, such that the decoupling approximation is more appropriate than the massless one.

VII. CONCLUSIONS

In this work, we have provided a variable flavor number scheme (VFNS) for inclusive final-state jets, taking the production of secondary massive quarks (see Fig. 1) for the thrust distribution as the concrete application. In the dijet limit, the singular terms factorize into a hard function given by a Wilson coefficient for the dijet production current, a jet function describing the hard collinear radiation within the jet, and a soft function describing soft radiation between the jets. The factorization is based on the fact that the typical invariant masses of the fluctuations described by these factors are widely separated, where the size of these scales depends on the thrust variable τ.

Including the radiation of secondary massive quarks, the situation becomes more complicated, since the quark mass adds another τ-independent scale to the situation that can lead to different kinds of hierarchies or relations with respect to the hard jet and soft scales. Apart from a more complicated analytic structure, one has to deal with potential mass singularities and the summation of logarithms of the mass—all with the requirement that the massive quark decouples in the infinite mass limit and that one obtains the well-known massless quark description in the limit that the quark mass vanishes.

The VFNS we provide is based on the hierarchy between the hard, jet, and soft scales and accounts in addition for the quark mass, for which, however, no assumption concerning a hierarchy with respect to the other scales has to be imposed. The effective theory description was explained in detail in Ref. [15] using the field theoretic analogy between secondary massive quarks and the radiation of "massive gluons." The four emerging effective theories are related to the four hierarchical regions of the mass with respect to the hard, jet, and soft scales, and deal with collinear and soft massless quarks and gluons as well as corresponding "mass modes." The treatment of these mass modes differs for each of the four effective theories and leads to modifications of the known factorization for massless quarks. These (i) add a quark mass dependence in the hard coefficient, the jet and soft functions, (ii) affect the RG evolution which is carried out with different flavor numbers above and below the quark mass scale and (iii) lead to additional massive threshold correction factors when the RG evolution of one of the structures crosses the mass scale. The factorization scale where this crossover is performed ("mass mode matching scale") can be varied in analogy to the renormalization scales. An essential aspect of the VFNS is that in a transition region between two neighboring effective theories, both of their descriptions can be used which ensures that the transition is continuous (up to perturbative terms from beyond the order that is employed in the description).

An important outcome of our mass mode treatment is that the way in which the massive quark contributes to the hard coefficient, the jet function, and the soft function as well as to their mass mode threshold factors can be determined for each of them individually without having to deal with the factorization theorem for the thrust distribution as a whole. This is related to the fact that the hard coefficient, the jet function, and the soft function are by themselves well-

defined field theoretical quantities that can be renormalized consistently. If the description includes the small-mass case (including the massless limit) the $\overline{\text{MS}}$ renormalization prescription is employed for the secondary massive quark corrections. On the other hand, if the description includes the large-mass case (including the decoupling limit), the on-shell (low-momentum-subtraction) renormalization condition is employed for the secondary massive quark corrections. For sufficiently large scale hierarchies, it may be possible to use massless quark results with the appropriate number of flavors for some of the structures as a good approximation. The transition regions are located where the quark mass is of the order of the hard, jet, or soft scales, and the difference of the renormalized quantities constitutes the mass mode threshold correction factors.

We have discussed the numerical impact of the secondary quark mass effects on the thrust distribution. These turn out to be small corrections in the tail region, but sizable at the peak, so that a phenomenological analysis of this region will have to take them into account. For the assessment of the renormalization-scale dependence, it is crucial to account for changes of the mass mode matching scale.

In this work, we have demonstrated the concept of a VFNS for final-state jets for the secondary massive quark effects in the thrust distribution. In subsequent publications, our proposed VFNS shall be applied also to the primary production of massive quarks [39], where new subtleties arise, as well as to other processes including deep inelastic scattering [40], where the relation to VFNS for initial-state massive quarks is elucidated.

ACKNOWLEDGMENTS

We thank the Erwin-Schrödinger Institute (ESI) for partial support in the framework of the ESI program "Jets and Quantum Fields for LHC and Future Colliders." P. P. would like to thank Bahman Dehnadi for helpful discussions and cross checks in parts of the numerical analysis.

Note added.—Recently, we received Ref. [41], where the $\mathcal{O}(\alpha_s^3)$ nonsinglet corrections to the heavy flavor matching of the parton distribution functions were calculated. Considerations in DIS for large x in analogy to this work [40,42] lead to a consistency relation similar to Eq. (145) involving this threshold correction, which implies

$$\begin{aligned}\mathcal{M}_3^{C,+} &= \frac{1}{4}\mathcal{M}_3^{J,+} = \frac{1}{4}\mathcal{M}_3^{S,+} \\ &= C_F T_F \Bigg\{ C_F \left(\frac{3337}{27} - \frac{604}{9}\zeta_3 + \frac{8\pi^4}{15} - \frac{32}{3}B_4 \right) \\ &\quad + C_A \left(-\frac{17726}{729} + \frac{824\pi^2}{243} + 30\zeta_3 - \frac{88\pi^4}{135} + \frac{16}{3}B_4 \right) \\ &\quad + T_F n_l \left(-\frac{12032}{729} + \frac{256}{27}\zeta_3 \right) \\ &\quad + T_F \left(\frac{6032}{729} - \frac{448}{27}\zeta_3 \right) \Bigg\}, \end{aligned} \tag{160}$$

where

$$B_4 = \frac{2}{3}\ln^4(2) - \frac{2\pi^2}{3}\ln^2(2) - \frac{13\pi^4}{180} + 16\text{Li}_4\left(\frac{1}{2}\right). \tag{161}$$

For $n_l = 4$ and $n_l = 5$ light flavors, one obtains the numerical values $\mathcal{M}_3^{C,+} = 34.9762$ and $\mathcal{M}_3^{C,+} = 33.2737$, respectively. We note that the numerical impact of the constants $\mathcal{M}_3^{C,+}$ and $\mathcal{M}_3^{J,+}$ in the analysis of Sec. VI is negligibly small.

APPENDIX: PLUS-DISTRIBUTIONS

We give the definition and integral prescription for the plus-distributions appearing in the nonlocal evolution factors, denoted by $[\ln^n(x)/x^{1+\omega}]_+$, for arbitrary (nonvanishing) ω. The prescription of these plus-distributions is based on an analytic continuation to a domain with a well-behaved convergence [38]

$$\left[\frac{\theta(x)\ln^n(x)}{x^{1+\omega}}\right]_+ \xrightarrow{\omega<0} \frac{\theta(x)\ln^n(x)}{x^{1+\omega}}, \tag{A1}$$

which leads to a definition that is based on the subtraction of strictly divergent terms located at $x = 0$ that can be generalized to arbitrary real values of ω in a straightforward way:

$$\left[\frac{\theta(x)\ln^n(x)}{x^{1+\omega}}\right]_+ = \lim_{\varepsilon\to 0}\left[\frac{\theta(x-\varepsilon)\ln^n(x)}{x^{1+\omega}} - \sum_{k=0}^{\infty}\delta^{(k)}(x)\frac{(-1)^k}{k!}\frac{\Gamma(n+1,(\omega-k)\ln(\varepsilon))}{(\omega-k)^{n+1}}\right]. \tag{A2}$$

This expression can be rewritten as an integral prescription

$$\int_0^X \mathrm{d}x \left[\frac{\theta(x)\ln^n x}{x^{1+\omega}}\right]_+ f(x) = \int_0^X \mathrm{d}x \frac{\ln^n(x)}{x^{1+\omega}}\left[f(x) - \sum_{k=0}^{\infty} f^{(k)}(0)\frac{x^k}{k!}\right] - \sum_{k=0}^{\infty} f^{(k)}(0)\frac{1}{k!}\frac{\Gamma(n+1,(\omega-k)\ln(X))}{(\omega-k)^{n+1}}, \tag{A3}$$

where the sums can be truncated for $k = N$ if $\omega < N + 1$.

[1] A. Juste, S. Mantry, A. Mitov, A. Penin, P. Skands *et al.*, arXiv:1310.0799.
[2] A. Jung, M. Schulze, and J. Shelton, arXiv:1309.2889.
[3] K. Agashe *et al.*, arXiv:1311.2028.
[4] S. Alekhin, J. Blümlein, K. Daum, K. Lipka, and S. Moch, Phys. Lett. B **720**, 172 (2013).
[5] H. Abramowicz *et al.*, Eur. Phys. J. C **73**, 2311 (2013).
[6] K. Kovařík, T. Stavreva, A. Kusina, T. Jezo, F. I. Olness, I. Schienbein, and J. Y. Yu, Nucl. Phys. Proc. Suppl. Ser. **222–224**, 52 (2012).
[7] J. Campbell, K. Hatakeyama, J. Huston, F. Petriello, J. R. Andersen *et al.*, arXiv:1310.5189.
[8] M. Aivazis, J. C. Collins, F. I. Olness, and W.-K. Tung, Phys. Rev. D **50**, 3102 (1994).
[9] M. Aivazis, F. I. Olness, and W.-K. Tung, Phys. Rev. D **50**, 3085 (1994).
[10] C. W. Bauer, S. Fleming, and M. E. Luke, Phys. Rev. D **63**, 014006 (2000).
[11] C. W. Bauer, S. Fleming, D. Pirjol, and I. W. Stewart, Phys. Rev. D **63**, 114020 (2001).
[12] I. W. Stewart, F. J. Tackmann, and W. J. Waalewijn, Phys. Rev. Lett. **105**, 092002 (2010).
[13] A. H. Hoang and I. W. Stewart, Phys. Lett. B **660**, 483 (2008).
[14] V. Mateu, I. W. Stewart, and J. Thaler, Phys. Rev. D **87**, 014025 (2013).
[15] S. Gritschacher, A. H. Hoang, I. Jemos, and P. Pietrulewicz, Phys. Rev. D **88**, 034021 (2013).
[16] S. Gritschacher, A. Hoang, I. Jemos, and P. Pietrulewicz, Phys. Rev. D **89**, 014035 (2014).
[17] R. Abbate, M. Fickinger, A. H. Hoang, V. Mateu, and I. W. Stewart, Phys. Rev. D **83**, 074021 (2011).
[18] A. H. Hoang and S. Kluth, arXiv:0806.3852.
[19] G. P. Korchemsky and G. F. Sterman, Nucl. Phys. **B555**, 335 (1999).
[20] M. D. Schwartz, Phys. Rev. D **77**, 014026 (2008).
[21] S. Fleming, A. H. Hoang, S. Mantry, and I. W. Stewart, Phys. Rev. D **77**, 074010 (2008).
[22] T. Matsuura and W. van Neerven, Z. Phys. C **38**, 623 (1988).
[23] T. Becher and M. Neubert, Phys. Lett. B **637**, 251 (2006).
[24] R. Kelley, M. D. Schwartz, R. M. Schabinger, and H. X. Zhu, Phys. Rev. D **84**, 045022 (2011).
[25] P. F. Monni, T. Gehrmann, and G. Luisoni, J. High Energy Phys. 08 (2011) 010.
[26] A. H. Hoang, A. Jain, I. Scimemi, and I. W. Stewart, Phys. Rev. Lett. **101**, 151602 (2008).
[27] A. H. Hoang, A. Jain, I. Scimemi, and I. W. Stewart, Phys. Rev. D **82**, 011501 (2010).
[28] A. K. Leibovich, Z. Ligeti, and M. B. Wise, Phys. Lett. B **564**, 231 (2003).
[29] J.-Y. Chiu, A. Fuhrer, A. H. Hoang, R. Kelley, and A. V. Manohar, Phys. Rev. D **79**, 053007 (2009).
[30] B. A. Kniehl, Phys. Lett. B **237**, 127 (1990).
[31] A. Hoang, Ph.D. thesis, Karlsruhe Institute of Technology, 1995.
[32] T. Becher and G. Bell, Phys. Lett. B **713**, 41 (2012).
[33] J.-Y. Chiu, A. Jain, D. Neill, and I. Z. Rothstein, J. High Energy Phys. 05 (2012) 084.
[34] J.-Y. Chiu, A. Jain, D. Neill, and I. Z. Rothstein, Phys. Rev. Lett. **108**, 151601 (2012).
[35] A. H. Hoang, A. Pathak, P. Pietrulewicz, and I. W. Stewart (to be published).
[36] R. Abbate, M. Fickinger, A. H. Hoang, V. Mateu, and I. W. Stewart, Phys. Rev. D **86**, 094002 (2012).
[37] S. Gritschacher, diploma thesis, Technische Universität, München, 2011.
[38] S. Fleming, A. H. Hoang, S. Mantry, and I. W. Stewart, Phys. Rev. D **77**, 114003 (2008).
[39] M. Butenschön, B. Dehnadi, A. H. Hoang, V. Mateu, and I. W. Stewart (to be published).
[40] A. H. Hoang, P. Pietrulewicz, and D. Samitz (to be published).
[41] J. Ablinger, A. Behring, J. Blümlein, A. De Freitas, A. Hasselhuhn, A. von Manteuffel, M. Round, C. Schneider, and F. Wißbrock, Nucl. Phys. **B886**, 733 (2014).
[42] A. H. Hoang, P. Pietrulewicz, and D. Samitz, arXiv: 1406.5885.